



A novel immune-competent murine model to evaluate the efficacy of a microRNA-based therapy for the pediatric brain tumor Medulloblastoma

Doctoral School in Neuroscience
curriculum Neuroscience and Neurotechnology
XXXVI cycle

Author: Letizia La Rosa

Supervisor: Davide De Pietri Tonelli, Ph. D.

University of Genova
Italian Institute of Technology

Copyright © 2023 by Letizia La Rosa
All Rights Reserved

TABLE OF CONTENTS

TABLE OF CONTENTS	iv
LIST OF TABLES	vii
LIST OF FIGURES	viii
LIST OF ABBREVIATIONS	ix
ABSTRACT	xii
CHAPTER 1 Introduction	1
<i>From Biogenesis to Biological Significance of microRNAs in mammalian Cancer and Central Nervous System</i>	
	1
MiRNA biogenesis: Canonical and Non-Canonical pathways	2
Annotation of microRNAs	2
<i>The functions of miRNAs in cell fate: pathological implications and therapeutic opportunities for brain cancer</i>	
	4
miRNA in Neurodevelopment	5
Cornerstones of CNS development	5
miRNA in CNS development	5
The roles of miRNAs in Cancer	6
miRNAs and Cancer Proliferation	7
miRNA and Apoptosis	8
miRNA and Angiogenesis	8
miRNA and EMT	8
Theragnostic role of miRNAs in cancer medicine	10
Diagnosis and prognosis	10
Therapy	11
Cancer Stem Cells: a new therapeutic target	12
Medulloblastoma: a paradigm to study the role and therapeutic potential of miRNAs in abnormal CNS development.	14
Development of the cerebellum	14
Medulloblastoma	15
Modeling the MB biology	16
Treatment of Medulloblastoma	16
CHAPTER 2 Rationale and Aims	18

CHAPTER 3	Results	20
	<i>An orthotopic xenotransplantation model of MB in an immuno-competent embryonic mouse</i>	20
	Human MB cells engraft and give rise to tumor-like masses wild type embryonic mouse brain	20
	Engrafted MB cells form a functional TME	23
	Human TXs are surrounded and infiltrated by the host immune cells	27
	<i>Validation of the neuron-like differentiation induced by a pool of 11 miRNAs in human cells</i>	29
	Validation of the pro-neural functions of 11 miRNAs in human iPSC-derived Neural Progenitor	29
	<i>Application of the in-utero MB model to assess the therapeutic efficacy of a pool of 11 miRNAs</i>	33
	Characterization of the tumor initiation upon in utero engraftment of MB pre-treated with 11 miRNAs <i>pool</i>	33
	In vivo proliferative capacity of DAOY cells is impaired upon the 11 miRNAs <i>pool</i> treatment	37
	Analysis of MB xenografts invasive patterns indicates mesenchymal-like transition	38
CHAPTER 4	Discussion & Conclusions	40
	Limitations and future perspective	45
CHAPTER 5	Experimental Procedures	46
	Human iPSC maintenance	46
	Human Neurons generation	46
	Human NPCs transfection and Neurite Outgrowth assay	46
	Animal care	47
	In utero transplantation	48
	BrdU labelling	48
	Immunofluorescence and imaging	48
	Immunocytofluorescence and imaging	49
	Image Analysis and Histological Measurements	50
	Maintenance and transfection of DAOY	51
	RNA extraction a real-time qPCR	51
	Statistical Analysis	52

ANNEX I. <i>In vitro</i> validation of the efficacy of the 11 miRNAs <i>pool</i> in a Medulloblastoma cell line	53
The 11 miRNAs <i>pool</i> transfection inhibits cell growth	53
Lower concentration of the treatment maintains the efficacy on cell growth	54
The 11 miRNAs <i>pool</i> induces pro-neural differentiation in vitro	55
The 11 miRNAs <i>pool</i> does not induce apoptosis in DAOY cells	57
REVIEWING PROCESS	58
<i>Reviewer #1 – Dr. Nereo Kalebic</i>	58
Author’s answer	59
<i>Reviewer 2 – Dr. Giancarlo Belenchi</i>	61
Author’s answer	61
REFERENCES	63

LIST OF TABLES

Table 1	- Genetic classification of Medulloblastoma subtypes	15
Table 2	- miRNA mimics used in the experiments.	47
Table 3	- List of Primary Antibodies used for Immunofluorescence in brain tissue samples.	49
Table 4	- List of Secondary Antibodies used for Immunofluorescence in brain tissue samples.	49
Table 5	- List of Primary Antibodies used for Immunocytofluorescence.	50
Table 6	- List of Secondary Antibodies used for Immunocytofluorescence.	50
Table 7	- List of primers used for qPCR.	52

LIST OF FIGURES

<i>Figure 1.1</i>	MiRNA biogenesis and functions.	3
<i>Figure 1.2</i>	Proposed mechanisms of action of miRNAs and their targets mRNAs.	4
<i>Figure 1.3</i>	Influence of miRNAs in cancer development, progression, invasion, and metastasis.	9
<i>Figure 1.4</i>	Schematic description of current methods for miRNA-based therapeutic approaches.	12
<i>Figure 1.5</i>	Cellular mechanisms of Cancer Stem Cells (CSCs).	13
<i>Figure 1.6</i>	Human MB integrate in brains of wt mice and maintain tumorigenic proliferation.	22
<i>Figure 3.2</i>	Tumor xenografts retain their human identity upon engraftment.	23
<i>Figure 3.3</i>	Functional TME surrounding the TX support perivascular CSCs niches.	25
<i>Figure 3.4</i>	Mature vasculature develops within engrafted MB tumors, contributing to the formation of a functional BBB.	26
<i>Figure 3.5</i>	TAMs are present and functional in the TME of TXs.	28
<i>Figure 3.6</i>	Human iPSCs Neuronal Differentiation and Characterization.	30
<i>Figure 3.7</i>	The effect of the <i>pool</i> of 11 miRNAs in human iPSCs correlates with a pro-neural differentiation phenotype observed in mouse cells.	32
<i>Figure 3.8</i>	Characterization of the MB xenograft model upon <i>in vitro</i> pre-treatment with the <i>pool</i> of 11 miRNAs.	36
<i>Figure 3.9</i>	The <i>pool</i> of 11 miRNAs reduced the number of proliferating cells in MB TXs.	38
<i>Figure 3.10</i>	TXs exhibit a morphological shift to a less invasive phenotype following treatment with the <i>pool</i> of 11 miRNAs.	39
<i>Fig. I. 1</i>	The 11 miRNAs <i>pool</i> reduces proliferation of human MB cell line.	54
<i>Fig. I. 2</i>	Titration of the 11 miRNAs <i>pool</i> .	55
<i>Fig. I. 3</i>	11 miRNAs <i>pool</i> stop cells in G0/G1 phase of cell cycle.	56
<i>Fig. I. 4</i>	The 11 miRNAs <i>pool</i> induces cancer stem cells neural differentiation <i>in vitro</i> .	56
<i>Fig. I. 5</i>	The 11 miRNAs <i>pool</i> does not induce apoptosis in MB cells.	57

LIST OF ABBREVIATIONS

ABC	ATP-binding cassette
AGO	Argonaute protein
ALDH	Aldehyde dehydrogenase
ATOH1	Atonal BHLH Transcription Factor 1
B7-H3	B7 homolog 3
BBB	Blood Brain Barrier
BCL6	B-cell lymphoma 6
BMP	Bone Morphogenetic Protein
BP	Basal Progenitor
BrdU	Bromodeoxyuridine
CAR-T	Chimeric Antigen Receptor T cell
CB	Cerebellum
CBFA	Core Binding Factor Alfa
cc	Corpus Callosum
CD133	Cluster Differentiation 133
CD31	Cluster Differentiation 31
CD68	Cluster Differentiation 68
Cdk	Cyclin-dependent kinase
c-miRNA	circulating-microRNA
c-Myc	cellular-Myc
CNS	Central Nervous System
cnt	control
CNU	Cerebral Nuclei
CpG	5'—C—phosphate—G—3'
CSC	Cancer Stem Cell
CSF	Cerebrospinal Fluid
Dcx	Doublecortin
DGCR8	DiGeorge Syndrome Critical Region 8
DIF	Day of differentiation
DMEM	Dulbecco's Modified Eagle Medium
DMSO	Dimethyl sulfoxide
E14.5	Embryonic stage 14.5
E18.5	Embryonic stage 18.5
E2F	E2 transcription factor
ECM	Extracellular Matrix
EF1 α	Elongation factor 1-alpha
EGFR	Epidermal growth factor receptor
EGL	External Granular Layer
EMT	Epithelial – Mesenchymal Transition
EPHA2	Ephrin type-A receptor 2
EV	Extracellular Vesicles
FACS	Fluorescence-Activated Cell Sorting
FAK	Focal adhesion kinase
FC	Frontal Cortex
FDA	Food and Drug Administration
FDM	Forebrain Differentiation Medium
FGF	Fibroblast Growth Factors
FMM	Forebrain Maturation Medium
FZD7	Frizzled-7
GalNac	N-acetylgalactosamine
GBM	Glioblastoma
GBX2	Gastrulation Brain Homeobox 2
GD2	Disialoganglioside

HB	Hind Brain
HDL	High-Density Lipoprotein
HER2	Human Epidermal growth factor Receptor 2
HIF	Hypoxia-inducible Factor
HIP	Hippocampal region
HuNu	Human Nuclei
IB	Inter Brain
IBA1	Ionized calcium-Binding Adapter molecule1
iPSC	Induced Pluripotent Stem Cell
IsO	Isthmic Organizer
KLF	Krüppel-Like Factor
KO	Knock out
LCA	Large Cell Anaplastic
Let-7	Lethal-7
LGE	Lateral Ganglionic Eminence
LNA	Locked Nucleic Acid
LSX	Lateral Septal Complex
LV	Lateral Ventricle
M	Mouse
MB	Medulloblastoma
MG	Microglia
MGE	Median Ganglionic Evidence
miRNA	Micro-RNA
MMP	Matrix Metalloproteinases
ncRNA	Noncoding RNA
NEC	Neural Epithelial Cells
NeuN	Neuronal nuclei
NGS	Next Generation Sequencing
NIM	Neural Induction Medium
NPC	Neural Progenitor Cell
NPM	Neural Proliferation Medium
nt	nucleotide
Oct4	Octamer-binding transcription factor 4
Otx2	Orthodenticle homeobox 2
p.t.	post transfection
p53	protein 53
P2	Post-natal day 2
P7	Post-natal day 7
Pax6	Paired box 6
PBS	Phosphate Buffered Saline
PBST	Phosphate Buffered Saline 0.1% Triton X-100
PD	Patient-Derived
PDOX	Patient-Derived Orthotopic Xenotransplantation
PECAM-1	Platelet Endothelial Cell Adhesion Molecule - 1
piRNA	Piwi-interacting RNA
PLO	Poly-L-Ornithine
pre-miRNA	Precursor microRNA
pri-miRNA	Primary microRNA
PTF1a	Pancreas associated Transcription Factor 1a
RG	Radial Glia
RISC	RNA-induced silencing complex
RL	Rhombic Lip
ROI	Region Of Interest
scr	Scramble
scRNA-seq	Single-Cell RNA sequencing
SFRP	Secreted Frizzled-Related Protein 4

SHH	Sonic Hedgehog
siRNA	Short-interfering RNA
SIRT-1	Sirtuin-1
Sox2	Sex determining region Y-box 2
Sox9	SRY-box transcription factor 9
STRd	Dorsal Striatum
SVZ	Sub-Ventricular Zone
TAM	Tumor-Associated Macrophages
Tbr2	T-box brain protein 2
TGF- β	Transforming Growth Factor beta
TLR	Toll-Like Receptors
TLX	homologue of the Drosophila tailless gene
TME	Tumor Microenvironment
TMem119	Transmembrane Protein 119
TsmiR	Tumor suppressor microRNA
TWIST	Twist-related protein 1
TX	Tumor Xeno-engraftment
UTR	Untranslated Region
VEGF	Vascular Endothelial Growth Factor
VZ	Ventricular Zone
Wnt	Wingless-related integration site
wt	wild type
XPO-5	Exportin-5
ZEB	Zinc finger E-box-binding homeobox
ZO	Zona Occludens

ABSTRACT

Accurate pre-clinical models of human cancer are essential for basic and translational research. The undeniable necessity of such models clashes with the reality of their ineffectiveness to replicate the context where human tumors form. Here is presented a new mouse model for human Medulloblastoma (MB) disease, a pediatric brain tumor with high incidence and frequent lethal recurrences, for which conventional treatments often cause lifelong drawbacks.

By leveraging the “immune-privileged” embryonic developmental time window, orthotopic xenotransplantation of human MB cells were successfully engrafted in immune-competent mice. The xenotransplants integrated into the host brain, reconstituting several tumor microenvironment characteristics by demonstrating infiltration, vascularization, and immune cell infiltration. Second, aimed to respond to the urgencies of new therapies, the MB model was here used to assess the efficacy of a *pool* of 11 microRNAs (miRNAs) that has been previously described to induce neuro-differentiation in neural progenitor populations. Non-coding RNAs play a fundamental role in cancer, with miRNAs occupying the frontlines being capable of either hijack or suppress tumor biology. Effective therapies cannot be devised if developed within a flawed system. We find that the engrafted MB tumors are responsive to the 11-miRNA *pool* pre-treatment, exhibiting reduced tumor proliferation and infiltrative-like features.

The approach here described enables the study of human MB formation and biology under conditions resembling its physiopathology, specifically in an embryonic and immune-competent environment. This mouse model can serve as platform to study efficacy of therapies, here demonstrated by means of miRNAs, offering significant opportunities for neuro-oncological research.

CHAPTER 1 Introduction

From Biogenesis to Biological Significance of microRNAs in mammalian Cancer and Central Nervous System

MicroRNAs are a class of small, non-coding RNA (ncRNA) molecules endogenously expressed as a single-strand that regulate the expression of the majority of the mammalian mRNAs⁸⁸. The length of miRNAs is approximately 23 nucleotides (nt)¹⁶⁴, which differentiate them from other small non-coding RNAs (i.e. piRNA, siRNA)¹¹⁷. miRNAs stand as the pioneers of small ncRNA discovery, having been first identified in 1993 by the Ambros group¹⁶⁴, and the subsequent discovery of their high conservation^{210,253} (with miRNA now recognized from the Bacteria kingdom^{40,2,335}) has prompted the formulation of hypotheses regarding the substantial roles these molecules have played in the evolution, leading to the finding of miRNAs as important post-transcriptional regulators of expressed transcripts^{6162,320,137}. The recognition of the cognate sequence relies on the “seed sequence” of the miRNA, a region situated a position 2-7 nt from the miRNA 5'-end, that controls miRNA binding to the target and the functional specificity^{167,88}. The gene-repressive functions of a miRNA are supported by the RNA-induced silencing complex (RISC), which guides the miRNA to its target mRNA through complementary base pairing. Once the miRNA is bound to its target mRNA, the RISC complex can initiate the process that leads to the inhibition of the translational machinery²⁴⁰ or degradation of the transcript¹³⁸. The choice between the two mechanisms hinges on the quality of binding between the target sequence and the miRNA, whether perfect or imperfect. In Metazoans, imperfect binding is prevalent^{254,18,118}, resulting in ribosomal stalling and subsequent release of the transcript, followed by its degradation. Additionally, alternative mechanisms have been identified, including direct cleavage or destabilization of mRNA^{254,152}, interference with ribosome function^{227,240,235,311}, and direct degradation of mRNA or the protein^{240,235}. In rare instances, inhibition also occurs through chromatin remodeling¹⁵². These discoveries were adeptly modeled mathematically in the systematic review conducted by Morozova in 2012²⁰⁹.

To understand the principles governing the function of miRNAs, comprehension of their *biogenesis* is crucial, as each phase significantly influences the specificity and effectiveness of the functional molecule (*Figure 1.1*). This aspect has fundamental importance in the development of therapeutic strategies that exploit these genetic tools, a concept that will be later discussed in detail. Primary miRNAs transcripts originate approximately equally from intergenic regions, being transcribed from autonomous genes¹⁶⁴ and from intragenic regions (mostly, introns)²⁶¹. The initial step in miRNA biogenesis entails the transcriptional process of RNA polymerase II^{36,164}, though a smaller fraction is transcribed by RNA polymerase III¹¹⁷. Transcription results in a long primary transcript known as *pri-miRNA*, characterized by a single-hairpin structure of about 80 nts. It is relatively common that miRNA can be derived from a polycistronic transcript, containing miRNA genes placed contiguously and generally defined as a cluster¹⁸. At this point, the maturation can proceed along two pathways: the *Canonical*, involving miRNA originating from intergenic regions, and the *Non-Canonical*, with the maturation of the miRtrons (intergenic origin).

MiRNA biogenesis: Canonical and Non-Canonical pathways

The primary mechanism for miRNA maturation is the canonical pathway²²². This mechanism involves the recognition of the pri-miRNA by the nuclear Microprocessor complex, DGCR8, and DROSHA (an RNase III enzyme). DGCR8 recruits DROSHA, guiding it to accurately cleave the stem-loop of the pri-miRNA. The miRNA precursor (*pre-miRNA*), of approximately 70 nts, is then released. Recognition by EXPORTIN-5 (XPO-5) and the GTPase-dependent protein Ran permits pre-miRNA to be transported to the cytosol. Here, the RNase-III DICER recognizes and cleaves the stem-loop of the pre-miRNA. The resulting duplex is then stabilized by AGO protein binding, and later assembled in the RISC complex. The strand loaded into AGO is defined as the *guide strand*, while the other, the *passenger strand*, is eventually degraded. Within the RISC complex, only one strand of the duplex is incorporated. Determination of which strand is selected relies on the thermodynamic stability at the 5' end of the miRNA duplex or the presence of 5' uracil at nucleotide position 1^{273,135}. This discrepancy is correlated to the cellular context and results in a strand bias with significant biological implications^{273,205,222,200}. Non-canonical biogenesis entails distinct maturation pathways, typically bypassing one or more steps of the more conventional one²²². These pathways can be categorized into Drosha/DGCR8-independent and Dicer-independent. A primary example of Drosha-independent generation of pre-miRNA are the miRtrons²⁰⁰ derived from mRNA introns during splicing. It is interesting to note that no miRtron has been identified as shared among the phyla of worms and the Mammalian and flies classes¹. The identification of hundreds of new mirtrons implies that, collectively, these molecules play a substantial role in gene silencing and evolution.

Although the above mechanisms account for the biogenesis of the majority of mammalian miRNAs, several exceptions were reported, such as Dicer-independent miRNAs, which are processed by Drosha from endogenous transcripts of short-hairpin RNA⁵⁰. Since their length is insufficient to be a Dicer substrate because they lack the microprocessor-binding sequence, these miRNAs necessitate Ago2 for trimming, completing the maturation process²²².

Annotation of microRNAs

The fundamental rules in the nomenclature of miRNAs, as outlined by Ambros et al.⁶, are here provided for ease in comprehension of subsequent parts of the text:

- The mature form of the miRNA product is denoted as "miR," followed by a hyphen and a number, determined by the historical order of discovery (i.e., miR-124 was identified and annotated before miR-425)
- Gene locus, pri-miRNA and pre-miRNA are collectively referred to as "mir"
- miRNAs that differ by a few nucleotides are annotated with a lowercase letter after the identification number. Example:

hsa-mir-15a	UAGCAGCACAU AA UGGUUU GUG
hsa-mir-15b	UAGCAGCACAU CA UGGUUU ACA

- Each miRNA should be preceded by three letters specific for each species, such as:

hsa-mir-376	belongs to <i>Homo sapiens</i>
mmu-mir-376	belongs to <i>Mus musculus</i>

- If two distinct loci produce identical mature products, an additional number is added after the full name. For instance, hsa-mir-515-1 and hsa-mir-515-2 are distinct miRNA genes that produce the same mature miRNA product.
- A suffix to the name indicates from which dsRNA the mature sequence originates. Examples:
 - hsa-mir-1228-5p from the 5' arm of the pre-miRNA
 - hsa-mir-1228-3p from the 3' arm of the pre-miRNA
- Clusters of miRNAs are generally indicated by the full name of the first miRNA composing the group, followed by a dash and the number identifying the last member. Example: miR-17 – 92

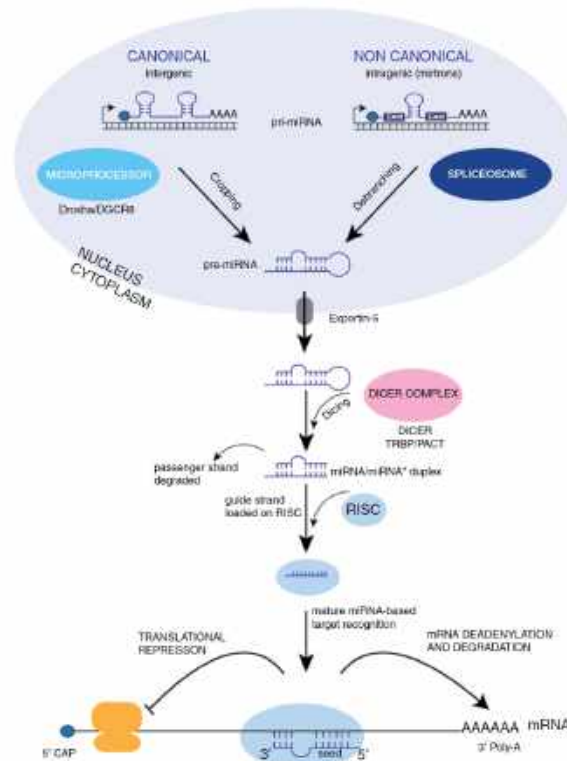


Figure 1.1 - miRNA biogenesis and functions. MicroRNAs (miRNAs) are initially transcribed as long, hairpin-containing precursor molecules known as primary miRNAs (pri-miRNAs). miRNAs that are encoded by their own genes and transcribed by RNA polymerase II as independent transcripts follow the canonical biogenesis pathway. In contrast, miRNAs that are encoded within introns of host genes, termed mirtrons, are transcribed along with their host genes and undergo a non-canonical biogenesis pathway. In the canonical miRNA biogenesis pathway, primary miRNAs (pri-miRNAs) are cleaved (cropping) by the microprocessor complex, composed of Drosha and DGCR8, to generate hairpin-shaped pre-miRNAs. In contrast, miRNA precursors in the non-canonical miRNA biogenesis pathway are processed (debranching) by the spliceosome complex to yield mature miRNAs. After being processed into pre-miRNAs, exportin-5 transports pre-miRNAs into the cytoplasm where the ribonuclease protein Dicer (dicing) further processes them into 18–22 nt duplexes. The mature miRNA is then incorporated into protein complexes called “RNA-induced silencing complexes” (RISC), where it exerts its gene-regulatory function by targeting specific mRNAs. The strand loaded into RISC complex is referred to as the guide strand, while the second passenger strand, is typically degraded, but in certain miRNAs, both strands are incorporated into RISC, leading to the formation of miR-“star” (miR-^{*}). In mammals, RISC-loaded miRNAs engage in imperfect base-pairing interactions with target mRNAs. Target specificity is dictated by the seed region of the miRNA, a sequence 6–8 nucleotides at the 5' end of the miRNA, which guides the binding site of miRNAs to any region of the target mRNA (i.e. 5' UTR, 3' UTR, or coding region). MicroRNAs utilize a range of mechanisms, such as ribosomal stalling, direct cleavage or destabilization of mRNA, and interference with ribosome binding, to effectively regulate their target expression. Each microRNA has the potential to interfere with hundreds of target mRNAs, while a single mRNA target can be modulated by multiple microRNAs in a synergistic manner^{242,170}. This convoluted regulatory network enables microRNAs to integrate diverse intracellular signals and regulate numerous signaling pathways. Adapted from de Luca et al., 2017¹⁸².

The functions of miRNAs in cell fate: pathological implications and therapeutic opportunities for brain cancer

NGS technologies ignited the era of miRNome studies, fostering transformative discoveries in basic research and application for personalized medicine²⁷⁴. There are around 2,300 mature miRNAs expressed in *H. sapiens*, as reported in miRBase (v.22)¹⁵⁶. It has been estimated that miRNAs play a role in the post-transcriptional regulation of at least 60% of all protein-coding genes¹⁷⁰, suggesting that the entire coding genome is likely under the influence of miRNAs. The human miRNome is organized into gene regulatory networks of greater complexity than previously thought. Indeed, miRNAs can act synergistically which means they can work together to produce an effect that would not be possible if they acted alone^{17,70,242,222}. miRNA targets have the capacity to regulate the expression of tens to hundreds of mRNAs, with several miRNAs potentially overseeing a single mRNA (Figure 1.2). Thanks to their complex functional programs, miRNAs influence key biological processes such as cell cycle^{49,311,202}, immune response^{154,214,217}, and cellular homeostasis^{7,97}. In essence, miRNAs are among the major effectors defining the boundary between physiological and pathological states^{7,256,214,70,97,145}.

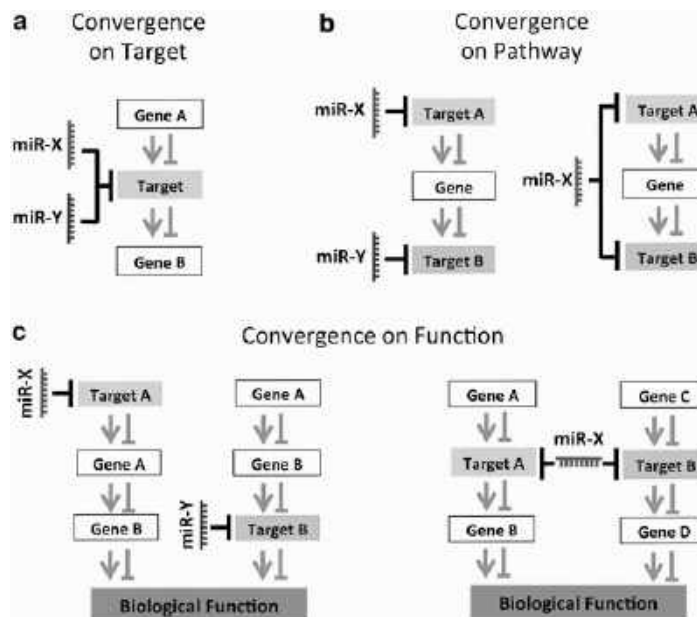


Figure 1.2 - Proposed mechanisms of action of miRNAs and their targets mRNAs. MiRNAs may cooperate in modulating several intrinsic and extrinsic signals. Among the demonstrated models can be find: (a) convergence on target, a single target is modulated by one or several co-expressed miRNAs; (b) convergence on pathway, more than a miRNA regulates multiple targets involved in the same molecular pathway; (c) convergence on function, multiple miRNAs define a network able to regulate coding genes with overlapping biological functions, or single miRNA controls different effectors of the same biological program. Adapted from Barca-Mayo et al., 2014¹⁷.

miRNA in Neurodevelopment

During embryogenesis, miRNAs are very abundant and exhibit specific spatial and temporal expression patterns in the developing central nervous system (CNS)^{144,276,288,17,346,282}, making them potential regulators of CNS development, maintenance and pathological processes³⁹. While the importance of miRNAs in brain development is recognized, the precise mechanisms of their influence remain unclear, as most studies lack thorough biological validation beyond predicted targets. This chapter explores fundamental neuronal development processes. Examples of the role of miRNAs in neurodevelopment and differentiation will follow.

Cornerstones of CNS development

The intricate development of the central nervous system (CNS) is initiated by the neural induction process, in which the interplay of Fibroblast Growth Factor (FGF) signaling, in particular FGF8, and the suppression of bone morphogenetic protein (BMP)^{290,173,271}, culminate in establishing the *neural plate*. During the process of neurulation, neural plate cells rearrange and give rise to the neural tube, the precursor structure of the CNS in mammals^{168,287}. This structure is composed of neuroepithelial cells (NEC) that undergo symmetric proliferative divisions to expand their pool before initiating the *neurogenesis*: asymmetric divisions generates a daughter NEC plus a differentiated cell, which can be a more committed progenitor cell or a neuron^{64,250}. The neural progenitor cells, the Radial Glia (RG) and Basal Progenitors (BP) progressively reduce the symmetric divisions and increase the asymmetric neurogenic divisions. This phase culminates in the generation of postmitotic neurons¹¹⁰. Later, neurons migrate from the germinative layers, the ventricular zone (VZ) and, in the telencephalon, the subventricular zone (SVZ) to their final destinations, where they will organize the different structures composing the CNS. In fact, here the neurons extend neurites (axons and dendrites) that form functional neural circuits²¹⁵. This process occurs within weeks in rodents but can take months in humans. The cerebral cortex develops from the telencephalon, the foremost region of the neural tube. During embryonic development, cell proliferation and differentiation events forge the final cortical architecture, a laminar structure with 6 layers (labeled, from the most surface-level to the deepest, I, II/III, IV, V, VI). The laminar organization is obtained by radial migration, and accumulates in an inside-out pattern^{193,148}. Each cortical layer contains neurons that have a lamina-specific projection pattern²⁵², therefore deep layer neurons project out of the cortex, whereas superficial layers contain neurons that form corticocortical projections^{252,148}.

miRNA in CNS development

Epigenetic mechanisms and miRNAs regulate neurogenesis as well as the neuronal differentiation and further maintain their proper functions³²⁸. MiRNAs also play an influential role in the wiring of brain network, as miR-218 that was recently correlated with the definition of hippocampal connection³⁰⁰.

Additionally, miRNAs' emerging roles in neurogenesis impact our understanding of nervous system evolution. The positive correlation between miRNA genes count and organismal complexity, particularly in cortex-dependent cognitive abilities, suggests that recently evolved miRNAs might contribute to higher cognitive functions in primates through neurogenesis regulation. The axis between miRNAs and NS was firstly postulated through experiments disrupting miRNA biogenesis factors like Dicer1^{20,62,239,151}. These studies demonstrated that functions of miRNAs in cortical development are time- and tissue-specific^{204,219,17,185}. The effects of miRNAs

on protective or disease-promoting function are the same as those seen in cancer (discussed in later sections). Loss- or gain-of-function experiments of specific miRNAs lead to these conclusions. The miR-17-92 family was shown to be essential for embryonic cell development^{292,306}, neural progenitor cell proliferation⁵³, axonal growth³⁴⁰ and the transition to intermediate progenitors²². Knock-out experiments revealed T-brain gene 2 (Tbr2; a key regulator of neurogenesis in the SVZ) is a target of the miR-17 – 92 cluster, resulting in suppression of cortical radial glial cells and expansion of the progenitor population²². miR-124, the brain's most abundant miRNA, plays a crucial role in neurogenesis. It gradually increases during neuronal differentiation to reach the peak in mature neurons^{157,192,48,267,4}. It was demonstrated, by manipulation in the level of miR-124, the involvement in adult neurogenesis (targeting Sox9)¹⁷⁷, neurogenesis and neural fate specification^{286,157,4}, and in axon growth¹²⁵. Like miR-124, also miR-9 is enriched in brain and controls neural stem cell numbers^{65,55} and the balance between neural stem cell renewal and differentiation³⁴¹. Moreover, miR-9 was shown to regulate neuronal migration and outgrowth⁵² as well as neural fate through epigenetic alterations that are able to convert fibroblasts into neurons^{331,247,328}. Important to note, miR-9 expression restricts the pool of neural progenitors in the boundary dividing midbrain and hindbrain¹⁶⁵. The diverse effects of miRNAs could be united through their convergence on TLX, a well-known upstream activator of the Wnt signaling pathway^{247,328}. This pathway's downstream effector, cyclin D1, is a key regulator of cell proliferation²⁸⁰. miR-137 is another relevant example of how TLX modulation can interfere in neuronal cell-specification³³⁰. Doublecortin (Dcx) is a well-known gene directly affecting neuronal migration²⁴¹. Levels of Dcx are influenced by miRNAs indirectly, through the inhibition of REST complex (miR-124 is a valid example)³⁰⁹ or directly, as for miR-134⁹⁴. Notably, miR-134 is located within the miR-379 – 410 miRNAs family, the largest known mammalian-specific miRNA cluster (which includes miR-134 and miR-376)¹⁵⁹.

The roles of miRNAs in Cancer

In cancer research, miRNAs were classically divided into two different categories¹⁷² based on their expression: i) miRNAs that act as oncogenes – *oncomiR*, and ii) miRNAs that act as *tumor suppressor miRNAs* (TsmiRs)^{38,119,305,263,108}. Genome-wide investigations revealed that many miRNA genes are located in regions harboring cancer-associated genomic regions^{334,105}. Interestingly to note, half of human miRNAs are localized in fragile chromosomal regions associated with chromosomal mutations causing tumor development¹⁷². Moreover, cancer-related genes are more frequently targeted by miRNAs compared to other classes of disease genes. The exact reason for this higher susceptibility of cancer genes to miRNAs remains unknown^{119,70,263}. Cancer-associated regions become oncogenic or tumor-suppressive depending on whether these regions are compromised by structural/functional amplifications (enhancing their tumorigenic potential) or maintained in their protective purpose. This relationship represents the fundamental framework on which the link between miRNAs and cancer relies. The first pioneering research connecting miRNA and cancer was performed by Croce's lab³⁸. This work has opened a field of investigation that is far from being concluded. Several studies have shown that miRNAs expression is tightly controlled by different transcription factors, so the abnormal expression of miRNAs in cancer could be due to dysregulation of some key transcription factors such as c-Myc⁹⁵ and p53²²³. The c-Myc transcription factor, famous for its oncogenic role, can induce the activation of the miRNA

cluster miR-17 – 92, playing as an oncomir, while suppressing the activation of the tumor suppressor miRNA let-7¹⁴³. The p53 protein functions as a tumor suppressor and is often inactivated in many cancer types. The p53 – miR-34 axis exemplifies how a transcription factor regulates miRNA expression to execute tumor-suppressive functions. Mendell and colleagues⁴⁴ demonstrated that p53 can stimulate the expression of miR-34a, which is known to promote cell-cycle arrest, cell senescence, and apoptosis. This, in turn, establishes a positive feedback loop by targeting SIRT1, a negative regulator of p53. Beyond c-Myc and p53, additional transcription factors have been identified as components of a mini-circuitry that controls miRNAs expression^{79,89}. Therefore, miRNA production is intricately regulated by multiple factors to maintain normal transcription, and any dysregulation in this process can lead to tumorigenesis. Other factors that are recognized to be linked with cancer are epigenetic alterations. There is a belief that miRNAs can undergo epigenetic modulation analogous to protein-coding genes²⁶⁶. The research group led by Nervi demonstrated how CpG methylation could impede the expression of miR-223⁹⁰. In the case of miR-127, which is also situated on a CpG island, a significant increase in expression was observed following treatment with DNA methylation and histone acetylation inhibitors. This upregulation was accompanied by the downregulation of the proto-oncogene BCL6⁴⁵. Similarly, decreased expressions of miR-124a is attributed to DNA hypermethylation in breast, lung, and colon carcinomas, respectively⁹⁰. The above evidence highlighted the role of epigenetic regulation in miRNA expression during tumorigenesis, implying that aberrant DNA methylation and histone acetylation of miRNA genes could serve as useful biomarkers for cancer diagnosis and prognosis.

miRNAs and Cancer Proliferation

One of the most emblematic features of cancers is abnormal cell proliferation. Deviance from the normal balance between cell proliferation and inhibition is the primary source of tumorigenesis. It recently came out how miRNAs are profoundly interlaced with pathways of cellular proliferation, thus being responsible for tumorigenesis initiation. E2F proteins are critical regulators of cell proliferation, and their expression is regulated by miRNAs^{113,321}. A member of this protein family, E2F1, induces target gene transcription during the G1 to S transition. Normally, miR-17 – 92 cluster controls the levels of E2F while the other components of E2F family (E2F2 and E2F3) in turn induces the expression of the cluster, creating a feedback system that controls the cell-cycle progression. In cancers, c-Myc is known to induce the overexpression of both E2F2 and miR-17 – 92, to exploit the cluster function to disrupt the feedback loop and eventually promote cell proliferation^{124,223}. Recently, it was shown that the expression levels of MYC/E2F/miR-17 – 92 network highly correlates with the progression of childhood malignant tumors of NS, being particularly high in medulloblastomas cancers¹¹³. The cell-cycle depends on cyclins, cyclin-dependent kinases (Cdks), and respective inhibitors, components regulated by miRNAs. Dicer-1 KO mutant of *D. melanogaster* germline stem cells are unable to proceed from G1 to S phase¹²³. In glioblastoma, p27^{Kip1} (Cdk inhibitor) is the target of miR-221/222²⁴⁸, and ectopic expression of miR-221/222 stimulated cell proliferation¹⁰³ establishing a causal link between miR-222/221 and tumorigenesis. Moreover, other studies reported the relation of miRNA to cancerous pathways by acting as modulator of Cdk and cyclin expression⁷⁵.

miRNA and Apoptosis

Tumor cells employ various tactics to restrict or bypass apoptosis, with the most prevalent approach being the impairment of the p53 tumor suppressor function. The reciprocal regulation between miRNAs and p53 has been proven by showing the presence of precise mechanisms involving miRNA to induce the activation of p53 directly or indirectly so that p53 acts as an effector to reduce the sensitivity of cells to apoptosis^{28,44,82}. Direct inhibition of proapoptotic factors was seen in ovarian and glioblastoma cancers^{68,5}, enhancing the relevance of miRNAs on the apoptotic activity and, as a result, in cell death.

miRNA and Angiogenesis

Angiogenesis is the process wherein new blood vessels emerge to meet the increased nutritional and oxygen requirements associated with tumorigenesis¹⁶⁶. Vascular endothelial growth factor (VEGF) is the reference angiogenic factor guiding endothelial cells to construct new vessels upon binding to its receptors⁸³. In the tumor microenvironment (TME), characterized by significantly lower oxygen levels than adjacent normal tissues, hypoxia assumes a critical role. Hypoxia-inducible factor (HIF) serves as the fundamental transcription factor responding to hypoxia¹⁵⁰ and influencing, among other genes, the expression of miRNAs. In this scenario, miRNAs targeting the HIF or VEGF signaling pathways are expected to exert a substantial influence on angiogenesis. For instance, miR-210 and miR-21 were correlated with hypoxia and sustainment of angiogenesis in association with the expression of VEGF^{175,264}. Additionally, miR-424 is induced by hypoxia in endothelial cells, facilitating angiogenesis both *in vitro* and *in vivo* by transcriptionally activating downstream VEGF expression¹⁰⁸. Claudins maintain the selective permeability of vascular endothelial cells, and in the particular case of the blood brain barrier (BBB), Claudin-5 represents the most present tight-junction protein^{112,343}. Deregulation of claudin and other tight junction proteins, e.g. occludin, and zona occludens (ZO) has been reported to link with tumor-specific phenotype in cancer cells²²⁶. Several miRNAs function as modulators of tight junction-related proteins such as KLF2/4 (Krüppel-Like Factor 2), a direct target of miR-25-3p that relocates in vascular endothelial cells upon miRNAs activation. This cluster is also implicated in the regulation of VEGFR2, ZO-1, occludin, and claudin 5, resulting in angiogenesis³³³. Jia and collaborators¹⁸⁷ performed the first proof-of-concept experiment revealing that the overexpression of Claudin-5 does alter the expression of several miRNAs, including miR-127, a well-known tumor suppressor in several human cancer^{313,304}. These studies, along with abundant evidence^{319,32,12,108}, affirm the complex regulation of angiogenesis by miRNAs.

miRNA and EMT

Epithelial–mesenchymal transition (EMT) can be considered as the pivot stage in metastatic cancer progression. Metastasis is the series of dynamic biological events characterized by the loss of cell adhesion, through the suppression of E-cadherin, and the activation of genes linked to motility and invasion. ZEB, SNAIL and TWIST are the main transcription factors involved in the activation of the metastatic cascade^{149,277}. miRNAs play a role also in the EMT and cancer metastatic phenotype²¹¹. This characteristic is linked to an increase in N-cadherin, a family of cell adhesion molecules, and vimentin, a type III intermediate filament protein that is a key component of the cell's cytoskeleton^{268,178}. Transforming Growth Factor- β (TGF- β), the master activator of ZEB, SNAIL, and TWIST transcription factors, is in turn regulated by miRNAs. miR-21/miR-31, miR-155, miR-

29a were causatively correlated to the acquisition of EMT behaviour in colorectal¹⁵⁸, cervical and human cancers^{153,98,234}. Experimental validation reported that overexpression of individual miRNAs can contribute to metastatic phenotype. The work of Ma and colleagues showed that miR-10b, highly expressed in metastatic breast cancer cells, induces invasion by promoting aggressive invasion in an *in vivo* immune-deficient mouse model¹⁸⁶. They also demonstrated that the expression level of miR-9 impairs the expression of E-cadherin. This is in line with the evidence that use of a miRNA 'sponge' targeting miR-9 reduces metastasis formation in the animal model, suggesting a therapeutic target. In contrast to the work of Ma and colleagues, it was observed that miR-9 suppresses MMP-14 expression by binding to the site in the 3'-UTR, consequently inhibiting the invasion, metastasis, and angiogenesis of the tumor cells³³⁶. This represents a significant example of how the cause-effect relationship can change depending on the context when dealing with miRNAs. Another notable illustrations of miRNAs as protectors against the EMT, is the miR-200 family²⁰⁷. These class of miRNAs are downregulated by TGF- β , and showed to inhibit the expression of ZEB1 and ZEB2 and, the demonstration of a negative feedback loop in which miR-200 primary transcript is also repressed by ZEB1 and ZEB2, reinforces the hypothesis of miR-200 as regulator in highly invasive breast cancer cells⁷⁶. The promoter of miR-203 is hypermethylated in highly metastatic breast cancer cells, and it was reported to inhibit tumor cell invasion *in vitro* and lung metastatic colonization *in vivo*⁷². Another significant aspect of the EMT is its association with chemoresistance, as demonstrated by Fischer in 2015⁸⁶. Counterintuitively, chemotherapy was followed by occurrence of lung metastasis by EMT cells. This phenomenon was linked to the overexpression of chemoresistance-genes. However, the overexpression of miR-200 successfully counteracted the resistance. Thus, EMT is involved in drug resistance and miRNAs could potentially counteract insensitivity of cancer cells to drugs. This concept, intimately linked to Cancer Stem Cells (CSCs), will be further explored in the section *Cancer Stem Cells: a new therapeutic target*.

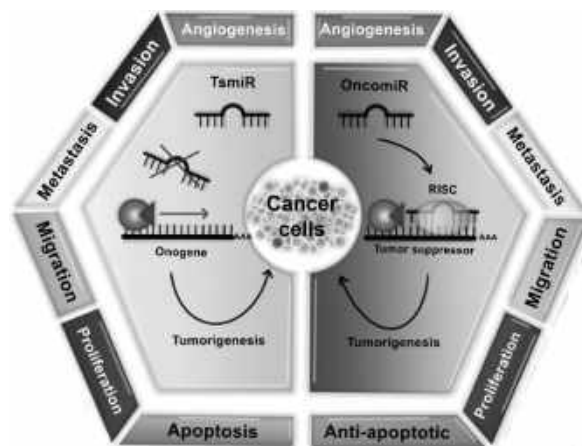


Figure 1.3 - Influence of miRNAs in cancer development, progression, invasion, and metastasis. A subset of miRNAs, classified as tumor-suppressive miRNAs (TsmiR) show reduced expression levels in cancer cells, while certain miRNAs (onco-miRs), exhibit increased expression in cancer cells and contribute to their proliferation, angiogenesis, invasion, and metastasis^{38,172,108}. The intricate mechanisms of action characteristic of miRNAs underlie the consequences of their deregulation. Reintroduction of tumor-suppressive miRNAs into cancer cells inhibits proliferation, induces apoptosis, reduces invasion and angiogenesis, and promotes cancer regression. Thus, therapeutic strategies targeting deregulated miRNAs could reprogram cancer cells to self-destruct or sensitize them to conventional therapies by liberating target genes from miRNA-mediated suppression^{91,70}. Adapted from Nurzadeh et al., 2021²²¹.

Theragnostic role of miRNAs in cancer medicine

So far, miRNAs have shown a role in various aspects of cancer. One opportunity, partially addressed by the emergence of NGS technologies, involves profiling miRNAs pathways. This process can aid clinicians in the use of miRNAs for predictive and therapeutic strategies. Their disease-specific nature and ability to serve as early indicators of disease make miRNAs a gold mine for cancer diagnosis and treatment. The following paragraph provides examples of how knowledge about miRNAs has been applied in the clinic, both for prognostic and therapeutic purposes. These examples were selected from the most relevant studies for their innovation and potential impact on clinical practice.

Diagnosis and prognosis

Liquid biopsies have revolutionized disease detection, monitoring, and personalized treatment, offering convenient alternative to traditional biopsies are impractical due to invasiveness or unavailability⁷⁰. Requiring small blood or liquor samples, liquid biopsies are more tolerable and quicker than surgical biopsies. This potential has held promises for cancer detection before emerging of clinical symptoms, as early diagnosis remains the critical step for a timely intervention and positive outcome. The detection of miRNAs in body fluids, known as *circulating miRNAs* (c-miRNAs), has emerged as a promising tool for cancer diagnosis and monitoring. Indeed, c-miRNA were proven to be more stable to conditions that normally degrade other RNAs (i.e. temperatures, pH, and RNase enzymes)¹⁹¹, probably because they are associated with extracellular vesicles (EVs) and RNA-binding proteins, such as Ago2 and HDL. Therefore, c-miRNA represents a non-invasive alternative for clinicians and patients, making them ideally suited for longitudinal and retrospective studies^{35,317}. Lu and colleagues were the first to report the use of a bead-based miRNA profiling method to evaluate the levels in normal and tumor tissues. The work revealed that distinct miRNAs expression patterns not only distinguish tumor origin but also determine the degree of differentiation and enable the classification of poorly differentiated tumor tissues¹⁷⁹. Several studies further identified miRNA signatures that can accurately diagnose specific cancer types. For instance, the use of a different subset of miRNAs was reported to specifically distinguish between tumoral and normal tissues for breast and hepatocellular carcinoma^{180,322}.

Biomarkers able to analyze the situation of each individual are also extremely useful to stratify the patient's cohort. In lung cancer, downregulation of let-7 in lung cancer tissues correlates with higher disease stages and poorer patient survival²⁹⁶. In 2011, Costa et al. utilized TaqMan Low Density Arrays to evaluate the expression of 365 miRNAs in ependymomas and normal brain tissue⁵⁷. They described the connection between the expression of specific miRNAs (let-7d, miR-596 and miR-367) that correlate with better prognosis. miR-448 and miR-383 were also identified to act as tumor suppressors in various cancers, including glioma³²³ and medulloblastoma¹⁶⁹. Due to the complexity of the underlying mechanisms driving cancer, the effectiveness of a singular treatment can vary, depending on the patient and the specific type of cancer. miRNAs are effective for therapeutic outcome prediction. The work of Costa et al.⁵⁷ found three miRNAs that successfully predicted the outcome upon EGFR monoclonal antibody therapy in colorectal cancer patients.

Therapy

The dual nature of miRNAs, functioning as oncogenes or tumor suppressors, offer two distinct approaches for miRNA-targeted therapy (Figure 1.4):

- Reduce the expression of oncomiRNAs, using miRNA inhibitors, mainly antisense oligonucleotides, or *sponge*³³⁸.
- Restore TSmRNAs expression by gene therapy or administration of synthetic mimics.

Use of miRNAs mimics as therapeutic has held promise for cancer treatment since their first study, in which miR-15/16 demonstrated efficacy in malignant pleural mesothelioma^{38,251}. In case of brain tumors, administration of miR-335 mimics to malignant astrocytoma cells resulted in growth arrest, reduced cell apoptosis, diminished invasiveness, and significant regression of astrocytoma xenografts²⁸¹. In gliomas, miR-381 has been shown to decrease cell proliferation and tumor growth²⁹⁷. Additionally, a miR-10b inhibitor is in the safety and dose escalation phase for glioblastoma treatment⁹⁶.

Despite promising preclinical results, miRNA therapeutics face significant hurdles in clinical translation, primarily due to the challenges associated with delivering miRNA mimetic/inhibitor molecules. One issue is, for example, the nuclease degradation in the extracellular space. Chemical modification of mimics has been proposed and accepted from Food and Drug Administration (FDA)¹³¹, but chemically modified miRNAs struggle to target tumor sites *in vivo*. Moreover, chemical modification might prevent the recognition of miRNA mimics by the maturation machinery. Covalent conjugation of specific moieties to miRNA mimics or inhibitors enhances their tissue-specific uptake, improving their therapeutic efficacy. Examples of such moieties include peptides, antibodies, aptamers, and sugars. One example is the N-acetylgalactosamine (GalNAc)-conjugated miR-122 exhibited ligand-specificity against the Asialoglycoprotein receptor of the hepatocytes⁶³. A clinical trial using Cobomarsen, a single strand oligonucleotide chemically modified²⁷⁸, reported the case of a treated patient of T-lymphoma whose tumor masses reduced significantly with no side effects. Packaging miRNA mimics or inhibitors in nanoparticles can improve uptake efficiency. Still, liposome nanoparticles are limited by their size and the lack of large extracellular spaces in solid tumors restricts liposomes uptake. A nanoparticle formulation of miR-10b is currently undergoing a dose escalation phase for breast cancer treatment (Patent of Transcode Therapeutics Inc.). Another approach leverages the unique characteristics of TME. MRX34, miR-34 mimic encapsulated in liposome nanoparticles utilizes this strategy (ClinicalTrials.gov, NCT01829971). In the acidic TME, MRX34 liposomes become positively charged, enabling them to adhere to negatively charged tumor cells via electrostatic interactions. While initial results are promising, data on target gene efficacy in various solid tumors is lacking, suggesting challenges in delivering miRNA mimics to tumors¹³³. Among these events, a strong immune-response was reported for two patients, highlighting the need for careful assessment of potential toxicities⁶⁰. In fact, innate immune responses triggered by exogenous RNA poses another challenge to miRNA therapeutics. Modifying nucleic acid drugs with chemical moieties like the 2'-O-methyl group can help mitigate TLR-mediated immune activation.

The effective delivery of miRNA therapeutics remains a critical challenge, preventing their widespread use in cancer treatment. As a result, no miRNA-based therapy has yet gained clinical approval.

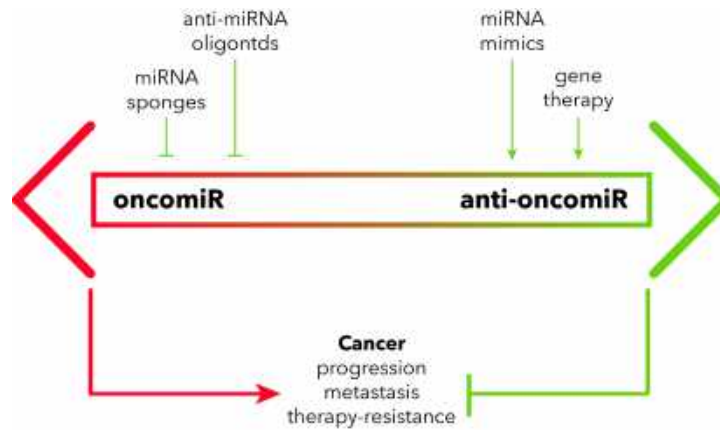


Figure 1.4 - Schematic description of current methods for miRNA-based therapeutic approaches.

Cancer Stem Cells: a new therapeutic target

Cancer stem cells (CSCs), also known as tumor-initiating cells, represent a subpopulation of cells within tumors accounting only 0.01–2% of the total mass^{25,23,324}. These “hidden” cells present the remarkable ability to self-renew indefinitely and differentiate into various cell types, contributing to tumor initiation, progression, metastasis, and recurrence^{284,23,51,14}. CSCs are similar to normal stem cells, sharing common regulatory signaling pathways (Wnt/ β -catenin, Sonic Hedgehog (SHH), Notch pathways, and PTEN)³²⁵ with fundamental roles in self-renewal and growth. Brain CSCs derived from patients express markers CD133 (Prominin-1) and Nestin, also called as neuroepithelial stem cell protein, which are also found in normal neuronal stem cells¹²⁷. Dirks and colleagues²⁸⁴ were the pioneers on identifying a population of brain stem-cell-like cells, isolated from aggressive glioblastomas or medulloblastomas. These cells were characterized by the expression of CD133, a marker also found on normal neural and hematopoietic stems. Notably, only CD133-positive cells induced tumor growth when injected into mice, suggesting that CD133 expression is a key signature of tumor-initiating cells²⁸⁴. CSCs possess innate resistance to conventional anti-cancer therapies. Normally, anti-tumor drugs are designed to target highly proliferating cancer cells²⁹¹, but CSCs, due to their quiescent state, can evade the detection and action of anti-tumor drugs^{228,93}. CSCs highly express ATP-binding cassette (ABC) transporters¹⁴¹, a class of proteins conferring a multidrug resistance trait. Solid tumors, including several brain tumors, exploit these proteins to become resistant to drugs³²¹. CSCs also employ aldehyde dehydrogenase (ALDH) as a defense mechanism against oxidative stress induced by chemotherapy¹⁴¹, thereby enhancing their resistance to these drugs^{141,230,321}. Interestingly, the ability to regulate oxidative stress and free radicals is also implicated in CSC resistance to radiation therapy^{109,285}. Moreover, CSCs possess enhanced DNA repair mechanisms, allowing them to counteract DNA damage more effectively than non-CSCs⁷¹. HIFs, regulator of cellular hypoxia responsiveness¹⁵⁰, were demonstrated to modulate the proliferation and fate of CSCs in medulloblastoma and glioblastoma multiforme¹²⁶. HIFs have been also linked to EMT¹⁵⁰, a process that is tightly intertwined with CSCs. Cancer cells undergoing EMT acquire stem-like features³²⁹, which is crucial for tumor initiation. In this sequence of events, the Wnt signaling pathway assumes a pivotal role¹⁵⁸, along with the Notch/Jagged²⁴ and hedgehog²¹⁶ signaling pathways.

Several miRNAs have been identified to regulate EMT directly influencing the CSC population^{344,345,46}. Examples include miR-10b^{169,13}, miR-210²⁹⁸, miR-5188¹⁷¹. In glioblastoma multiforme (GBM), miR-504 has been shown to function as a negative regulator of the Wnt- β -catenin pathway by directly suppressing FZD7 expression. Overexpression of FZD7 was able to reverse the EMT inhibition induced by miR-504¹⁷⁶. These pathways regulate the expression of genes involved in EMT and CSCs, leading to their acquisition of stem-like properties and drug resistance²³⁰. miR-135a/b is also predicted to target SFRP4, a protein that inhibits Wnt/catenin¹¹⁴. miRNAs can also revert other CSCs pro-tumor characteristics such as drug-resistance, as demonstrated using U87MG cells (human GBM cell line) in which the inhibition of miR-127, an important regulator of ABC transporters, restored the drug sensitivity⁸¹.

The tight regulation of CSCs self-renewal is a critical factor in the process of tumorigenesis. Disruption of this regulatory balance leads to unrestrained CSC self-renewal, ultimately ending with tumor development. Six essential factors, namely Nanog, Sox2, Oct4, KLF4, Lin28, and c-Myc, are indispensable for maintaining stem cell pluripotency. A subset of miRNAs, such as miR-470, miR-296, and miR-134, were shown to exert an inhibitory effect on the expression of self-renewing factors Oct4, Sox2, and Nanog²⁹⁹. Other examples were extensively reported in the review of Gangaraju and Lin⁹². The origin of CSCs remains unclear, with two possibilities: they may arise from normal stem cells or from normal progenitor/differentiated cells that have reverted to a stem-like state. Further research is needed to determine the true source of CSCs. Furthermore, the limited ability of cancer cells to allow tumor regrowth implies that treatment relapse is likely caused by the persistence of CSCs, presenting a promising avenue for cancer therapy.

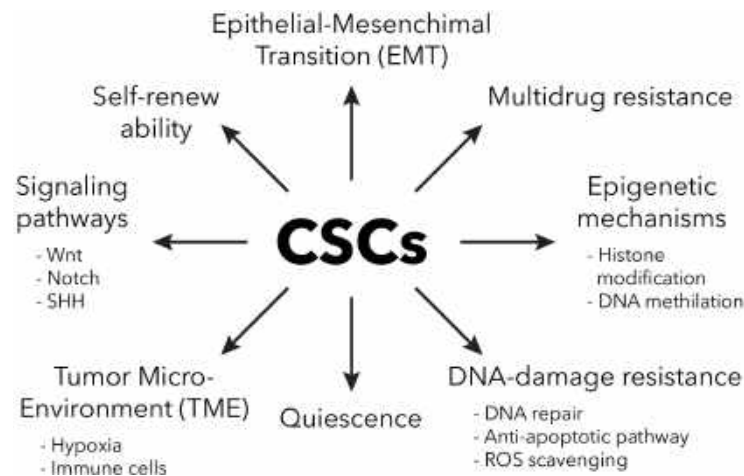


Figure 1.5 - Cellular mechanisms of Cancer Stem Cells (CSCs). CSCs evade therapeutic agents through a complex interplay of signaling pathways and cellular modifications, with signaling pathways promoting self-renewal and EMT. EMT, influenced by the tumor microenvironment, contributes to drug resistance. This process is modulated by effectors acting on epigenetic modifications, DNA repair, and DNA remodeling, potentially leading to a quiescent state, which in turn sustain drug resistance^{141,329,93,24,158,216,14}. Adapted from Phi et al., 2018²³⁶.

Medulloblastoma: a paradigm to study the role and therapeutic potential of miRNAs in abnormal CNS development.

Medulloblastoma (MB) has origin from neural progenitor cells in the cerebellum due to malfunctions in the developmental process at certain points. Given the tumor critical time of development and location, understanding the fundamentals of cerebellar development is crucial. This section will provide an overview of cerebellar development before delving into the specifics of MB disease.

Development of the cerebellum

The cerebellum is a small hindbrain structure that, beside the predominantly known role in motor movement and balance, it has also integral function in sensorimotor and cognitive networks, influencing cognitive processes, visuospatial reasoning, associative learning, emotional regulation, behaviour, and psychiatric disorders^{54,8}. The cerebellum harbors nearly half of the brain's neurons, organized in a dense cellular layer³⁴, and it stands out as one of the most elaborate regions of the CNS³⁴. The anatomical structure consists of two hemispheres connected by a narrow midline structure known as the *vermis*, a characteristic feature of mammals³⁴. Like the telencephalon, the cerebellum is composed of grey and white matter. The outer grey matter, the cerebellar cortex, is divided into three distinct layers: the molecular layer (at the outermost surface), the Purkinje cell layer, and the granular layer (the innermost layer)^{31,258}. Embedded within the white matter, underneath the cerebellar cortex, there are the four cerebellar nuclei, the output structures of the cerebellum. Arising from the dorsal hindbrain¹²¹, the cerebellum undergoes a four-step developmental process: 1) cerebellar territory organization; 2) establishment of the cerebellar progenitors; 3) granule cell migration; 4) formation of cerebellar nuclei and circuitry⁷³. After the neural tube closure, the initial subdivision starts with the expression of the transcription factors Orthodenticle homeobox 2 (Otx2; defining the Forebrain and Midbrain) and Gastrulation Brain Homeobox 2 (Gbx2; in the Hindbrain), delimiting the midbrain-hindbrain boundary^{195,174}. The isthmus organizer (IsO), arising from this border, expresses FGF8, a crucial growth factor for cerebellar development²⁶⁹. Other neural tube products, including WNT1, SHH, BMP, and TGF- β , interact with the IsO to specify the anterior-posterior axis and rhombomere segmentation⁷⁸. Within Rhombomere 1, the proteins ATOH1 and PTF1a serve as distinct markers for the rhombic lip (RL) and the ventricular zone (VZ), respectively^{3,134,314}. The lower portion of the RL differentiates into transient pseudostratified epithelium, the *roof plate*, and gives rise to choroid plexus cells. These specialized cells produce cerebrospinal fluid (CSF), a critical component for brain development¹¹. Alterations in CSF volume have been linked to cerebral growth impairments and neurological disorders^{69,198,9}. Cerebellar nuclei neurons are the first to emerge from the RL and the VZ²⁵⁹. The development of cerebellar nuclei initiates with a transient "nuclear transitory zone" located in a marginal position. Neurons of the RL will migrate tangentially into the ventral and isthmus^{314,111} and will give rise to the External Granule Layer (EGL). This latter, under the influence of FGF8 and SHH signals, undergoes a clonal expansion phase during the late pregnancy period, that will culminate in the formation of a six-eight cells layer around the second year of life in humans^{249,78}.

Medulloblastoma

MB is a devastating malignant tumor affecting the cerebellum, predominantly striking children, though it can also occur in adults²²⁵. Brain tumors represent the most common neoplasms in pediatric cases and are the second leading cause of tumor-related deaths, following leukemia²²⁵. MB falls under the category of cancers that affect the posterior fossa, including also astrocytoma, ependymoma, and cerebral glioma. The average age at diagnosis of MB is 13 years, with a peak incidence in children aged 2 to 7 years, being this tumor very rare in the adult population (over 21 years of age)¹⁹⁹. The annual incidence is estimated at 0.5 per 100,000 children under 15 years of age¹⁹⁹. Symptoms include loss of balance, lack of coordination, diplopia, dysarthria, and, due to the involvement of the fourth ventricle (for which obstructive hydrocephalus is common), the signs of hydrocephalus, including headache, nausea, vomiting, and unstable gait^{34,54}. MB is a heterogeneous disease with four distinct molecular subgroups^{146,244}: WNT, SHH, group 3, and group 4, which are generally linked to specific histological features. *Table 1* correlates genetic subtypes, histology and localization details, characteristics that have implications for prognosis and treatment of MB²⁰³.

Table 1.- Genetic classification of Medulloblastoma subtypes

Tumor subtype	Histology features	Localization	Prognosis
WNT	Classic type	Cerebella peduncle	Good
SHH	Desmoplastic type	Rostral hemispheres	Good
Group 3	LCA type	Midline	Poor
Group 4	Classic type	Midline	Poor

The prognosis of MB disease is generally favorable, however in 30% of cases, the tumor is subject to relapses and often proceed in metastases, which involves the subarachnoid space of brain and spinal cord and, even if rare, also in the liver, bone marrow and lungs²²⁵. Relapses, occurring in almost one third of the patients, are considered mostly incurable, hence leading to fatality in the majority of cases^{115,243}. A consensus among researchers suggests that the root cause of tumor relapse is the presence of CSCs^{56,196,26}, which possess an inherent strategic ability to evade the effects of chemo- and radio-therapy, allowing them to repopulate and revitalize the tumor at later stages. This hypothesis is further supported by the notion that MB originates from neural progenitors that failed the neuronal lineage commitment and remain in a pluripotent state^{107,8,129}. Yang et al.³²⁶ provided one of the first evidence that MB resulted from mutations in the SHH pathway in neuronal stem cells. Interestingly, they also showed that when the altered commitment involved the stem cells, the resulting tumors were more aggressive. In a recent study, Hendrikse et al.¹²⁹ established a connection between the emergence of MB-group 4 and the CBFA complex, which is expressed early in neural progenitor cells of the RL, preventing their maturation. Through OTX2 depletion, they were able to reverse this developmental arrest. The unique developmental characteristics of the RL in humans and its high susceptibility to altered progenitor cell fate contribute to a potential explanation for the increased human predisposition to MB.

Modeling the MB biology

The increasing categorization of MBs into subgroups underscores the necessity for the creation of precise models that faithfully replicate each subgroup. This is essential for the effective utilization of these models in preclinical studies. Mouse models and cell lines aid in studying MB onset and mechanisms. Current models used in MB research studies were meticulously reviewed by Roussel et al.²⁶⁰. Here are reported the general categories, with pros and cons.

In vitro models: cell lines (i.e. DAOY) or patients-derived (PD) cells. Despite their ease of cultivation and common use in preclinical drug testing, recent molecular analysis reveals that established human tumor lines do not always accurately represent primary tumors due to the acquirement of mutations or loss of genetic material²⁶⁰. Moreover, PD cells were reported to be difficult to generate stable lines or even maintain their intrinsic subtype-specific signaling signature when cultured²⁶⁰. Moreover, primary tumor cell lines generated from surgically removed tumors represents the final stage of tumor development, characterized by transformed cells and accumulated genetic rearrangements²⁹³.

In vivo models: mice are the most used animal models. The induction of MB tumor can be achieved by 3 main approaches: i) Mice carrying genetic mutations involving the different regulatory pathways known for MB disease, meaning SHH^{107,272}, the WNT¹⁰¹, Group 3²⁹⁵ and Group 4⁸⁷; ii) Implantation of cells harboring a MB-inducing mutations mice cortex or cerebellum. The engraftment can be syngeneic or xenogeneic, depending on the type of cells used. For example, Huang et al.¹³⁶ reprogrammed human Induced Pluripotent Stem cells (human iPSCs)-derived NEC to reproduce the Group-3 MB subtype. Engraftment location can be orthotopic or heterotopic (as the engraftment in the flank⁴¹, one gold standard in cancer research); iii) PD-orthotopic xenografts were specifically developed to mirror the TME of human MB, a feature otherwise absent in the other *in vivo* alternatives above-mentioned²⁶⁰). Following the initial processing of the tumor sample, there are no intermediary *in vitro* stages, eliminating artifacts or genetic drift that may occur during cell culture.

Specific genetic models are useful for targeted therapies, while syngeneic orthotopic models are invaluable for exploring the immune landscape²⁶⁰. The increasing implementation of Patient Derived Orthotopic Xenografts (PDOXs) in preclinical testing reflects the limitations of cell lines in accurately mirroring primary MB tumors. The focus of preclinical MB research was first performed on the SHH and Group 3 subgroups, driven by the need for improved therapies in these high-risk groups. Several drugs and small molecules have shown efficacy in suppressing MB in mouse models; however, most studies have employed established cell lines and flank-model tumors. Crucially, in xenogeneic engraftments, the inclusion of biological material from a distinct individual necessitates the utilization of immune-deficient animals, thereby excluding the influence of the immune system in the studies. Moreover, surpassing the blood-brain and blood-tumor barriers still poses significant challenges, limiting the number of drugs effectively available for treating MB patients. Hence, there is the urgent need for better preclinical models of human MB.

Treatment of Medulloblastoma

In most cases, the disease is responsive to existing therapies. A systematic overview of the current therapies is recapitulated in the review of Prados et al.²⁴³, It has been described that, the most common therapy in clinical

practice is the surgical resection of the tumor mass followed by radio-chemotherapy regimens. However, treatments often lead to impairment of the cognitive-affective behaviours, with several deficits that concerns the expressive language and word-finding ability, emotional apathy, visual-spatial function and memory^{255,257}. Immune modulation, particularly in the context of challenging-to-treat relapses, remains under investigation in MB, encompassing the exploration of use of chimeric antigen receptor (CAR)-T cells strategy, oncolytic viruses and vaccines. Targets of these approaches are predominantly membrane receptors or typical components of tumorigenic cells (i.e. HER2, B7-H3, EPHA2, GD2), or cytokines produced by Immune cells (such as Interleukin 13)²⁴³. The use of small molecules against the cancer thread is giving encouraging answers^{160,189,308}. However, hereby quote prof. Prados, to highlight the fact that there is a pressing demand to discover and apply new techniques and approaches in cancer research:

“[...] A “one size fits all” approach is no longer relevant given the degree of biologic differences that exist with subgroups and clearly within individual patients. A major challenge going forward is to optimize the use of clinical trial designs that take into account both the rarity and heterogeneity found in relapsed disease”.

To best of our knowledge, there are no active clinical trials investigating the use of miRNA-based therapies for MB patients³¹⁵. Injecting Locked Nucleic Acid (LNA) antimiRs into the bloodstream that specifically target miRNAs from the miRNA-17 – 92 cluster was shown to reduces tumor growth in syngeneic mouse models of SHH-subtype of MB²¹³. Xenotransplant mouse models treated with nanoparticle-conjugated miR-192 mimic resulted in a significant reduction in the number of metastatic lesions and improvement in survival¹⁵. Restoration of the downregulation of miR-34 and miR-124, two miRNAs commonly suppressed in MB, holds promise for miRNA-based treatments, as shown in engrafted animals with MB cell lines^{238,283,305}. Pannuru et al.²³² showed how targeting chemoresistance-associated miRNAs could restore the sensitivity of MB cells to therapeutic agents. As one prevalent challenge for MB is drug-resistance induced by chemotherapeutic agents^{232,246}, co-delivering of miRNA mimics or antimiRs with chemotherapeutic agents could offer novel hope for treating hard-to-manage MB cases. Further preclinical trials are necessary to confirm the feasibility of employing miRNA mimics to treat MB. However, similar approach are now under preclinical studies to evaluate the potential of miR-124 nanoparticles in Parkinson's disease and prostate cancer models^{213,279}, catalyzing more interest in new paradigms for therapies, with miRNAs emerging as a promising therapeutic target.

CHAPTER 2 Rationale and Aims

The validity of better preclinical cancer models remains a recurring concern, especially when translating basic findings to human therapy. The definition of “model” *per se* implies the feasibility to accurately replicate human disease conditions, which is crucial for inferring treatment efficacy and safeness. Only 8% of tested drugs reaches the patients, and the most ineffective route connecting research to clinical therapies is the one covered by oncological treatments^{190,188,212}. The low success rate of translating animal studies to human therapies highlights the limitations of models in accurately mimicking human diseases. While 2D cell culture models can shed light on cellular mechanisms, they fail to replicate the complex molecular patterning and the interactions between cell types and their microenvironment^{190,188,260}. Therefore, 3D cell cultures have been employed to address this limitation (i.e. organoids, assembloids, organ-on-a-chip). Despite their real-time readout and imaging capabilities, these devices fail to reproduce vascularization and immune system commitment consistently with their natural counterpart^{188,339,348}. Indeed, such miniaturized devices sure lack the complexity for predictive applications, highlighting the still reductive nature of these methods³⁴⁸. On the other side, animal models for MB research offer an answer to these limitations, aspiring to simulate a more realistic and comprehensive system, but this endeavor requires compromising the immune system of the receiving host. A full complete immune system is of tremendous necessity for deeply understanding cancer development and progression¹⁰⁶. Indeed, the absence or suppression of the immune system in many *in vivo* preclinical studies has led to severe immune responses and incomplete outcomes⁶⁰. The first immunocompetent xenotransplantation in mouse brain reported (as far as our knowledge) has been presented by our lab in the work of Hoffman et al.¹³², describing the xenotransplantation of human Glioblastoma cells in mouse brain. The prevailing hypothesis stating that MB has origin from faulty neural progenitor cell development in the hindbrain has gained extensive support, implying that its actual origin lies principally during embryonic development. Therefore, preserving this scheme of tumor origin is essential to reconstruct its genesis more accurately. For the reasons presented above, the first aim of this study is the **generation and characterization of an orthotopic xenotransplantation model for MB in brain of immune-competent mice.**

The profound impact of miRNAs on cancer biology has been widely reported over the last two decades^{38,119,305,263,108}. One of the main aspects of this influence involves the maintenance of miRNA-mediated regulatory mechanisms that preserve specific features enabling a subpopulation of cells to remain in an undifferentiated, quiescent state. The theory supporting this phenomenon is directly related to the existence of the CSC population^{284,23,51}. In the scenario of MB, this implies that cells retain their stem-like properties, exhibiting a progenitor-like profile. miRNAs have been demonstrated to either sustain this process or reverse it, inducing differentiation and resulting in decreased proliferation, tumor volume downsize, and the reduction of tumorigenic and metastatic capabilities^{344,345}.

Our laboratory found a particular combination of different miRNAs able to induce the neuronal differentiation of mouse Neural progenitor cells²⁴². Based on the correlations between neural progenitors and MB cells, it is

possible to hypothesize the use of the 11 miRNAs as saboteur of the proliferative and tumorigenic phenotype to contrast the MB malignancy. However, to identify and test therapeutic targets against MB, we need to develop models that mimic the initiation and progression of the disease. Attempts to overcome this challenge resulted in the use of PD cells, but these strategies had reached a partial success as cell lines isolated from tumor resections represent the final stage of the tumor development, encompassing transformed cells that accumulated genetic alterations²⁹³. While miRNAs exhibit high conservation^{210,253,156}, direct evidence of the neuronal differentiation-inducing effect of the 11 miRNAs combination remains lacking in the human context. To effectively translate this approach to human MB, is urgent to have an experimental system that resembles the one employed in the previous study. Human iPSCs, characterized by minimal genetic modifications compared to tumor cells, can be considered a valuable platform for conducting the required initial assessment. By inducing the human iPSCs to a neural progenitor identity, we could recreate the cellular environment that is thought to initiate MB formation, allowing to study the human Neural Progenitor Cells (hNPC) response to the *pool* of 11 miRNAs. For the reasons presented above, the second aims of this study are the: **evaluation of the ability of a *pool* of 11 miRNAs to induce pro-neuronal differentiation in human iPSCs**; and the ***in vivo* validation of the effect of a *pool* of 11 miRNAs in MB engraftments**.

CHAPTER 3 Results

An orthotopic xenotransplantation model of MB in an immuno-competent embryonic mouse

A fundamental limitation of human tumor engraftment models is the requirement of immune-suppressed mice. This minimal presence of tumor-host immune system interaction can result in histopathological results that differ significantly from that naturally occurring in human tumors. Syngeneic models present an alternative approach, but their inability to study therapies for human-specific tumors due to their identical origin to the host limits their applicability both on embryonic and adult mouse brain tumor models. In fact, the immune response via innate pathway is already active during embryonic development of the mice, contrary to the adaptive one^{206,85}. Therefore, we proposed the employment of the embryonic immune-privileged time frame which allows the injection of human MB cells in mice brains while maintaining their wild-type (wt) immune background.

Human MB cells engraft and give rise to tumor-like masses wild type embryonic mouse brain

To evaluate the engraftment of MB tumor initiation in immunocompetent mice, we aimed to determine if the presence of a human MB cell line could be observed at various time points during developmental stages pre- and post-natal. In the model established by Hoffman et al.¹³², the peak of tumor growth occurred at the developmental post-natal day 7 (P7). Reinforced by the principal aim to study infant brain tumor engraftment, we consequently selected our final time point to coincide with the predicted period of maximum growth and tumorigenic potential. DAOY cell line, a commercially available and commonly used desmoplastic MB line isolated from a 4 years-old Caucasian male¹⁴⁰, was first transduced with a lentivirus harboring the mCherry fluorescent protein under the control of the human promoter Elongation Factor 1 α (EF-1 α) promoter, to enable the rapid identification of the engrafted cells in the host. Single-cell suspension of 50.000 DAOY mCherry⁺ cells were injected into the lateral ventricle (LV) of immune-competent mouse brains at embryonic stage 14.5 (E14.5) following an *in utero* procedure (Figure 3.1 – A). The survival rate of embryos undergoing the *in utero* surgery was around the 90%, as expected for this procedure^{265,132}. To estimate the effectiveness of the *in utero* transplantation, we checked at different time points the number of pups that presented red fluorescent masses in the brain, as a positive indication of DAOY mCherry⁺ cells, therefore indicating the engraftment of tumor cells. Analysis at E18.5, P2 and P7 of the animals that survived the procedure showed that almost the totality of brains was positive for tumor xeno-engraftment (TX) at all stages analyzed (Figure 3.1 – B), confirming the success of the *in utero* engraftment. Hence, wt mice were confirmed to immune-tolerate the external source of the implanted cells, allowing the maintenance of the engraftments at least up to 14 days after the surgical procedure. Tumors displayed the ability to grow over time within the host tissue, as qualitatively observed, and did not show a specific preference for engraftment within the host brain (Figure 3.1 – C). This observation was confirmed by positive staining for the Ki67 proliferation marker (Figure 3.1 – D). Human nuclei from both E18.5

and P7 explants exhibited a high proliferative state, supporting the conclusion that the TXs retain a tumorigenic capacity, resulting in the growth of tumor masses.

Previous studies have shown fusion events between the transplanted embryonic human neural stem cells and neurons of the host³⁰, which resulted in the exchange of genetic material between donor and host cells. While the phenomenon of cell-fusion is recognized, explanations regarding its significance and potential implications are still unknown. To assess whether the transplanted DAOY cells in the embryonic mouse underwent cell-fusion events with the host cells, immunohistochemical analysis with a Human-specific nuclei (HuNu) antibody was performed. Brain slices from the harvested brains were examined for their intrinsic mCherry fluorescence and analyzed for the immunoreactivity to HuNu antigen. As shown in *Figure 3.2 – A*, DAOY mCherry⁺ cells maintain their human identity, as all the human nuclei within the region marked by the red fluorescent signal being co-stained with HuNu signal. Huang and colleagues³¹⁶ reported that the species-specific morphological features of human nuclei can be used to distinguish human from the mouse's cells. Indeed, HuNu⁺ nuclei are not enriched in nucleoli, whereas mouse nuclei show several nucleoli (*Figure 3.2 – B*). This, using the coexisting presence of the mCherry signal, eliminated the need to include the discriminative HuNu signal in the subsequent analysis. Together, these observations indicate that human MB cell line engrafts and grow over time in brain of immune-competent mouse embryos, which shows that the presented model can be suitable to study infant brain tumors behaviour in an immune-competent brain TME.

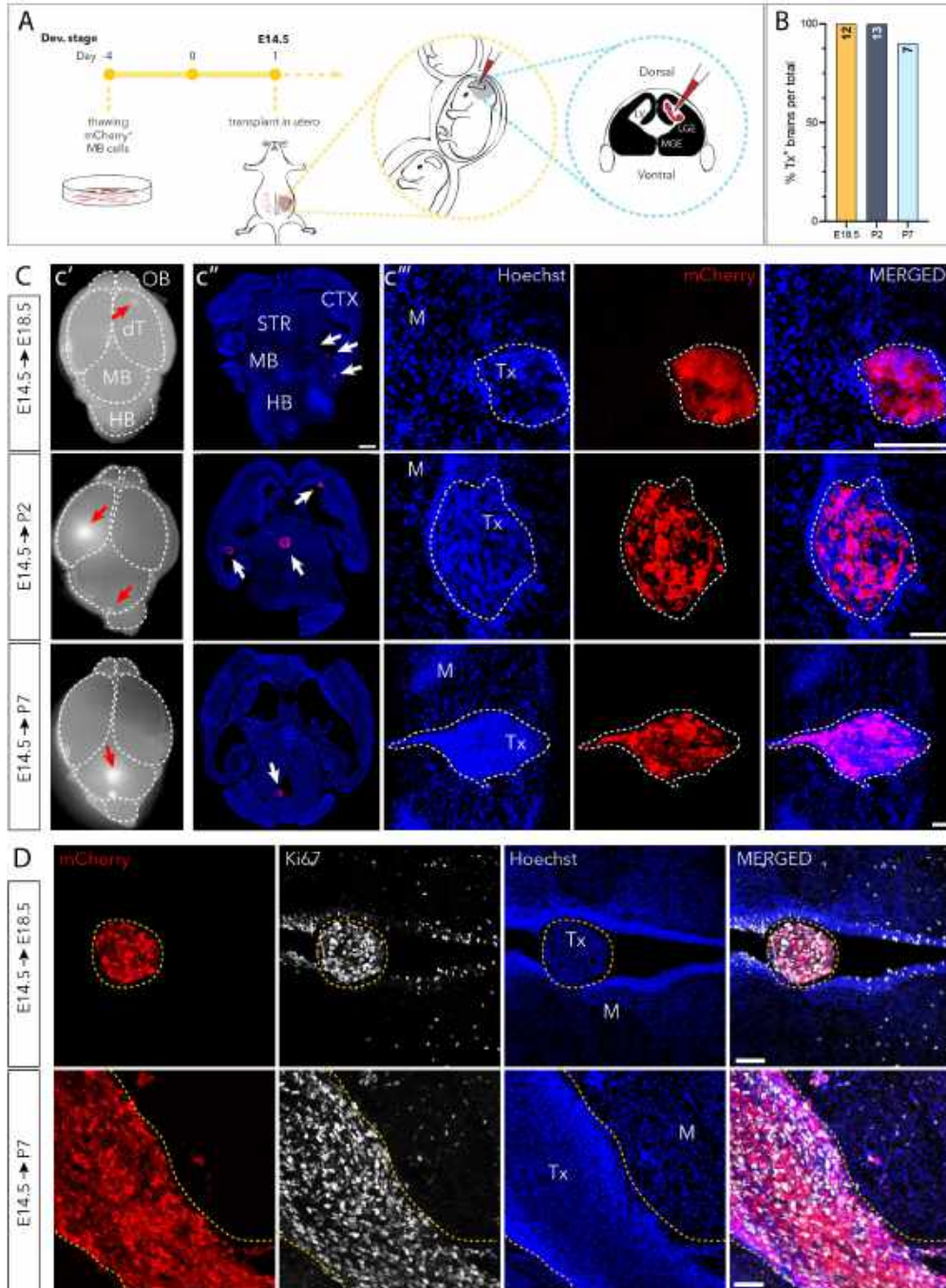


Figure 3.1 - Human MB integrate in brains of wt mice and maintain tumorigenic proliferation. (A) Experimental procedure. Human MB cells are plated 4 days before the in utero transplantation. Single cell suspension is injected in the later ventricle (LV) of E14.5 embryos. (B) Percentage of brains showing tumor xenotransplant (TX) over the total litter. Sample size per each time point is reported at the top of the histogram bar. (C) E18.5, P2, P7 mice brains in dorsal view (c'), red arrows indicated the TX (white spots); (c'') immunofluorescence of a cryosection in transversal plane or coronal plane (c''') at the indicated ages, composed by mCherry⁺ cells; in (c'') the white arrows indicate the TX. Scale bar: 500µm. (D) Immunofluorescence images of cryosections in coronal plane at the indicated ages, showing proliferating cells (Ki67, white) within the tumor. Blue: nuclei (Hoechst), red: TX (mCherry), white (Ki67). Scale bar: 50µm. Dashed lines indicate tumors borders.

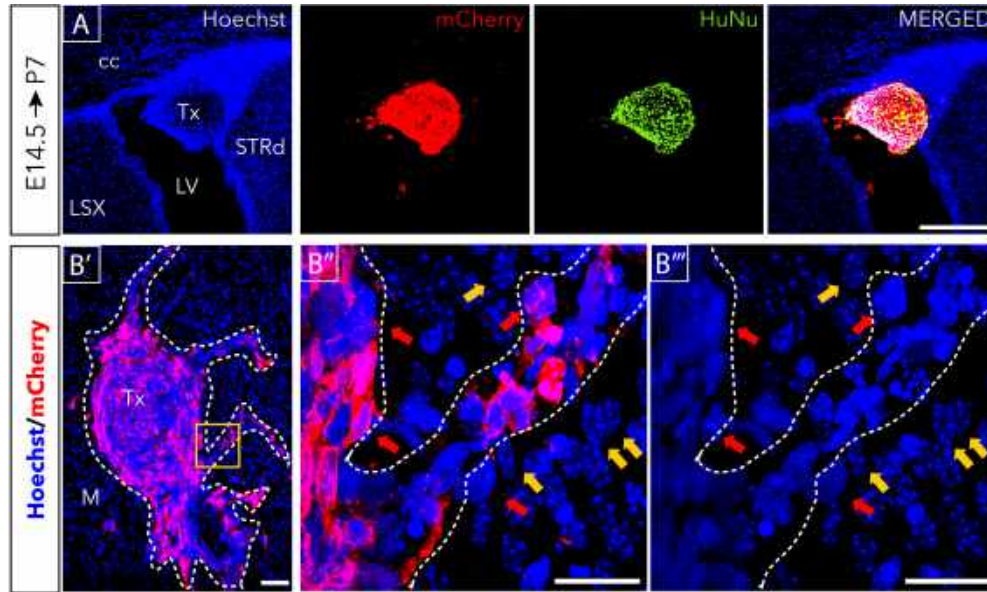


Figure 3.2 - Tumor xenografts retain their human identity upon engraftment. Immunofluorescence images of cryosections in coronal plane of P7 mouse. (A) Nuclei (blue) within the TX (red) overlapping with Human Nuclei (HuNu) marker. Scale bar: 200µm. In (B) magnification of morphological characteristics distinguishing human (red arrows) and mouse (yellow arrows) nuclei. (B' and B''') Human nuclei co-stain mCherry signal of the TX. Scale bar: 20µm. Dashed lines indicate the tumor borders.

Engrafted MB cells form a functional TME

Given the observed growth trend, which is in line with existing literature, we focused our attention on the two developmental stages E18.5 and P7, to characterize the features of tumor progression over time.

The presence of functional blood vessels surrounding the tumor plays a crucial role in all the stages of tumor formation, e.g. engraftment, proliferation, metastatic activity, and resilience, due to their active character on exchange of oxygen and nutrients, removal of CO₂ and metabolic wastes^{83,150}. The proper formation of the blood vessels is, therefore, an important component that enables the analysis of the ongoing tumor behaviour. Located inside the patient skull, tumor core and metastatic areas are accessible to the pharmacological drugs depending on the local permeability, being selective or not, of the angiogenic structures, either neo-formed or re-designed. Also, the angiogenic degree of brain tumors is a signature of their grade of malignancy. For these reasons, it is crucial to characterize tumor and TME blood vessels content and structure. To verify whether our model exhibits angiogenesis, we investigated the presence of specific proteins associated with a functional vascular system. VEGF, a family of secreted glycoproteins, has been associated with an increased tumor microvessel density, leading to a higher risk of recurrence and a poor prognosis^{83,77,264}. Cluster of differentiation 31 (CD31), also known as Platelet Endothelial Cell Adhesion Molecule (PECAM-1), is constitutively expressed by the endothelial cells. This marker indicates vascular formation²¹⁸ and is often found in solid tumors¹⁹. In the TXs of MB, presence of these markers was examined using immunofluorescence, and positivity was observed in both E18.5 and P7 mice (*Figure 3.3 – A* and *Figure 3.3 – B*), indicating that TXs establish vascular connections with the host tissue. By comparing the expression of the two markers over time, at E18.5 the expression of CD31 was more well-defined in the periphery and spread in the internal part of the mass in later stages of P7 mice (*Figure 3.3 – B*). Furthermore, the vessels within the mCherry⁺ region exhibit enlarged diameters, a

characteristic feature of brain tumors and considered a hallmark of angiogenic vessels^{104,67,155}. As demonstrated by others³⁷, brain orthotopic xenotransplants revealed that CSCs exploit vascular niches enriched with secreted factors from endothelial cells, which aid in maintaining the stem cell-like state of tumor cells. We hypothesize that this phenotype could represent a strategy for tumor cells to remain inside niches that promote quiescence, serving as a reservoir for tumor repopulation and/or metastasis within the host. Our finding aligns with previous research and presents an intriguing avenue for further exploration of this phenomenon in a model possessing an unaltered immune system at both brain- and systemic- level. In line with those results, we found colocalization of the human-specific neural progenitor marker Nestin with CD31 in TXs of P7 mice (*Figure 3.3 – C*), indicating a close interplay between *bona fide* CSCs and endothelial cells.

Another important feature of the brain's vasculature is the BBB. Claudin-5 is the most abundant tight junction protein that actively contributes in a significant manner to the selective permeability of the BBB, acting as a gatekeeper in brain endothelial cells. Moreover, laminin, a critical component of the basement membrane¹²⁰, plays a substantial role in modulating BBB function since all the different isoform of laminin regulate the distinct cellular processes and signaling pathways within the neurovascular unit³³². Previous studies have demonstrated a major disorganization in laminin net within tumor tissue compared to healthy tissue^{104,130}. Therefore, laminin organization was investigated in E18.5 and P7 slices collected from TX⁺ brains. Laminin is present within the tumor mass as early as E18.5 (*Figure 3.4 – A*) exhibiting a mildly disorganized appearance close to tumors. The most striking observation is the directional invasion of blood vessels from the surrounding tissue inward the tumor, clearly traversing tumor boundaries, as shown in *Figure 3.4 – B* and magnification *Figure 3.4 – b'*. These observations suggest the possibility of vessel co-option, a non-angiogenic mechanism of tumor vascularization where cancer cells utilize pre-existing blood vessels instead of inducing new blood vessel formation. Immunoreactivity for Claudin-5, a marker of endothelial tight junctions, was observed in peritumoral vessels within the brain parenchyma (*Figure 3.4 – A*). Dense vascularized structures were also prominently visible at the boundaries of the ventricle (*Figure 3.4 – C*). Co-staining of Laminin and Claudin-5 indicates maturity of the vasculature, as the presence of the basal lamina is needed to exert the homeostatic properties of BBB^{120,130}, while presence of Claudin-5 marks functional vessels, thus confirming that the vasculature surrounding the TME is functional. This observation supports the occurrence of angiogenesis.

Our findings demonstrate that the TXs are integrated into the host's blood vessel network as early as 4 days post transplantation, and they are enveloped by a functional BBB. The intratumoral vasculature seems likely to originate by both co-option and angiogenesis, as evidenced by the robust VEGF expression within the mCherry⁺ area. Further studies are needed to investigate whether the localized expression of Claudin-5 and VEGF contributes to the structural aspects of tumor growth and infiltration. Additionally, elucidating their impact on vascular permeability is essential. The presence of Nestin⁺ stem cells further highlights the model's ability to mimic a CSC niche, emphasizing the intriguing potential of this model for future studies. Even if only qualitative analysis were performed, these results show that the CSCs are seamlessly connected to the host's blood vessel network, which is the same as saying to the functional BBB.

Together, these findings demonstrate that tumor engraftment recapitulates MB-typical behaviour through the development of a functional vasculature, paving the way for novel approaches in investigating the TME specific of human MB in an immunocompetent mouse model.

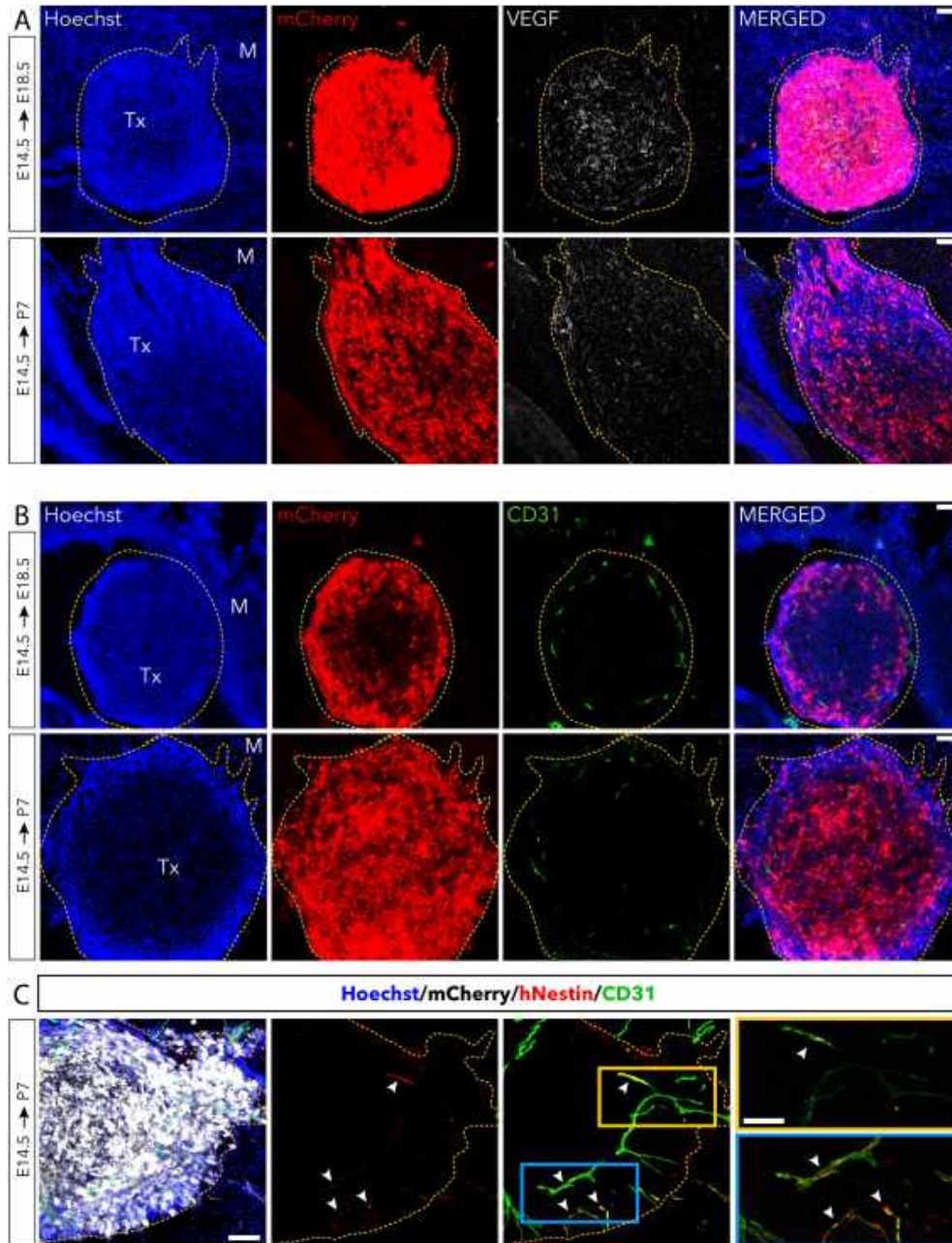


Figure 3.3 - Functional TME surrounding the TX support perivascular CSCs niches. Immunofluorescence images of cryosections in coronal plane at the indicated ages. (A) VEGF (white) is highly present within the TX (red) of E18.5 mice and maintained in P7 animals. Scale bar: 100µm. (B) At E18.5 marker for endothelial cells (CD31 – green) are predominantly at the periphery of the TX, while diffuses within the mass in P7 animals. Scale bar: 100µm. (C) Increased vessel dimensions in P7 animals showing signal overlap with human-specific marker of neural stem cells Nestin (red) as indicated by white arrows. Scale bar: 100µm. Dashed lines indicate tumors borders.

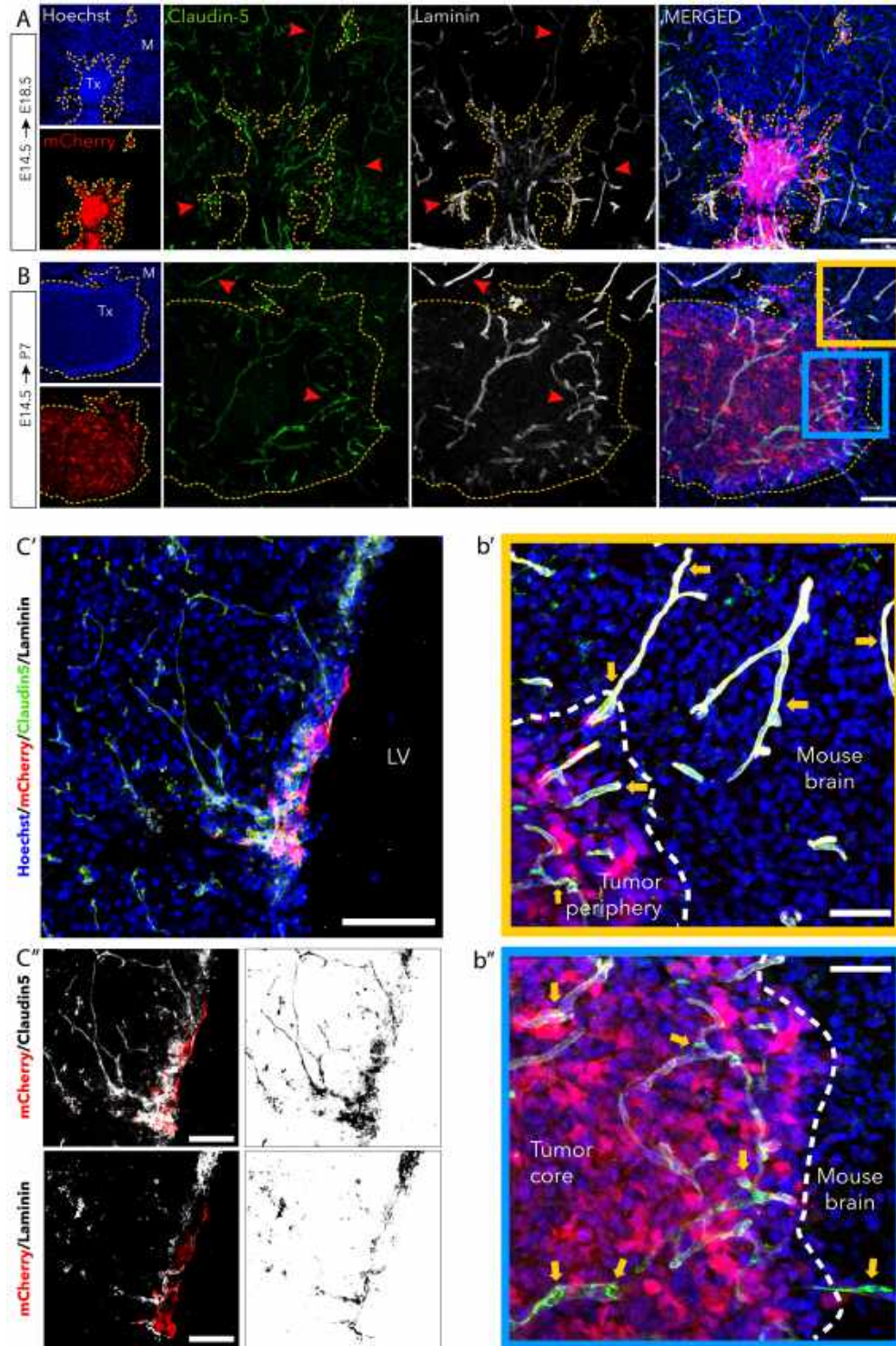


Figure 3.4 - Mature vasculature develops within engrafted MB tumors, contributing to the formation of a functional BBB. Immunofluorescence images of cryosections in coronal plane. (A and B) Laminin (white) and Claudin-5 (green) signal of both E18.5 and P7 mice brains demonstrate higher density and disorganized assembly within the TX (red) when compared to the host tissue surrounding the tumor (red arrows). Scale bar: 100µm (A and B). (b' - yellow box) High magnification of vessels co-stained by laminin and Claudin-5 crossing tumor borders in P7 brain (yellow arrows); (b'' - light blue box) Detail of low vascular organization within the TX. Blue: nuclei (Hoechst), red: TX (mCherry), green: Claudin-5, white: laminin. Scale bar: 200µm (b' and b''). (C) Immunoreactivity of laminin and Claudin-5 defining dense association with TX on the LV borders of P7 brain. Scale bar: 100µm. (C'') Increased vessel dimension is visible also in smaller tumors. Blue: nuclei (Hoechst), red: TX (mCherry), white: Claudin-5/laminin. Scale bar: 100µm. Dashed lines indicate tumors borders.

Human TXs are surrounded and infiltrated by the host immune cells

Within the tumor-infiltrating cells of the tumor, the predominant population comprises microglia (MG) and macrophages (making up to 30% of the tumor mass)²⁷⁵. These cells are known to directly degrade the extracellular matrix (ECM), and modulate the immune-response of the non-neoplastic tissue, facilitating tumor expansion^{262,99,27}. Also in the case of MBs, tissue-resident MG and tumor-associated macrophages (TAMs) constitute the most represented tumor-infiltrating cell population¹⁹⁴. It was demonstrated that TAMs can promote tumor growth by suppressing T-cell activity, stimulating angiogenesis, and establishing immunosuppressive TME through the production of growth factors, cytokines, and chemokines²³¹. In the particular case of SHH-MB tumors, TAMs play a crucial role, as gene expression profiling showed increased infiltration of these immune cells compared to other MB subgroups¹⁹⁴. The non-specific response (which includes also the MG) is already functional at E18.5^{10,289}. Therefore, I aimed to investigate the involvement of MG (and other TAMs populations) in the TXs. To perform these analysis, immunostaining of ionized calcium-binding adapter molecule 1 (IBA1) was valuated over time. At E18.5, IBA1⁺ cells were randomly distributed within the tumor region (*Figure 3.5 – A'*). Double-staining with CD68 (a marker for macrophages and activated MG when co-localized with IBA1³⁴⁷) showed positive immunoreactivity only in cells located away from the tumor margins (*Figure 3.5 – A'*). In contrast, at P7, activated MG cells were present both in surrounding areas and within the tumor mass (*Figure 3.5 – A'*), indicating a dynamic colonization of the tumor by the innate immune cells. Interestingly, while MG surrounding the tumor at P7 exhibited a ramified, active morphology^{310,233,307}, double positive IBA⁺/CD68⁺ cells located distant from the tumor in E18.5 brains displayed an amoeboid shape, visible in *Figure 3.5 – B*. This amoeboid morphology could be indicative of macrophages or microglia in a "reactive" state, potentially associated with a response to stress conditions such as infections or pathological conditions^{233,307}. However, the amoeboid morphology is not associated with phagocytic activity²³³. Consistent with these findings, qualitative observations in areas distant from the TX or adjacent to the tumor (*Figure 3.5 – B*) were compared within the same brain slice, revealing that the regions outside the tumors lack the ramified morphology observed for IBA1⁺/CD68⁺ cells close to the TX, exhibiting instead the amoeboid observed in E18.5 mice. Co-localization of IBA1⁺/CD68⁺ cells with mCherry⁺ signal, in some observed events, suggests the presence of phagocytic activity directed towards tumor cells (*Figure 3.5 – C*). Furthermore, this hint gains relevance by the presence of observed disrupted mCherry⁺ nuclei, which is consistent with the phagocytic activity of MG/TAM cells (for a reference figure, please refer to Fig.4 of Zhao et al., 2016³⁴²). Together these findings demonstrate the presence of competent TAMs, including *bona fide* tissue-resident microglia, capable of recognition, migration, and phagocytic activity of MB cells of the TX. While IBA-1 and CD68 are not entirely capable of distinguishing between the various TAM populations (i.e. microglia and macrophages)²²⁴, the use of microglia-specific markers, such as TMEM-119^{33,147}, a type I transmembrane protein specifically expressed by resident microglia, but not by blood-born macrophages, could be employed to elucidate the relative contributions of microglia versus macrophage-derived populations. The implementation of the presented model could potentially elucidate the mechanisms governing the interactions between TAM subpopulations and brain cancers^{99,27}.

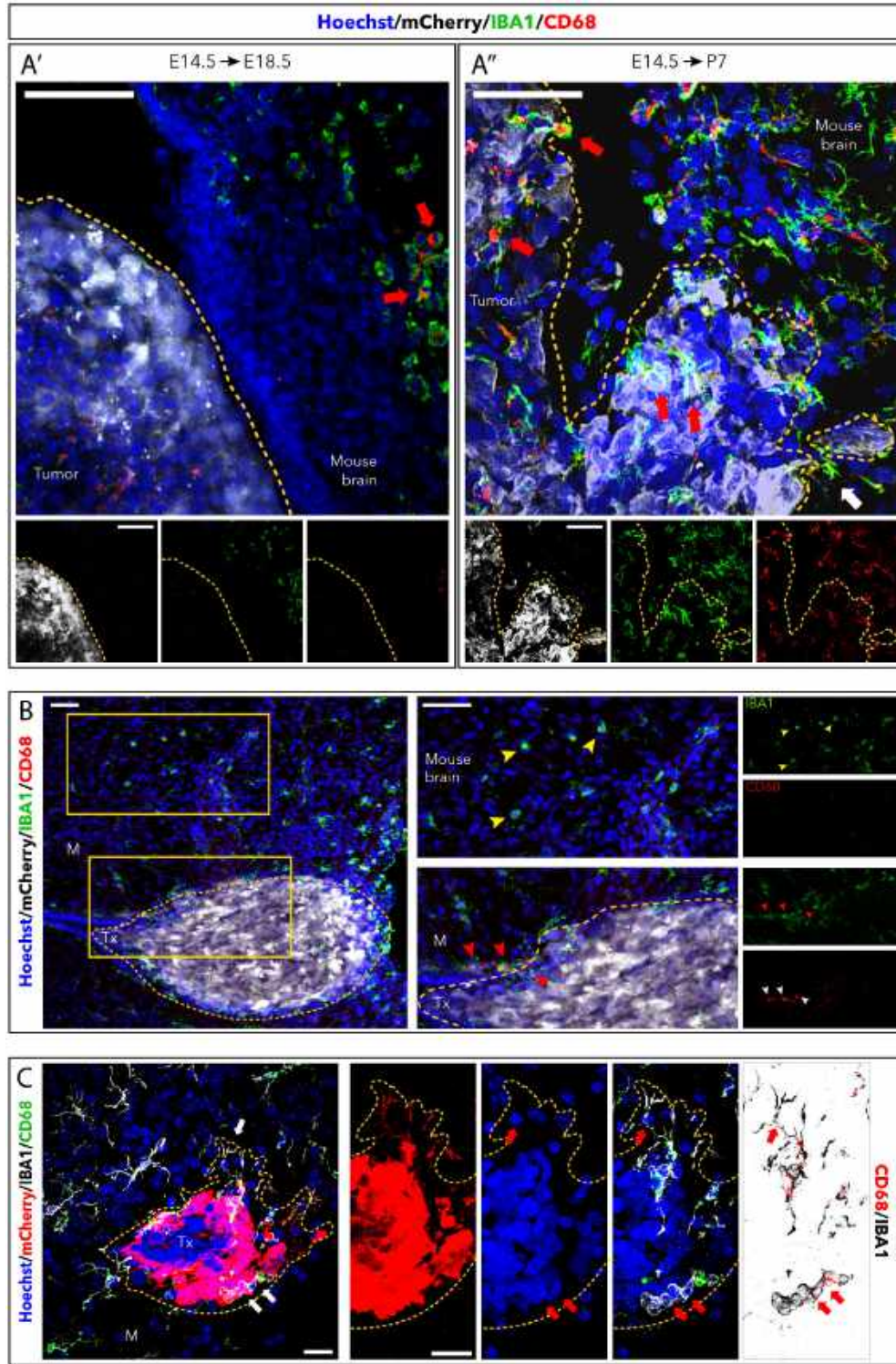


Figure 3.5 - TAMs are present and functional in the TME of TXs. Immunofluorescence images of cryosections in coronal plane. (A'' and A') In E18.5 embryos, TAMs marker IBA1 (green) is already present, but IBA1⁺ cells show lower levels of the marker of activation CD68 (red) compared to the TME of P7 mice (A''), confirmed also by typical morphology of activation. Scale bar: 50µm (A' and A''). (B) P7 brain slice showing IBA1⁺/CD68⁺ cells not in close proximity to the tumor displaying an amoeboid shape (yellow arrows, magnification box), while expressing an activated morphology when adjacent to the TX (red arrows, magnification box). Blue: nuclei (Hoechst), white: TX (mCherry), green: IBA-1, red: CD68. Scale bar: 100µm. (C) Active IBA1/CD68 double-positive cells colocalize with mCherry signal where small nuclei debris are found, indicating phagocytosis activity (white arrows in low magnification and red arrows in higher magnification). Scale bar: 20µm. Dashed lines indicate tumors borders.

Validation of the neuron-like differentiation induced by a *pool* of 11 miRNAs in human cells

The previous work from our laboratory demonstrated that a *pool* of 11 miRNAs upregulated during early stages of adult neurogenesis was necessary and sufficient to sustain the neuronal fate of adult neural stem cells at the expense of astrogliogenesis²⁴². Individual administration of the miRNAs composing the *pool* was ineffective, indicating that the presence of all the 11 miRNAs were necessary to support the pro-neural role of the miRNA *pool*. Interestingly, 9 of the miRNAs have never been reported for their relevance in mouse neurogenesis.

Although the miRNA composing the mentioned *pool* are conserved in human species^{210,253,156}, the proof that the same effect is exerted also in human progenitors have never been demonstrated. To validate this, the *pool* of 11 miRNAs was transfected in an episomal line of human iPSCs.

Validation of the pro-neural functions of 11 miRNAs in human iPSC-derived Neural Progenitor

To define an experimental setting that could be used to evaluate the pro-neural functions of the 11 miRNAs in a reproducible manner, a “zero-footprint” (viral-integration-free) iPSC line was used and differentiated using minimally defined media and manufacturers’ protocol. Cells were first characterized to assess the baseline of the neuronal differentiation performance.

Originally starting with 4×10^6 iPSCs in one well of a six-well microplate, the first phase of differentiation as described in *Figure 3.6 – A* provided approximately 3.3×10^6 human Neural Progenitor Cells (NPCs). During the single-cell differentiation phase, the doubling time of human NPCs cells was maintained around 50 hours, with a slight decrease during the 2nd passage (*Figure 3.6 – B* and *Figure 3.6 – C*), possibly due to the neural selection occurring during the differentiation. The viability of cells followed the same tendency. In order to confirm the NPCs character, human cells were analyzed by immunofluorescence microscopy (*Figure 3.6 – E*) using Nestin, Pax6 and Sox2 antibodies. The intermediate filament Nestin is known to be expressed in dividing precursor cells of the NS and its detection was consistent with its characteristic cytoplasmic staining in almost all the cells (*Figure 3.6 – E*). Pax6 coordinates neurogenesis and proliferation. All the human NPCs in *Figure 3.6 – E* were Pax6 positive. In agreement with previous reports, Pax6 was mostly observed within the nuclei of the human NPCs. Moreover, the expanded human NPCs retained their characteristic neural rosette morphology during the neuronal induction (*Figure 3.6 – E*). Cells were further differentiated to a Forebrain Neuronal Fate, to address the functional differentiation potential.

During the differentiation of human NPCs, reduction in growth rate was observed, likely due to the occurrence of differentiation-induced programmed cell death. Cells were maintained in neuronal maturation medium for up to 70 days of differentiation (DIF 70). In *Figure 3.6 – D* are reported representative images of cells during differentiation. Immunocytochemistry for neuronal markers was performed at DIF28, DIF45, and DIF70. *Figure 3.6 – E* reports the validation of the differentiation through Immunocytochemistry, by using typical neuronal differentiation antibodies (doublecortin – DCX, neuron-specific class III beta-tubulin – Tuj1, neuronal nuclear protein – NeuN).

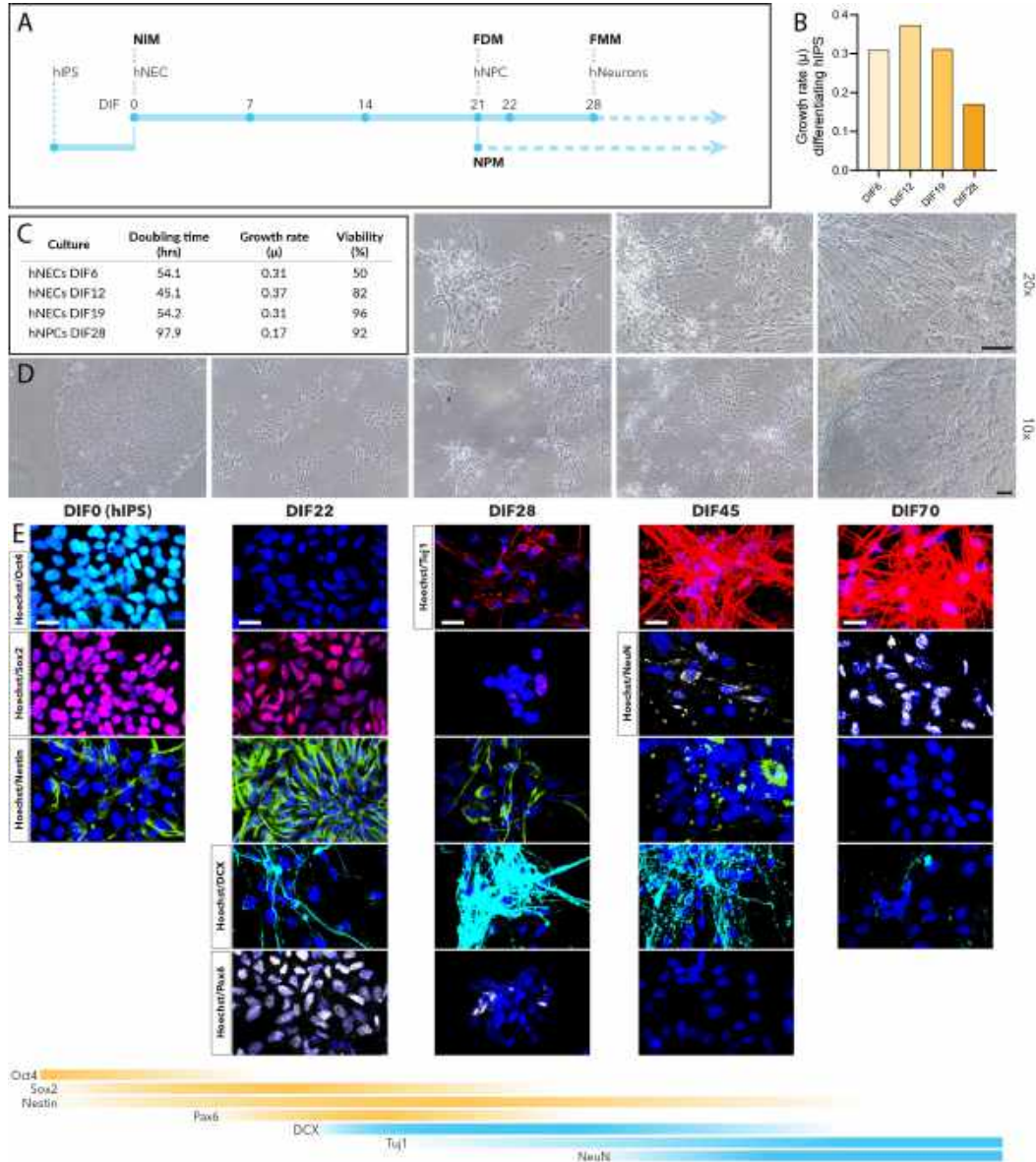


Figure 3.6 - Human iPSCs Neuronal Differentiation and Characterization. (A) Schematic representation of the differentiation protocol. (B) Growth rate (μ) of differentiation hIPSC (hNECs) at the indicated days of differentiation. (C) Summary table of cell biological characteristics during differentiation. (D) Representative images of human iPSC during distinct stages of neuronal differentiation protocol. Below: magnification 10x, above: magnification 20x. (E) Immunofluorescence images of human iPSC for different differentiation markers during the indicated DIF (above). Scale bar: 20 μ m. human iPSC: human Induced Pluripotent Stem cells, hNEC: human Neural Epithelial Cells, hNPC: human Neural Progenitor Cells, hNeurons: human Neurons, NIM: Neural Induction Medium, FDM: Forebrain Differentiation Medium, FMM: Forebrain Maturation Medium, NPM: Neural Proliferation Medium, DIF: day of differentiation, hrs: hours.

The extension of neurites is a fundamental process in neuronal differentiation, serving as the primary factor required for the generation of both axons and dendrites^{201,74,301}. This feature is also used as a phenotypic assay in pharmaceutical screening, due to its time-effectiveness and clear-cut results¹¹⁵. The phenotypic “Neurite Outgrowth assay” was therefore chosen to study the impact of the 11 miRNAs on human NPCs in a live-cell imaging system.

To better follow the dynamics of neurites upon differentiation, human iPSCs-induced NPCs were transduced with a lentivirus harboring mCherry fluorescent protein under the constitutive EF1 α . Cells were followed for 3

passages after the transduction, demonstrating no substantial difference in cell morphology or viability compared to the wt cells (*Figure 3.7 – B*). To identify the most effective miRNA transfection method, cells were initially evaluated using the SiGLO Green transfection indicator that localizes to the nucleus and emits at $\lambda_{\text{max}}=520\text{nm}$. Green fluorescent signal was observed upon transfection with two different lipid-based transfection reagents, Lipofectamine 2000 and Lipofectamine Stem, 48 hours after the transfection. Quantification of the transfection efficiency reported a better performance for the Lipofectamine 2000 agent (75.5% SEM \pm 8.8 against 55.7% SEM \pm 7.4) (*Figure 3.7 – C*”).

Next, human NPCs were transfected with synthetic mimics of the 11miRNAs *pool* at a final concentration of 250nM of mimics transfected. After 5 hours, the medium was replaced with the Forebrain Differentiation Medium (FDM) to induce differentiation of human NPCs as previously shown for mouse NPCs in the work by Pons-Espinal et al.²⁴². The neurite extension and the number of branch points were followed from 24 hours p.t. up to 6 days, corresponding to 144 hours – 168 hours pt. Comparison with the *scramble* (biological ineffective RNA) control, the total neurite length and number of branch points showed a clear positive trend (*Figure 3.7 – D*). The average number of branch points for the *scramble* was $0.6 \pm \text{SEM } 0.4$ at time point 0 and increased to $1.1 \pm \text{SEM } 0.7$. The 11 miRNA-treated cells presented a mean initial number of branch points of $1.0 \pm \text{SEM } 0.3$ reaching the value of $2.0 \pm \text{SEM } 0.6$ at the end of the experiment, suggesting no effect on the rate of neurite emission. However, the number of branch points was twice that of the *scramble* control at the baseline. This suggests that miRNA administration may lead to an increase in the number of emission cones within the first 24 hours. Supporting this hypothesis, neurite elongation, measured as the sum of the total length in the measured area, exhibited a significantly higher average upon *pool* transfection, compared to the *scramble* control (*Figure 3.7 – D*”), reaching approximately four times the initial length (from $270.6 \text{ mm} \pm \text{SEM } 12.4$ to $801.1 \text{ mm} \pm \text{SEM } 0.4$). *Scramble* samples only doubled their length ($128.3 \text{ mm} \pm \text{SEM } 89.4$ reaching $283.5 \text{ mm} \pm \text{SEM } 224.3$). These results confirm that the *pool* of the 11 miRNAs retain a pro-neural function as indicated by the neurite outgrowth assay. Because the transfection protocol differs from the standard neuronal differentiation protocols (see *Figure 3.6 – A* and *Figure 3.7 – A*) and neuronal differentiation is a sensitive process which critically depends on cell seeding density and adherence to established procedures^{43,116} (and author’s personal experience) possibly leading to heterogeneous results, I also investigated whether the effect of miRNAs could also be observed specifically in Neural Proliferation Medium (NPM). Human NPCs were treated with 11 miRNAs *pool* [250nM] or *scramble* [250nM] and after 5 hours, maintained in NPM. After 24 hours from the transfection, the number of branch points for the *scramble* was $0.5 \pm \text{SEM } 0.4$ and $1.0 \pm \text{SEM } 0.4$ for the *pool*, replicating the same outcomes observed for FDM (*Figure 3.7 – D*). Interestingly, by the end of acquisition, the *scramble* condition reached an average number of branch points of $0.9 \pm \text{SEM } 0.6$ whereas miRNAs-treated hNPCs exhibited around a 2.5-fold increase ($2.6 \pm \text{SEM } 1.5$). Regarding the second parameter, the neurite length extended in the same fashion observed for the NPM (time point 0, *pool* $270.5 \text{ mm} \pm \text{SEM } 78.6$, *scramble* $115.2 \text{ mm} \pm \text{SEM } 92.5$; after 144 hours, *pool* $930.4 \text{ mm} \pm \text{SEM } 287.8$, *scramble* $208.9 \text{ mm} \pm \text{SEM } 161.7$). In sum, irrespectively from culture conditions, the *pool* strongly impaired cell growth (*Figure 3.7 – E*’ and *Figure 3.7 – E*”), compared to *scramble* transfection, possibly due to the induced differentiation.

Collectively, these experiments suggest potential pro-neural effects of the 11 miRNAs in human NPCs, confirming previous observation in mouse cells. It is intriguing that the 11 miRNAs *pool* elicited similar effects on cells plated in presence of forebrain differentiation medium or neural proliferation medium, suggesting the 11 miRNAs could be used as a strategy to induce differentiation. Confirming this observation would mark the first demonstration in a human context that a combination of miRNAs is sufficient to bypass the need for specific differentiation factors.

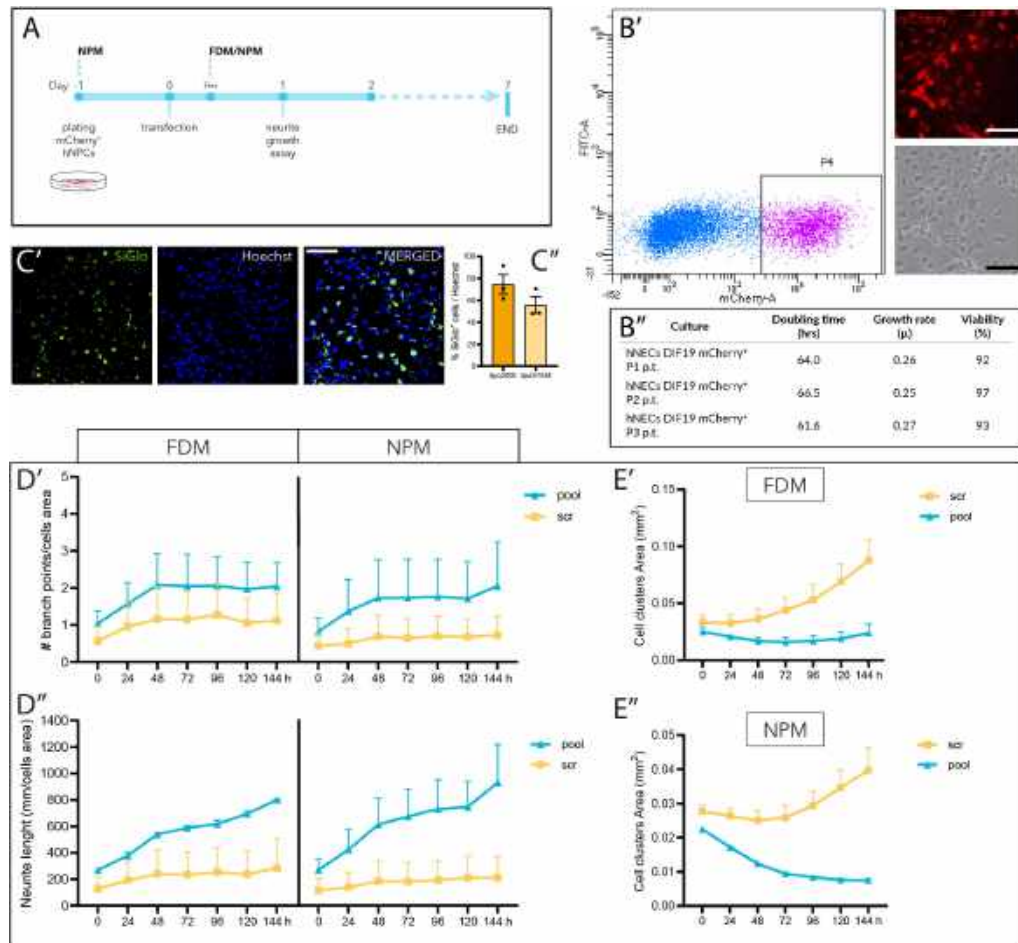


Figure 3.7 - The effect of the pool of 11 miRNAs in human iPSCs correlates with a pro-neural differentiation phenotype observed in mouse cells. (A) Schematic representation of the differentiation protocol. (B') FACS sorting gate of hNPC transduced with a lentivirus harboring EF1 α -mCherry; on the right, a representative image of sorted mCherry⁺-hNPCs is reported (above: red epifluorescence, below: brightfield). (B'') Table with growth and viability values for 3 passages of mCherry⁺-hNPCs after cell sorting. Scale bar: 100 μ m (C) Immunofluorescence images of mCherry⁺-hNPCs upon transfection with 250nM SiGlo (green) using Lipofectamine 2000. (C'') Number of green fluorescence-positive nuclei over the total nuclei (Hoechst, blue) after transfection with Lipofectamine 2000 (lipo2000; n=3) or Lipofectamine Stem (lipoSTEM; n=3). Scale bar: 100 μ m (D' and D'') Cumulative curve normalized on cell area (area of the acquisition field occupied by cells) of the number of branch points (D') and neurite length (D'') for mCherry⁺-hNPCs plated in FDM (left graphs) or NPM (right graphs); the respective growth curves are reported for FDM (E') or NPM (E''). Light blue: pool, yellow: scramble. n = 2 wells. Data are represented as mean \pm SEM.

Application of the *in-utero* MB model to assess the therapeutic efficacy of a *pool* of 11 miRNAs

The experimental findings hinted at the potential pro-neurogenic effect of the 11 miRNAs *pool*, prompting the hypothesis of utilizing the *pool* to induce differentiation of the abnormally de-differentiated population identified in MB. The pro-neural differentiation effect of the *pool* was further studied in DAOY cells, a human cell line model of SHH-subtype of MB. *In vitro* experiments were conducted in our laboratory to characterize the effects of the *pool* in this cellular system. For more details, please refer to Annex I. In brief, transfection with the 11 miRNAs *pool* in DAOY cells triggered a differentiation-like response, characterized by reduced proliferation and a shift towards neuronal fate. Quantitative analysis of differentiation markers corroborated this effect, demonstrating that the used miRNAs promote neuronal differentiation in DAOY cell line.

Prior experiments conducted in our laboratory demonstrated that the *in utero* injection of GBM cells gave rise to the formation of glioblastoma tumors over time and can successfully engraft and sustain the formation of a complex TME¹³². A similar approach has also been recently employed by Barbieri et al. with human meningioma tumors, proving that our *in utero* approach can be suitable for different brain tumors¹⁶. These findings encouraged the exploration of this paradigm for studying MB biology, bridging the divide between *in vitro* evidence and pre-clinical studies toward the development of a potential miRNA-based therapy.

Given that MB tumors with a neuronal differentiation profile commonly exhibit a more favorable prognosis with higher survival rate, we aimed to evaluate whether pre-treatment with the 11 miRNAs *pool in vitro* could replicate the differentiation-inducing effects also in our *in utero* model. Therefore, our objective was to determine whether the *pool* of miRNAs could affect MB growth, potentially by promoting neuronal differentiation *in vivo*.

Characterization of the tumor initiation upon in utero engraftment of MB pre-treated with 11 miRNAs pool

DAOY mCherry⁺ cells cultured *in vitro* were transfected with the 11 miRNAs *pool* or *scramble* control and, after 1 day, cells were injected into the embryonic lateral ventricle of the mouse brain at E14.5 according to the protocol described above. Two different miRNAs concentration, [10nM] and [125nM], were tested. These two concentrations exhibited an effect on DAOY cells *in vitro* (see Annex I). A *scramble* control with the same relative concentration was used as a control. Given that the study focuses on an infant brain tumor and knowing that several authors use models centering their analysis at P7 stage^{294,303} and corroborated by Hoffmann's model that showed the highest proliferation for GBM TX at P7 mice, the study was directed towards mice with engraftment in the post-natal stage at P7. This time point corresponds to 14 days after the *in vitro* pre-treatment of DAOY cells (Figure 3.8 – A, for a schematic representation of the experimental procedure). As first goal, we aimed to determine the time length for which the transfected miRNAs persisted within the MB xenografts. Considering that mature miRNAs delivered during transfection may undergo additional dilution due to cell division, especially given the highly proliferative nature of tumor cells, the analysis aimed to assess the dynamics of the 11 miRNA mimics presence within the MB tumors. Embryonic brains were collected at E18.5 and P7 and MB xenografts were manually dissected to extract RNA.

The presence of miRNAs relied on the detection of the human-specific hsa-miR-376b-3p, different from the mouse counterpart and not detectable in mouse-origin tissues. Quantitative real-time analysis confirmed the presence of hsa-miR-376b-3p at E18.5 (4 days p.t.) and remained detectable at P7 (though not significant), as shown in Figure 3.8 – E.

Because the structure of the mouse brain is not fully developed at E14.5, the ongoing development can eventually facilitate communication between the ventricles, which might facilitate the movement and engraftment of tumor, injected in the forebrain, in various regions of the host brain. Therefore, I first aimed to assess whether the *in vitro* pre-treatment of tumor cells could result in a distinct tumor tropism of tumor foci throughout the entire brain. Four brains per condition were collected, and the entire brains were sectioned rostro-caudally while rigorously maintaining fixed anatomical references, ensuring that each slice represented the same position in each of the brains (Figure 3.8 – B). The mCherry⁺ red fluorescence was then examined using an epifluorescence microscope and the presence was annotated slide-by-slide, to reconstruct the virtual distribution of tumor foci per each brain. The cumulation of subsequent slides that presented the MB cells signal was considered as a *tumor mass*. Only tumor masses present in more than 5 consecutive slides were considered in the subsequent analyses. The rationale behind imposing this threshold is based on not considering as “tumors” cell aggregates that did not proliferate within two weeks after the injection, thus deeming them as dispensable for the aim of this study. The result is illustrated in Figure 3.8 – C. The map distribution of tumor foci showed that MB cells are able to successfully engraft in different regions of the brain, from the rostral to caudal areas. The distribution of tumor foci was dispersed throughout the longitudinal brain axis (as is also reported in Figure 3.8 – D), with a minor concentration around the lateral ventricles of the forebrain, consistent with the fact that this is the site where the injection was performed. Moreover, this analysis indicated that the *in vitro* pre-treatment did not influence the preferential positioning of MB cells in the host brain, as shown by the comparison of the MB cells transfected with the 11 miRNAs and the controls. This analysis provided a preliminary validation of internal consistency and reproducibility of the *in utero* procedure. This also indicates the reliability of the technique, which ensures the accuracy of future analyses.

The tumor masses were then counted. The treatment with *pool* at [125nM] resulted in a higher number of tumors (Figure 3.8 – F). This finding may seem in contrast with the expectation that the 11 miRNAs *pool* treatment would reduce proliferation of tumor cells. However, when the volume of the MB masses was quantified, it was found that the treatment with the *pool* at [125nM] significantly reduced the volume of the MB masses when compared to the relative *scramble* control (Figure 3.8 – H). The combination of these two parameters suggests that the efficacy of the *pool* treatment becomes apparent at the higher concentration, leading to the development of smaller tumor masses.

Next, cell density was quantified within the engrafted MB tumors, measured by counting human nuclei within several Regions-Of-Interest (ROI) in the TXs. Analysis indicated a higher cell density in the *pool* at [125nM] (Figure 3.8 – G). This result could be attributed to two distinct factors: i) smaller cell nuclei or ii) closer cell bodies and nuclei. Considering the former scenario would be consistent with numerous studies demonstrating that reducing nuclear size correlates with a reduced cancer aggressiveness, as this attribute is associated with nuclear rupture^{59,142}. However, definitive consensus on the precise role of nuclear size in cancer development is

still under debate^{142,270}. The latter possibility would suggest, instead, a potential hypoxic condition ongoing within the tumor mass. Hypoxia is a widely recognized hallmark of the propensity of tumors to metastasize and reinforce their aggressiveness¹²⁶. It is crucial to determine which of the two situations applies in our experimental setting to comprehending the *pool*'s impact on tumor biology. However, as the enquiry into nuclear properties deviates from the scope of this study, the focus shifted to other aspects that can also shed light on this question and ascertain whether the *pool* exerts an effect on proliferation/differentiation of MB cells *in vivo*.

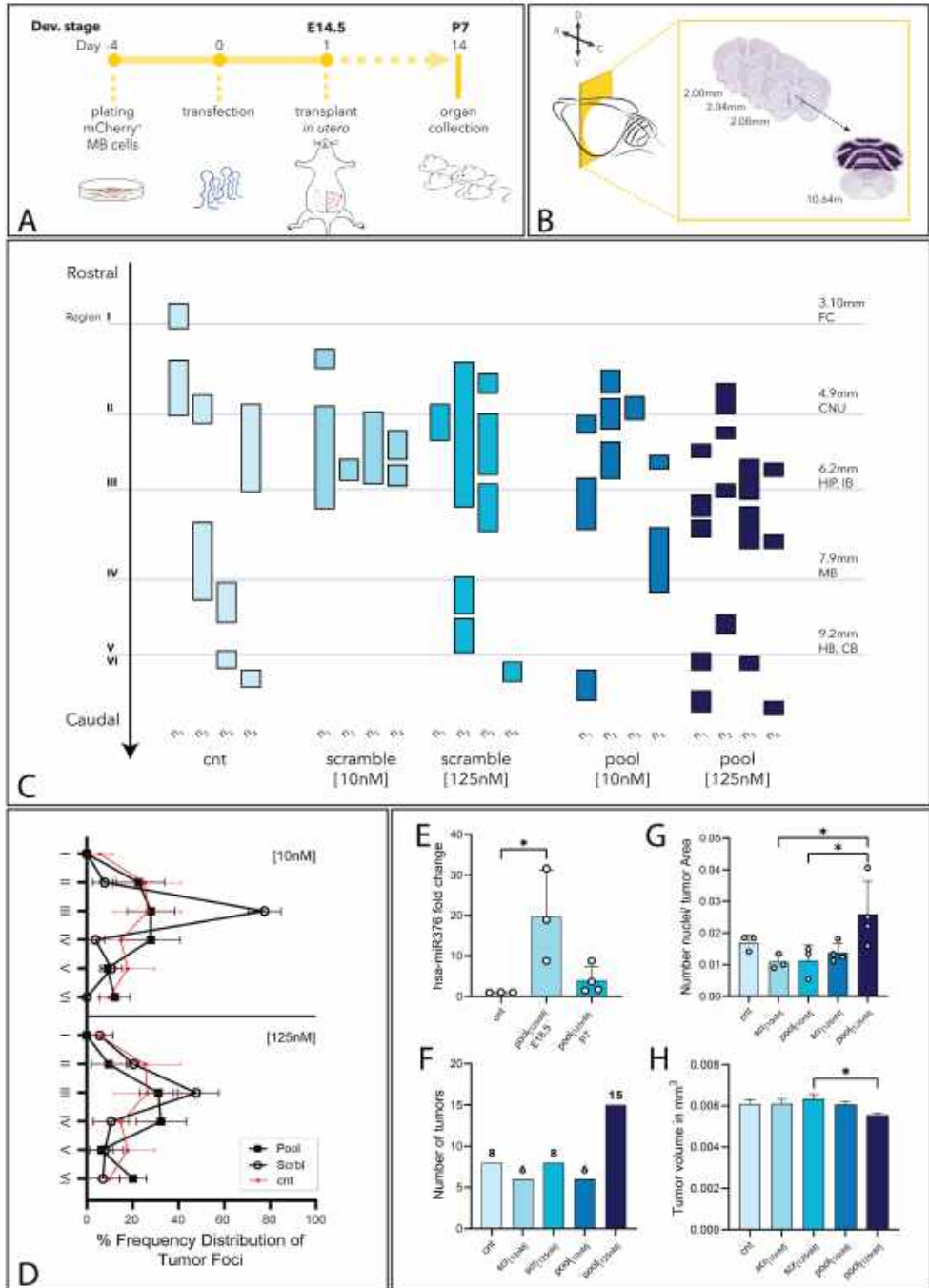


Figure 3.8 - Characterization of the MB xenograft model upon in vitro pre-treatment with the pool of 11 miRNAs. (A) MB cells are plated the day before the transfection (control condition is not transfected). 24 hrs p.t., cells are injected in LV of immune-competent mouse embryos and sacrificed at P7 (corresponding to 14 days after the in vitro transfection for the treated cells). (B) Brain explants are sectioned in coronal planes (40 μ m thick) under fixed, reproducible anatomical parameters. Coronal sections from the Allen Mouse Brain Atlas, 2011⁶¹. (C) Map of the spatial distribution of tumor masses (rectangles) across six distinct brain anatomical regions. Each rectangle represents the set of consecutive brain slices containing a tumor focus. Relative condition is reported below. Only tumor masses with thickness >200 μ m are considered. FC: Frontal Cortex, CNU: Cerebellar Nuclei, HIP: Hippocampal region, IB: Interbrain, MB: Mid Brain, HB: Hind Brain, CB: Cerebellum. n = 4 brains per condition (D) Percentage of tumor foci present in each region relative to the total number of brain tumor foci in pool or scramble [10nM] (up) or [125nM] (down). Both conditions are represented with the percentage relative to the control condition (red line). (E) hsa-miR-376 fold change in pool [125nM] - treated brains at E18.5 (n = 3 brains) or P7 (n = 4 brains) compared to control (n = 3 brains), (F) total number of tumors for control (n = 8 tumors in 4 brains), scramble [10nM] (n = 6 in 4 brains), scramble [125nM] (n = 8 in 4 brains), pool [10nM] (n = 6 in 4 brains), pool [125nM] (n = 15 in 4 brains). (G) Number of cells (cell nuclei) on tumor area in coronal section. n = 4 brains. (H) Volume of tumors for control (n = 8 tumors in 4 brains), scramble [10nM] (n = 6 in 4 brains), scramble [125nM] (n = 8 in 4 brains), pool [10nM] (n = 6 in 4 brains), pool [125nM] (n = 15 in 4 brains). Data are represented as mean \pm SEM, statistical significance revealed by using one-way ANOVA and Tukey's multiple comparisons test; * p value < 0.05.

In vivo proliferative capacity of DAOY cells is impaired upon the 11 miRNAs pool treatment

Transfection with the 11 miRNAs *pool* resulted in a significant reduction of MB cells growth (see Annex I). To ascertain these findings *in vivo*, the proliferative index of tumor cells was assessed by immunostaining the pre-treated MB xenografts in mouse brains. Mice at P6 were injected with BromodeoxyUridine (BrdU), a thymidine analogue that is incorporated in DNA during its synthesis. After 24 hours, mice were euthanized, and immunostaining was performed to determine the proportions of cells that incorporated BrdU. (*Figure 3.9 – C*) To further address proliferation potential of tumor masses, engrafted MB cells were co-stained with Ki67, a protein that localizes in the nucleus of cells in proliferative state. This marker is also employed in diagnosis and prognosis of tumoral aggressiveness in a direct fashion: the higher the percentage of cells, the more aggressive the tumor is considered⁶⁶. Co-localization of the BrdU and Ki67 signals indicates that the labeled cells were replicating 24 hours before sacrifice and persist in their proliferative state at the time of sacrifice.

Brain slices were stained for the two markers, and the number of BrdU⁺ and/or Ki67⁺ cells was normalized to the total number of mouse cells within the TX ROI. Since the primary effect of the *pool* was observed only at the higher concentration of the 11 miRNAs, we focused exclusively on the 125nM condition. Interestingly, the miRNAs treatment led to the reduction of the proportion of both Ki67⁺ and BrdU⁺ cells compared to the scramble (*Figure 3.9 – A, B, D, E*). Analyses of the double staining for the two markers led to the same conclusion (*Figure 3.9 – F*), providing further support to this observation. This result confirms the *in vitro* data and supports an anti-proliferative role of the 11 miRNAs in MB TX *in vivo*.

To further validate these findings and gain a broader understanding of the miRNAs impact on tumor biology, it is essential to assess the differentiation status of tumor masses. This analysis can reveal whether the effects extend beyond proliferation control. That could influence the differentiation program, as demonstrated *in vitro*. Currently, data regarding tumor differentiation is still being collected and analyzed. Once complete, this data will provide insights into the ability of the 11 miRNAs *pool* to modulate tumor cell differentiation and potentially suppress tumor progression.

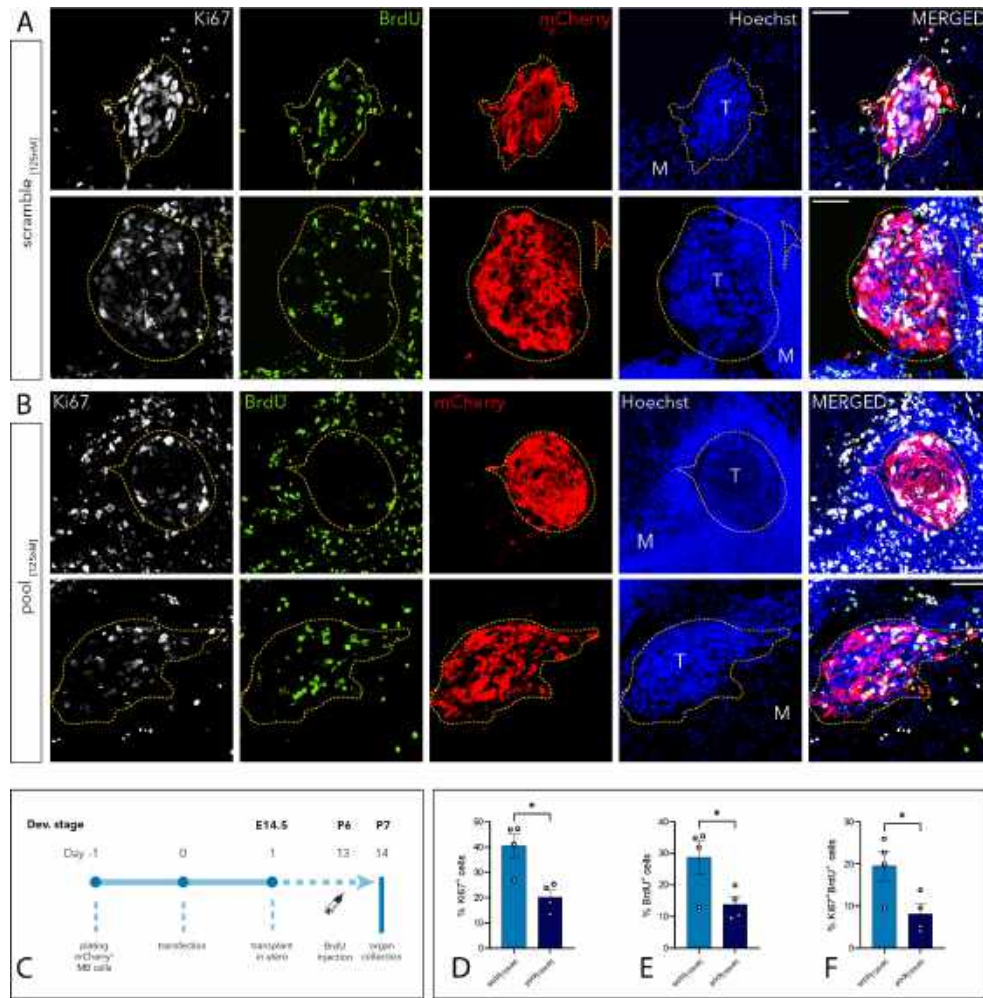


Figure 3.9 - The pool of 11 miRNAs reduced the number of proliferating cells in MB TXs. (A and B) Immunofluorescence images of cryosections in coronal plane of P7 brains. Scale bar: 100µm. Dashed lines indicate tumors borders. (C) Experiment diagram of BrdU injection. (D, E and F) Percentage of number of Ki67⁺, BrdU⁺ and Ki67⁺/BrdU⁺ double-positive cells on the total nuclei within the TX area. n = 4 brains. Data are represented as mean ± SEM, statistical significance revealed by using t-test; * p value < 0.05.

Analysis of MB xenografts invasive patterns indicates mesenchymal-like transition

Cancer cell adaptation to hypoxic conditions¹⁵⁰ has been demonstrated to modulate the proliferation and fate of CSCs in MB¹²⁶. CSCs are characterized by a high capacity to evolve in EMT¹⁵⁰, a process which leads the stem cellular compartment to re-initiate the tumorigenesis or mobilize into metastatic processes³²⁹. In fact, EMT features are directly correlated to high aggressiveness and invasiveness in solid tumors²⁰⁸. Remarkably, our model demonstrated a diverse range of tumor cell infiltration patterns, spanning from cohesive collective cell migration to mesenchymal-like migration of single cells (Figure 3.10 – B' and Figure 3.10 – B''). The control group demonstrated an equal representation of both invasive and non-invasive phenotypes (Figure 3.10 – C'), suggesting that a distinct prevalence for either invasive or non-invasive behaviour of transplanted MB cells is not expected. These observations align with the inherent heterogeneity of tumor cells and the multiple factors that influence their motility, making more likely that the probability of observing a particular phenotype is random. In contrast, a dose-dependent increase in the representation of non-invasive morphology was observed

in samples treated with the *pool* (Figure 3.10 – A' and Figure 3.10 – A''), as compared to their respective *scramble* controls (*pool* [125nM] $\chi^2 = 7.66$, $p = 0.0056$; *pool* [10nM] $\chi^2 = 38.86$, $p < 0.001$). The percentage of the observed morphologies and the respective dataset are reported in Figure 3.10 – D' and Figure 3.10 – D''. Although, this observation requires further analysis of roundness versus irregularity shape, which is currently underway, this finding is intriguing as it points toward a possible role of the 11 miRNAs to prevent EMT characteristics. To further elucidate whether tumor mass behaviour relies on deterministic versus probabilistic model, we are currently including immunohistochemistry analyses against EMT markers in our study.

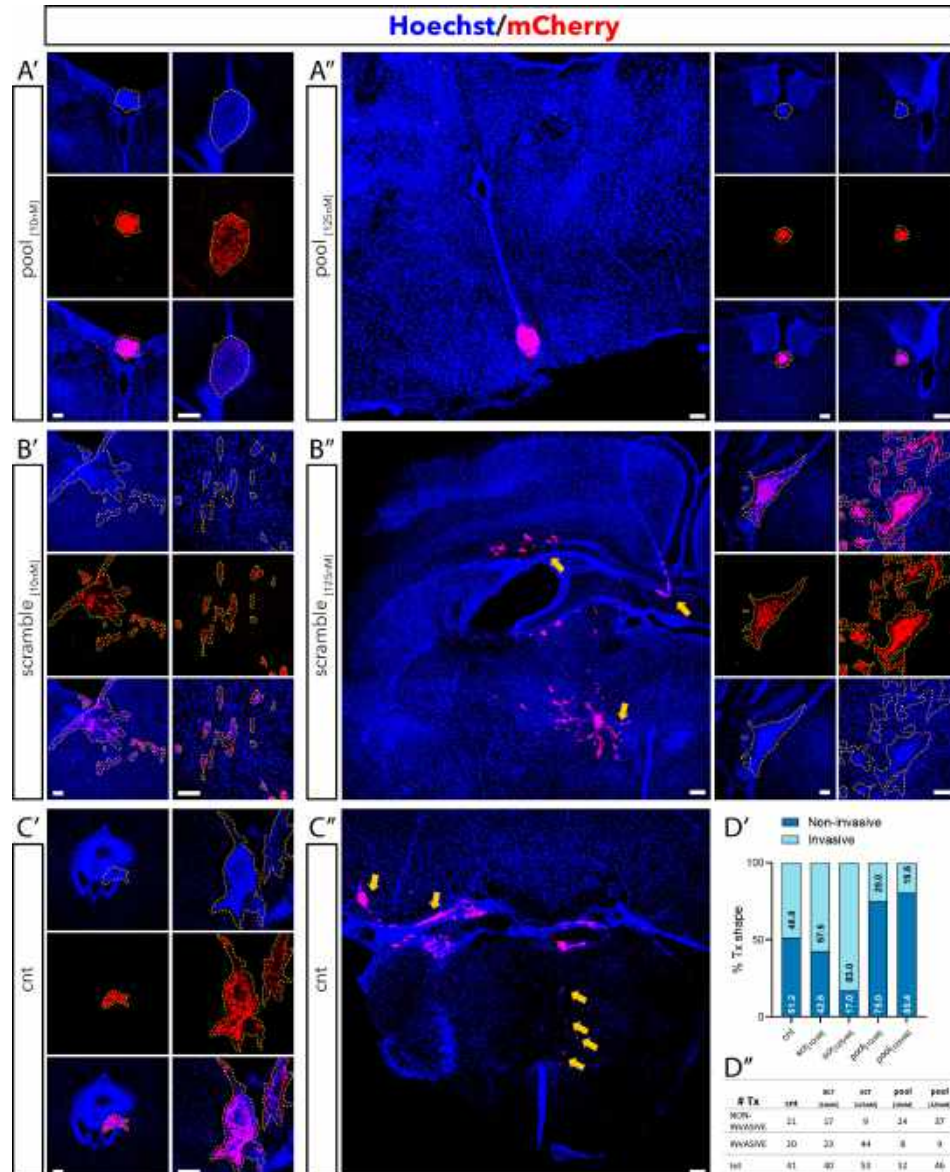


Figure 3.10 - TXs exhibit a morphological shift to a less invasive phenotype following treatment with the pool of 11 miRNAs. (A, B and C) Immunofluorescence images of cryosections in coronal plane of P7 mice showing rounded shape commonly observed for *pool* – treated samples (A' – [10nM] and A'' – [125nM]) as opposed to the invasive-like patterns in *scramble* (B' – [10nM] and B'' – [125nM]) or control (C' and C''). High-field images showing the broadened diffusion of TX borders in *scramble* and control (B'' and C'') indicated with yellow arrows, in comparison to the spherical morphology of *pool* (A''). Scale bar: 200 μ m. Dashed lines indicate tumors borders. (D') Percentage of shape category found relative to the total number of sections considered in the indicated condition (values are reported within the bar). The original dataset number is reported in (D'').

CHAPTER 4 Discussion & Conclusions

Cancer modeling is crucial for elucidating cancer biology and evaluating therapeutic interventions. Despite being well-established, *in vitro* models inadequately mimic at systemic level the TME and all the factors that govern cancer dynamics and CSCs involvement^{293,129}. Animal models offer a more comprehensive approach, but lack realistic human-specific cancer behaviour^{190,188,161}. On the other hand, xenograftments of human tumor cells introduce human-specific players, but the requirement of immunodeficient mice, alters tumor growth characteristics and inflammatory conditions involved in tumor development and progression^{77,21}. Moreover, the immunocompromised host eliminates the possibility of studying the immune system reaction to a tested therapeutics, leading to the high failure of pre-clinical studies^{60,190,106}. Pediatric oncology is more influenced by these limitations, as the use of adult animals or patient-derived tissues may capture later stages of the disease, deviating from natural pathology progression²⁹³. MB, as a brain cancer primarily affecting children, underscores the critical need for refined models.

This thesis implemented and validated a new mouse model for human MB by *in utero* engraftment of human MB cells in the embryonic brain of immunocompetent mice, thus addressing the limitations of existing models of MB.

This was achieved by leveraging the natural immune suppression of mouse embryos, in which the adaptive immunity matures after birth^{206,85}. By introducing in wt mouse embryos a human cell line of SHH-MB, the DAOY cell line, cells were shown to form tumor masses which proliferate in the mouse tissue and develop functional connection within the host tissue. A previous approach, developed by Semenkow et al.²⁷⁵, reported the generation of an immune-tolerant mouse model of glioblastoma. However, such a model was generated by chemical suppression of the T-cell activation since the first week of postnatal life. As a result, this model can not be considered fully immunocompetent and does not adequately address the aforementioned limitations of animal models in replicating the complexities of the original system. Noteworthy, T-cells play a crucial role in TME. Their suppression by TAMs is necessary in order to permit immunosuppression, by the production of growth factors, cytokines, and chemokines and establishing angiogenesis^{229,231}. However, T-cells can also indirectly limit the angiogenesis^{229,302}. Their eradication before the tumor implantation is therefore detrimental to the study of tumorigenesis. Overcoming these limitations, a previous study from our group¹³² has developed a mouse model of orthotopic xenotransplantation of human glioblastoma in wt mouse embryos. This thesis leverages this model to implement and validate the first immunocompetent orthotopic model of MB in wt mouse embryos, establishing a human-based system that reflects the embryological origin of the tumor.

Our model shows the presence of MG and macrophages associated to the tumor foci which also showed a morphology typical of activation. Moreover, MG-like cells exhibited the ability to identify and engulf foreign cells, consistent with their established phagocytosis role. TAMs, which are abundant in the SHH subgroup of MB¹⁹⁴, have emerged as promising therapeutic targets. However, their role in MB remains a subject of debate, with some studies supporting their pro-tumorigenic role^{163,231}, akin to their established function in glioblastoma⁴⁷, while others suggest a potential tumor-suppressive role in MB^{197,337}. Hence, further elucidation

of the mechanisms underlying TAM involvement in MB is fundamental. The generation of the presented model enables the possibility to elucidate the reciprocal role of MG and TAM cells in either promoting or hindering MB expansion. Furthermore, a complex interplay exists between angiogenesis and TAMs. As fundamental part of the TME, TAMs promoting tumor-supportive angiogenesis or suppress it depending on their specific function^{122,245}. For instance, TAMs produce pro-angiogenic factors and degrading the ECM²²⁹, triggering the vasculature proliferation. Additionally, TAMs are known to accumulate in hypoxic tumor regions, where they indirectly induce VEGF secretion and where HIF1 α , a key regulator of macrophage-endothelial cell interactions, represents another layer of linkage between vasculogenesis and immune-cells in the tumor. Calabrese et al.³⁷ showed in *in vivo* orthotopic xenografts that tumor growth is also linked to functional vasculature thanks to the presence of CSCs adjacent to the endothelial cells, and that co-injection of CSCs with primary-human endothelial cells enhanced this growth³⁷. Using our model, we show the colocalization of endothelial marker CD31 and MB CSCs marker Nestin^{127,284,37}. Many other aspects remains unknown about the fine composition of CSCs niches and molecular mechanisms controlling their stemness, dormancy and chemo-immuno resistance, particularly in relation to their ability to evade detection within the abnormal tumor-induced vasculature¹⁴. Different authors^{327,229,14} proposed the CSCs as promising therapeutic target, to eliminate this subpopulation through the angiogenetic component of the CSCs niches. However, the most recent experimental evidence supporting the causative association between CSCs and perivascular niches in MB remains the last one (as far as the author found)^{327,14}. Further studies are needed to finely understand the key players of the angiogenesis-CSCs-TAMs circuit in the TME. Our model, by mimicking TME of human MB in an immune-competent mouse, could offer valuable perspectives.

A major obstacle in testing brain tumor treatment is overcoming the BBB, which hinders the delivery of therapeutic drugs due to its impermeability to large molecules³¹². Notably, SHH-subtype of MB is characterized by an intact BBB, as formally demonstrated by the work of Phoenix et al.²³⁷, making it less responsive to treatment compared to MB subtypes with a more permeable BBB, such as the WNT subtype²³⁷. Therefore, exploring strategies to selectively target the BBB within the tumor zones could enhance tumor accessibility and treatment efficacy. Our study revealed the presence of the BBB. Indeed, we were able to show the formation of tight junctions between endothelial cells, particularly Claudin-5, within and surrounding the tumors. The vascular morphology observed in our study closely resembles that described by Phoenix et al.²³⁷, suggesting the possibility of similar non-permeability characteristics. Though our model did not definitively prove BBB formation and functionality, its future exploitation would open up new avenues for therapeutic delivery to the tumor.

As related to research and development of new therapies for MB, growing evidence underscore the significant role of miRNAs in the earliest stages of brain development and how the dysregulation of specific miRNAs contributes to pathological adult and pediatric MB. The *in vitro* screening by Luo et al.¹⁸⁴ revealed downregulation of the 14q32 miRNA cluster, specifically miR-376b, miR-370, miR-411, and miR-708 in SHH-subtype MB. Microarray analysis in SHH-subtype of MB from human samples found downregulation of many miRNAs of the same cluster. Among these miRNAs, in particular miR-124, miR-127, miR-134, miR-139, miR-370, miR-382, miR-411¹⁸³. A distinct miRNA signature was identified MB CSCs, with miR-135 significant

downregulated¹²⁸. Reintroduction of the miR-135 with a viral construct showed the efficient downregulation of its target *Arhgef6*, notably involved in MB CSCs, highlighting it as a potential therapeutic target for MB¹²⁸. When reintroduced, miR-370 reduced glioma proliferation and progression¹⁸¹.

The functionality of miRNAs expands beyond their role in cancer, reaching the complex pathways involved in brain development and functioning. By viewing brain cancer as a brain tissue that has escaped the control of normal regulatory pathways, the study of miRNAs in healthy brain tissue remains highly informative.

For example, miR-134 is recognized for its ability to induce neuronal differentiation by suppressing self-renewal transcription factors²⁹⁹. In glioblastoma, miR-134 levels are significantly reduced, and restoring its expression has been shown to inhibit cell proliferation²²⁰. miR-218, implicated in CNS pathologies³⁰⁰, is also downregulated in MB. Restoring miR-218 expression in MB cell lines has demonstrated significant growth inhibition³⁰⁵. miR-708 plays a role in neural differentiation and exhibits dual functionality as both a tumor suppressor and an oncomir⁴². Additionally, it targets vimentin, an intermediate filament protein associated with cancer progression. And also miR-135 regulates angiogenesis by targeting FAK, regulator of VEGF expression⁷⁰.

It has been proposed that miRNAs can be employed to modulate the expression or activity of one or more other miRNAs^{70,42}. In 2017, Pons-Espinal et al.²⁴² showed the synergic effect of 11 miRNAs to induce the differentiation of murine adult neural stem cells. A significant portion of the miRNAs included in the combination had been identified as potential players in MB by several previous researches.

Here, we exploited the synergistic effects of the 11 miRNAs *pool* and validated the efficacy of this treatment to induce differentiation of MB cells.

Initially, to confirm the pro-neural effect of 11 miRNAs in a human setting, we assessed the impact of the 11 miRNAs *pool* on human iPSCs-derived NPCs, representing a 'molecular blank state' where evaluate its potential effects in a human context. Subsequently, we validated and established the transfection conditions of the 11 miRNAs in the DAOY cell line model of MB (subgroup SHH). As expected, the *pool* was able to reduce *in vitro* the proliferation and migration of the human iPSC-derived NPCs, and to exert a pro-neural differentiation of the cells.

To confirm the ability of the 11 miRNAs *pool* to reduce tumor growth *in vivo*, we performed *in utero* orthotopic xenograftment in immune-competent mouse embryos. Following transfection with the *pool* at [125nM], engrafted MB cells diminished their proliferative potential resulting in smaller tumors volume. This conclusion is in line with the *in vitro* studies (Annex I) and indicated that the *pool* could slow down the tumorigenesis of MB cells *in vivo*. As related to proliferation, however, further validation needs to be performed. The proliferative potential of MB cells was performed by considering BrdU and Ki67, common markers used to evaluate the duplication and the proliferative potential in cancer cells, respectively. Ki67 protein is detectable during all active phases of the cell cycle (G1, S, G2, and mitosis), but is absent in cells in the G0 cell cycle phase. The observed volume reduction could be attributed to either induction of CSCs differentiation or their quiescence. The quiescence is a characteristic mainly linked to the CSCs population^{71,93,102}. On the other hand, BrdU can be incorporated in the DNA not only during the S phase of cell cycle, but also in case of DNA repair or by general DNA-remodeling events. These events are extremely common in quiescent CSCs to respond to therapeutic agents^{93,102}. If the 11 miRNAs induce quiescence in tumor cells, a rise in BrdU incorporation could be expected.

On the contrary, a reduction in BrdU⁺ cells was observed, indicating that the cells were likely undergoing a differentiation process rather than quiescence. Although the cell cycle index (determined by BrdU-Ki67⁺/BrdU⁺ cells) displayed only a non-significant trend (data not shown), increasing the sample size could increase the statistical power of this analysis. Either quiescence or differentiation would be the underlying mechanism, the administration of BrdU approximately 14 days after treatment might have occurred beyond the time window when BrdU incorporation could effectively capture treatment-induced DNA remodeling or cell cycle exit. Investigating earlier time points for BrdU assay in subsequent experiments could provide deeper insights into the fate determination of MB upon the *in vitro* treatment. We also reported an increase in cell density within the tumor masses of sample treated with *pool* at [125nM]. The observed reduction in nuclear size could explain the increase density and would be consistent with decreased cell proliferation. While the role of nuclear size in tumorigenesis remains a topic of debate²⁷⁰, there is a general consensus that higher nuclear size in MB tumors correlates with increased anaplasia, a highly de-differentiated malignant condition used for patient stratification^{100,318}.

Our results revealed a higher number of tumor masses upon treatment with the *pool* at [125nM] compared to other conditions. This result seems to be in apparent contradiction with the proposed therapeutic role of miRNAs. Although it can not be excluded that the effect of the treatment with several miRNAs together is different from the effect of a single one, this observation would be in agreement with previous data showing that the treatment with a single miRNA *in vivo* can induce the dissemination of tumors in non-SHH MB¹⁵. The synergistic effect of a combination of miRNAs in an immunocompetent mouse has never been evaluated, thus it is plausible that this *pool* induces a slowing down of growth, in association with an increased risk of metastasis. Indeed, the engraftment was found to occur with no discernible difference between treated and control groups. Hence, the observation of larger tumor masses with smaller volumes suggests the possibility that engraftment remains constant, but the proliferation capacity of each engrafted cell is reduced. This could lead to the fragmentation of the overall tumor mass when viewed as a single entity.

This “pro-metastatic” behaviour of the *pool* was unexpected given the established role of several miRNAs composing the *pool* in suppressing metastasis. In fact, miR-411 downregulates vimentin, a protein associated with metastasis^{70,42}. Additionally, miR-124 is known to target Sox9, a key driver of MB metastasis^{315,211}, and EMT transcription factors¹³⁹. Mir-127, whose expression is regulated by Claudin-5, is downregulated in several brain metastatic tumors and act as a functional tumor suppressor¹⁸⁷. Metastasis are interlaced with EMT, which initiates cellular remodeling, including morphological changes, which are seldom associated with spherical/shapes. The observation that treated samples rarely exhibit typical invasive behaviour, preferring a rounded morphology, provides indirect support for the hypothesis that tumor fragmentation is not a result of metastasis. Measuring the compactness index²⁹ of tumor morphologies would provide a formal assessment of the degree to which control and treated samples differ in terms of morphology.

Regardless of the efficacy against metastasis, this approach offers a valuable tool to evaluate the collective role of miRNAs in the *pool* for metastasis, a crucial question to address. In sum, **while the specific mechanism of the 11 miRNAs on proliferation and metastasis remains unclear, this study provides the first evidence of synergistic action of a combination of miRNAs in MB *in vivo*.**

The exploration of these miRNAs as a concrete therapeutic approach is still in its preliminary stages. Significant challenges remain in the development of miRNA-based therapeutics. Firstly, effective and safe delivery strategies for miRNAs have yet to be established, hindering their clinical translation^{60,315,133}. To date, no miRNA-based therapies have gained FDA approval. Moreover, for brain cancer specifically, the ability to cross the BBB remains a significant hurdle^{237,315}. Secondly, further research is needed to elucidate the molecular mechanisms by which these miRNAs exert their effects. This includes identifying the genes that these miRNAs target and the mechanisms by which they repress gene expression. The re-purification of engrafted MB cells (i.e. by FACS) could provide a unique perspective into their molecular identity post-implantation. This would dissect not only the intrinsic influence of the host environment but also reveal the distinct molecular signatures induced by the treatment on these cells. It is essential to emphasize the unique value of analyzing engrafted cells rather than studying them under *in vitro* settings. A comparison of gene- and protein-expression profiles between pre-treated MB cells and the respective controls from *in utero* engrafts can pinpoint the specific molecular pathways modulated by the 11 miRNAs. This, in turn, allows us to understand the mechanism through which MB cells adapt and evolve within the living organism. Therefore, identifying the targets of 11 miRNAs *pool* in MB engrafted cells could serve as a pivotal guide, enhancing the precision and focus of our subsequent studies. To further elucidate the compensatory potential of synergistic action, an intriguing approach could be to deplete the targets primarily targeted by miRNAs and involved in the described tumor-related mechanisms. Assessing whether the 11 miRNAs *pool* maintains its impact would provide valuable insights into the ability of synergistic action to mitigate the effects of missing molecular players.

Functional studies of miRNAs face challenges due to the absence of physiological conditions, as miRNAs typically act in low amounts and target multiple genes concurrently. In our model, the effect was exerted at the higher dosage, the quantification of has-miR-376 in brain tissue suggest that miRNAs become significantly diluted in the tissue relatively fast, probably due to the high proliferation rate observed also in normal conditions. Nevertheless, it is established that upon transfection, mimics are incorporated into the RISC complex and act almost instantaneously. Hence, even in the absence of miRNAs, their potential impact might persist over time, or it is plausible that the remaining low concentration two weeks post-treatment is exerting an effect with a more physiological fashion. This method could therefore provide a novel strategy for deciphering gene regulatory networks influenced by miRNA-mRNA interactions in human tumor molecular networks.

Ultimately, our model can be viewed as a platform for versatile purposes. For example, the model can be readily adapted to investigate other MB subgroups, such as group 4, where only a limited number of models have been developed^{237,260,129}. Moreover, the utilization of human iPSCs, achieved through either patient reprogramming or genetic modification, can be applied to establish personalized disease models. Subsequently, the findings from these models can be firstly validated in animal models and then confirmed in clinical tests for their relevance and translatability. Overall, this pilot study provides proof-of-concept for researchers engaged in human MB cancer research and the study of miRNA interactions and sets the stage for further development in the field.

Limitations and future perspective

- For the *in vitro* validation of the 11 miRNAs, we omitted the consideration of a control for the transfection vehicle. Nevertheless, incorporating a mock control would more accurately depict the baseline condition of the transfection procedure.
- Given that the adaptive immune system is recognized to reach full development after the first month postnatal, it becomes crucial to assess whether this complete maturation of the immune system would lead to the rejection or absorption of the engraftment. Therefore, expanding the analysis would provide valuable insights in this direction.
- To assess the differentiative potential exerted by the 11 miRNAs *pool*, it is essential to evaluate the expression of neuronal markers in the tumor masses and compare the expression level between treated and control groups.
- For similar reasons, the assessment of EMT marker expression is of interest to determine whether the observed differential preferences in the morphological shape of the tumor are attributable to the EMT remodeling process.
- The TME is intricately shaped by the composition of TAMs. Investigating the potential influence on the relationship between TME and TAMs orchestrated by the miRNAs could provide novel insights in this field.
- It would be intriguing to optimize the 11 miRNAs *pool* for a human-specific context. Utilizing scRNA-seq analysis could help identify the miRNA profiling of CSCs in human MB cells, specifically DAOY cells in our study. By comparing this profiling to that of human iPSCs undergoing canonical differentiation, we can refine miRNAs primarily involved in the differentiation of human NPCs and highlight the differences with (undifferentiated) MB cells. Consequently, this approach may validate a freshly customized *pool* of miRNAs tailored specifically for humans, potentially enhancing its effectiveness in supporting the differentiation process.
- Separate the engrafted MB cells upon transplantation is crucial to understand their true molecular identity and response to the treatment. Analyzing their coding and non-coding profiles can reveal key information about how MB cells adapt and evolve in the living organism and delve into the specific effects of the 11 miRNAs for identifying potential targets for future studies.

CHAPTER 5 Experimental Procedures

Human iPSC maintenance

Human Episomal iPSCs (Gibco, A18945) were cultured at 37°C, 5% CO₂ and ambient oxygen level on Geltrex-coated plates in mTeSR1 medium (STEMCELL Technologies, 05850). For passaging, hiPSC colonies were incubated with ReLeSR (STEMCELL Technologies, 05872) for 5 min. Pieces of colonies were washed off with mTeSR1 and gently resuspended in mTeSR1 supplemented with 10μM Y-27633 (STEMCELL Technologies, 72304) for the first hour after the seeding. A daily medium change followed. Cells were routinely tested for mycoplasma.

Human Neurons generation

Human Neurons were generated following according to the manufacturer's instructions. Briefly, iPSCs were dissociated into single cells using StemPro Accutase Cell Dissociation Reagent (Life Technologies, A1110501) and plated within the concentration of 1x10⁶ single iPSCs/well into a single well of a Geltrex-coated 6-well plate in STEMdiff Neural induction medium with SMADi (STEMCELL Technologies, 05833). Medium was changed daily. For passaging, human NPCs were washed with 5ml of DMEM/F-12 and incubated with StemPro Accutase Cell Dissociation Reagent for 4 min. Cells were washed off with DMEM/F12, centrifuged for 5min at 300g and resuspended in STEMdiff Neural induction medium with SMADi. After the third passage, cells were expanded in STEMdiff Neural Progenitor Medium (STEMCELL Technologies, 05833) or further differentiated. For neural differentiation, cells were plated in Poly-L-Ornithine (PLO)/laminin coating at a concentration of 1.25x10⁴ cells/cm² in STEMdiff Neural induction medium with SMADi. The following day, the medium was changed to STEMdiff Forebrain Neuron Differentiation Medium (STEMCELL Technologies, 08600) (FDM) and daily full medium change was performed. Once confluence was reached, cells were detached as previously and plated in STEMdiff Forebrain Neuron Maturation Medium (STEMCELL Technologies, 08605). Seeding concentrations of 3-4x10⁴ cells/cm² was preferred for short-term cultures (< 30 days of maturation), or 5-6x10⁴ cells/cm² for long-term cultures (> 30 days of maturation). Medium was changed every other day. Cell counting and viability estimation was performed with automated Cell Counter (Cell Drop, DeNovix). Viability is calculated as:

$\frac{\text{number of viable cells}}{\text{total number of cells}} \cdot 100\%$. Growth rate (μ) was obtained by: $\mu = \frac{\ln\left(\frac{\text{number of cells seeded}}{\text{number of cells harvested}}\right)}{\text{hours of growth}} \cdot 24\text{hrs}$. Doubling time (t_d) was calculated with the formula: $t_d = \frac{\ln(2)}{\mu} \cdot 24\text{hrs}$.

Human NPCs transfection and Neurite Outgrowth assay

mCherry⁺ human iPSCs-derived NPCs (hNPCs) were obtained with transduction of EF-α1_mCherry lentivirus. Positive clones were selected by fluorescence activated cell sorting (FACS) on BD FACS Aria III cytofluorometer to obtain a pure population, using a non-transfected sample of NPCs as negative control to set the gating strategy for cell sorting. For transfection, cells were plated in standard culture condition (37°C, 5% CO₂, ambient O₂ levels) within the concentration of 2x10⁴ /cm² in each single well of a Geltrex-coated 24-well plate in

STEMDiff Neural Progenitor Medium (NPM – referred in the main text as Neural Proliferation Medium). The day after, cells were transfected. For testing the optimal transfection conditions, siGlo Green transfection indicator (Dharmacon, D-001630-01) was transfected at a final concentration of 250nM in a ratio 1:1 using Lipofectamine Stem Transfection Reagent (Invitrogen, STEM00015) or Lipofectamine 2000 Transfection Reagent (Invitrogen, 11668019) in MegaCell RPMI-1640 medium (Merck, M3817). For Neurite Outgrowth assay, cells were transfected with a *pool* of mimics or *scramble* negative control (Dharmacon, CN-001000-01-05) at a final concentration of [250nM] using Lipofectamine 2000 Transfection Reagent in ratio 1:1. Transfection medium was replaced with fresh medium (NPM or FDM) after 5 hours. The list of miRNA mimics is reported in Table 2. Analysis for Neurite Outgrowth started 24 hours p.t. using IncuCyte S3 (SARTORIUS) with Incucyte Neurotrack software module. Plates were scanned every 6 hours over a 144 hours period using a 10x objective. Nine images per well were captured and images were analyzed for neurite length, branch points, cell-body clusters number and area. The masks/filters adjustment for Neurotrack red Fluorescent image analysis were as follows: Segmentation mode: Texture; Hole fill: 0; Adjust size: -5 μ m; Min cell width: 8 μ m; Neurite filtering: Best; Neurite sensitivity: 0.5 μ m; and Neurite width: 2 μ m. The following parameters were quantified: Cell-Body Clusters (CBC) = total number of cell body clusters/area of image field; Cell-Body Cluster Area (CBCA) = sum of areas of all cell-body clusters pooled/area of image; Neurite Length (NL) = sum of lengths of all neurites pooled/ area of image field; Neurite Branch Points (NBP) = total number of branch points/area of image field. Raw data were collected from the instrument and further analyzed.

Table 2 - miRNA mimics used in the experiments.

miRIDIAN microRNA	Reference Dharmacon	Sequence
mmu-miR-124-3p	C-310411-05-0002	5'-UAAGGCACGCGGUGAAUGCC-3'
mmu-miR-127-3p	C-310616-07-0002	5'-UCGGAUCCGUCUGAGCUUGGCU-3'
mmu-miR-134-5p	C-310568-07-0002	5'-UGUGACUGGUUGACCAGAGGGG-3'
mmu-miR-135a-5p	C-310576-05-0002	5'-UAUGGCUUUUUAUUCCUAUGUGA-3'
mmu-miR-139-5p	C-310822-01-0002	5'-UCUACAGUGCACGUGUCUCCAG-3'
mmu-miR-218-5p	C-310397-07-0002	5'- UUGUGCUUGAUCUAACCAUGU-3'
mmu-miR-370-3p	C-310409-05-0002	5'-GCCUGCUGGGGUGGAACCUUGU-3'
hsa-miR-376b-3p	C-300741-03-0002	5'-AUCAUAGAGGAAAAUCCAUGU-3'
mmu-miR-382-5p	C-310607-05-0002	5'-GAAGUUGUUCGUGGUGGAUUCG-3'
mmu-miR-411-5p	C-310987-01-0002	5'-UAGUAGACCGUAUAGCGUACG-3'
mmu-miR-708-5p	C-310391-05-0002	5'-AAGGAGCUUACAAUCUAGCUGGG-3'

Animal care

None of the animals used in our experiments had been previously used for other procedures. All subjects were test- and drug-naïve. The animals presented a healthy status and were employed independently of their gender for each experiment. Mice were housed under standard conditions at the animal facility of Istituto Italiano di Tecnologia (IIT), Genoa, Italy. All experiments and procedures were approved by the Italian Ministry of Health (Permits No804/2020-PR Ref. # IIT-186) and IIT Animal Use Committee, in accordance with the Guide for the Care and Use of Laboratory Animals of the European Community Council Directives. Wild-type CD1 females

and males were crossed, and mouse embryos were used for *in utero* xenotransplantation procedure at the indicated day *post coitum* (dpc). The vaginal plug was defined as Embryonic day 0.5 (E0.5).

In utero transplantation

At the day of injection, cultured cells were detached with Trypsin, counted, and re-suspended in sterile PBS at final concentration of 50.000 cells/ μ l and 10% sterile Fast Green (1% stock solution in H₂O, Fast Green FCF, Sigma Aldrich). Surgery of a pregnant time-mated wt dam (14.5 dpc, E14.5) was performed under standard anesthesia conditions (2.5% Isoflurane (Isocare, Animalcare) and 1.5% oxygen). The pregnant dam was placed on a heating plate (37°C) exposing the abdomen. Pre-surgically Voltaren (2.5ml/kg bodyweight, Novartis) was subcutaneously injected at the forelimb. Abdomen was shaved, wiped with 70% ethanol and disinfected with Betadine (Superfarma). Laparotomy was performed by a 1.5 cm long cutaneous incision and followed by a slightly smaller incision of the abdominal wall next to the *linea alba* to expose the uterus from the abdominal cavity. Single cell suspension was loaded to a pulled-glass capillary (Sutter Instruments, I.D.: 0.69 mm, O.D.: 1.2 mm, Length: 10 cm; BF120-60-10 and Micropipette Puller P-97, Sutter Instruments) and directly connected to the microelectrode/pipette holder (5430-1.0, MPH6S, WPI). Glass capillary was aligned perpendicular to the telencephalon of the mouse embryo *in utero* and injection of the single cell suspension into the lateral ventricle done by 1-2 short manual pulses (vent pressure, ~15 psi (~1.1 bar) (max. 20 psi), Pneumatic PicoPump PV820 – WPI) until the ventricle was filled (1 pulse \cong 1 μ l). During surgery, the uterus was moistened with filtered PBS (Filter Type 17597, 0.2 μ m, Sartorius Stedim Biotech) pre-heated at 37°C. After injections uterine horns were placed back in the peritoneal cavity and the abdominal wall was sutured (VICRYL EP (5/0) V385H; C-3, 13mm, 45cm; Ethicon) and further disinfected with Betadine. Pregnant mice or mothers were sacrificed by cervical dislocation at the indicated times and embryos or pups were decapitated, dissected, and further processed.

BrdU labelling

P6 mice were weighted and injected with 50 mg/kg of BrdU (Sigma-Aldrich) resuspended in phosphate buffer saline (PBS). Intraperitoneal injections of P6 mice were performed with 27-gauge needle to avoid liquid spillage. Mice were sacrificed 24 hours after the BrdU injection. Brains were processed immediately after the sacrifice.

Immunofluorescence and imaging

Immediately after the sacrifice, brains were dissected in cold 1x PBS and rapidly analyzed under stereo microscope (Olympus SZX16 with Olympus U-RFL-T) to define brain with engraftments. Positive and negative brains were post-fixed in 4% paraformaldehyde (Sigma-Aldrich, P6148) O/N at 4°C. The day after, brains were de-hydrated in 30% sucrose at 4°C, cryo-embedded in Tissue-Tek O.C.T and stored at -20°C until use. Coronal cryosections (20 μ m (E18.5-P2) and 40 μ m (P7)) were prepared at the indicated ages and processed for immunofluorescence. Cryosections were re-hydrated in 1x PBS and (when specified) subjected to antigen retrieval with 10 mM citric acid at pH 6.0 for 10 min at 95°C, followed by 20-30 minutes of cooling and permeabilized with progressive steps in 0.3% and 0.1% Triton X-100 in 1x PBS (PBST). Blocking was performed

in 0.1% PBST + 5% normal goat serum for 1 hr at RT. Sections were then incubated with primary antibodies diluted in blocking solution O/N at 4°C. Extensive washing in 0.1% PBST was followed by incubation with secondary antibodies diluted in blocking solution for 2 hrs at RT. Washing steps in 0.1% PBST and then 1x PBS were performed, followed by nuclear counterstain with Hoechst 33258 (1:300 in 1x PBS from a stock solution of 1 mg/ml in dimethyl sulfoxide, DMSO, Sigma Aldrich) for 30 min. Cover-slips were immediately mounted with ProLong Gold Antifade (Invitrogen), air-dried O/N in the darkness, and sealed with nail polish (Electron Microscopy Sciences). For BrdU staining, the procedure was modified by additional incubation, prior to the blocking step, in 2N HCl for 30 minutes at 30.2°C and then washed three times in 1x PBST at RT. All images were acquired using the Nikon A1 and Nikon ECLIPSE Ti. Images were taken with 10x, 20x or 60x (oil-immersion) objective. Table 3 and Table 4 list the Primary and Secondary Antibodies and specification for labeling. In all immunostaining analysis of brain sections, anti-mCherry antibody was added to counterstain the constitutive expression of the DAOY cells.

Table 3 - List of Primary Antibodies used for Immunofluorescence in brain tissue samples.

Antigen	Vendor	Dilution	Antigen retrieval
Anti-BrdU	Abcam (ab6362)	1:100	yes
Anti-CD31	BD pharmigen (550274)	1:100	no
Anti-CD68	Abcam (ab53444)	1:100	no
Anti-mCherry	Abcam (ab206402)	1:500	-
Anti-Claudin-5	ThermoFisher (4c3c2)	1:100	no
Anti-IBA1	Fujifilm (019-19741)	1:500	no
Anti-Ki67	Abcam (ab15580)	1:100	yes
Anti-Laminin	Abcam (7463)	1:500	no
Anti-hNestin	Abcam (ab105389)	1:200	no
Anti-VEGF	Abcam (ab52917)	1:100	no

Table 4 - List of Secondary Antibodies used for Immunofluorescence in brain tissue samples.

Antigen	Vendor	Dilution
Goat anti-rabbit AlexaFluor 647	ThermoFisher (A21245)	1:1000
Goat anti-rat AlexaFluor 488	ThermoFisher (A11006)	1:1000
Goat anti-chicken AlexaFluor 568	Abcam (ab175477)	1:1000
Goat anti-mouse AlexaFluor 488	ThermoFisher (A11029)	1:1000
Goat anti-rabbit AlexaFluor 647	ThermoFisher (A21245)	1:1000

Immunocytofluorescence and imaging

During the experimental passages, human iPSC cells and their differentiated progeny were seeded onto coverslips in 24-well plates and maintained under identical culture conditions as the parent population. The day of fixation, plates were washed three times with 1x PBS at RT and fixed in 4% paraformaldehyde (Sigma-Aldrich, P6148) for 10-15 min at RT. Fixative was removed by washing plates for three times with 1x PBS and plates were stored at 4°C until use in 1x PBS. For immunofluorescence, cells were permeabilized with 0.1% Triton X-100 in 1x PBS (PBST). Blocking buffer (BB) was prepared in 0.1% PBST + 5% normal goat serum for 1 hr at RT. Primary antibody solution was prepared in BB and coverslips incubated O/N at 4°C, in the darkness. Extensive

washing in 0.1% PBST was followed by incubation with secondary antibodies diluted in blocking solution for 2 hrs at RT. Washing steps in 0.1% PBST and then 1x PBS were performed, followed by nuclear counterstain with Hoechst 33258 (1:300 in 1x PBS from a stock solution of 1 mg/ml in dimethyl sulfoxide, DMSO, Sigma Aldrich) for 15 min. Cover-slips were immediately mounted with ProLong Gold Antifade (Invitrogen), air-dried O/N in the darkness, and sealed with nail polish (Electron Microscopy Sciences). All images were acquired using the Nikon A1 and Nikon ECLIPSE Ti. Images were taken with 10x or 20x objective. The antibodies used in the analysis are listed in the following tables.

Table 5 - List of Primary Antibodies used for Immunocytofluorescence.

Antigen	Vendor	Dilution
Anti-DCX	Millipore (ab2253)	1:250
Anti-Tuj1	Abcam (ab9354)	1:250
Anti-Oct4	Biologend (3A2A20)	1:200
Anti-Nestin	Millipore (ab5326)	1:250
Anti-NeuN	Millipore (ab377)	1:250
Anti-Pax6	Millipore (ab5603)	1:250
Anti-Sox2	Biologend (901301)	1:250

Table 6 - List of Secondary Antibodies used for Immunocytofluorescence.

Antigen	Vendor	Dilution
Goat anti-rabbit AlexaFluor 647	ThermoFisher (A21245)	1:1000
Goat anti-mouse AlexaFluor 488	ThermoFisher (A11029)	1:1000
Goat anti-mouse AlexaFluor 647	ThermoFisher (A150123)	1:1000
Goat anti-guinea pig AlexaFluor 647	ThermoFisher (A21450)	1:1000
Goat anti-chicken AlexaFluor 568	Abcam (ab175477)	1:1000
Goat anti-mouse AlexaFluor 568	ThermoFisher (A11031)	1:1000
Goat anti-rabbit AlexaFluor 488	ThermoFisher (A11008)	1:1000

Image Analysis and Histological Measurements

All images were analysed with Nikon software version 4.11.0 (NIS Elements Viewer) and processed with ImageJ version 1.48v (Wayne Rasband, National Institutes of Health, USA). Number of positive brains was obtained by identifying fluorescent masses constituted by DAOY mCherry⁺ cells injected in the lateral ventricles of mouse embryos at E14.5 and observed under stereo microscope (Olympus SZX16 with Olympus U-RFL-T) upon dissection.

Reconstruction of tumor masses and distribution within the brains: coronal sections of 40 μ m were collected from 4 brains per each condition. The entire brains were sectioned rostro-caudally while rigorously maintain fixed anatomical references. This ensured that each slice occupied the same position across all brains. Brain slices were categorized into six principal anatomical *regions* for ease of representation. A single brain slice possessing mCherry signal is considered a *tumor focus*. The set of consecutive brain slices presenting *tumor foci* (mCherry fluorescence signal) is defined as a *tumor mass* (or simply, *tumor*); n = number of brains

Frequency Distribution of tumor foci: tumor foci count per brain region, normalized to the total number of tumor foci in the whole brain; n = number of brains (average of values from single brains)

Number of tumors: n = tumor masses (data from a single brain were pooled considering treatment conditions and considered as a whole)

Tumor volume: was measured in coronal sections of embryonic brains by the diameter (d) of each tumor in its greatest dimension and volume (V) was estimated with the following ellipsoid formula⁸⁴: $V = \frac{4}{3}\pi ab^2$, where *a* and *b* corresponds to the sagittal and axial plane, respectively. mCherry fluorescence signal defined *tumor area*. Analysis was restricted to tumor masses that occupied at least 6 consecutive brain slices; n = tumor masses (data from a single brain were pooled considering treatment conditions and considered as a whole)

Cell proportions measurements: for cell density within the tumor area, Hoechst⁺ nuclei were counted within tumor area (defined by mCherry fluorescence) and divided by the tumor area; proportion of cells were calculated as the number of cells Ki67⁺ or BrdU⁺ or Ki67⁺BrdU⁺ over total Hoechst⁺ nuclei within tumor area (defined by mCherry fluorescence) and normalized to the tumor area. During the count, cells were considered also for their morphology in order to exclude mouse nuclei³¹⁶. Counting was performed by considering different regions of the tumor mass and different regions of the brain (when applicable); n = number of brains (average of values from single brains).

Maintenance and transfection of DAOY

DAOY mCherry⁺ cells (ATCC, HTB-186) were obtained with transduction of EF- α 1_mCherry lentivirus. The DAOY cells were cultured at 37°C, 5% of CO₂ and 95% of relative humidity with DMEM High Glucose (Dulbecco Modified Eagle Medium; Sigma Aldrich) containing 10% of FBS (fetal bovine serum, Sigma Aldrich), 1% of penicillin-streptomycin antibiotics (ThermoFisher) and 1% of L-glutamine (Lonza Srl). For transfection, cells were seeded in 12-well plates at a concentration of 15x10³ cells/cm². The day after cells were transfected with a *pool* of mimics or *scramble* negative control (Dharmacon, CN-001000-01-05) at a final concentration of [10nM] or [125nM] in ratio 1:1 using Lipofectamine 2000 Transfection Reagent in MegaCell RPMI-1640 medium. After 6h, the medium was substituted with serum-free Neurobasal (ThermoFisher) containing 1% of penicillin-streptomycin antibiotics and 2% of B-27 (Life Technologies).

RNA extraction a real-time qPCR

Total RNA from 3 brains for E18.5 (non-injected and mCherry⁺) and 4 brains for P7 mice was extracted for quantification of miRNAs in fresh brain tissues. Expression levels of hsa-miR-376b-3p in all the samples were quantified as a measure of the residual miRNAs levels of the *pool* in the tissues. This miRNA was selected due to its high discriminatory power, as it is absent in mouse tissue (confirmed by additional ongoing laboratory studies – data not shown). For injected mice, the mCherry⁺ brains were carefully dissected under a stereomicroscope with a scalpel to isolate the mCherry-positive regions. Tissues were snap frozen in dry ice and stored at -80°C. For RNA extraction, frozen tissue was added 700 μ l of Qiazol (Qiagen) and homogenized using a TissueLyser II (Qiagen) with 5 mm stainless steel beads pre-treated for RNase and DNase. Homogenization

consisted in 3 × 1 min cycles at 30 Hz and then samples were cleared by centrifugation at 10,000 × g for 5 min at 4 °C. RNA extraction was performed following QIAzol protocol (Qiagen) according to the manufacturer's instructions. A volume of 8µl of total RNA was treated with DNase I (Sigma) and then quantified using a Nanodrop ND-1000 spectrophotometer (Thermo Fisher Scientific). The purity of RNA was evaluated using the 260/280 and 260/230 absorbance ratios. For both ratios, a value of ~ 2.0 was considered indicative of good quality RNA. cDNA was synthesized using miScript II RT kit (Qiagen) according to the manufacturer's instructions. Real-time qPCR was performed with QuantiFast SYBR Green PCR Kit (Qiagen) and expression level was determined relative to U6 snRNA level, using the delta-delta Ct method.

Table 7 - List of primers used for qPCR.

Gene	Catalog #	Sequence
hsa-miR-376b-3p	MS00007399	5'-AUCAUAGAGGAAAAUCCAUGUU-3'
RNU6		5'-CUCGCUUCGGCAGCACAUAUACUAA-3'

Statistical Analysis

Data were analyzed by GraphPad Prism 9 and are shown as mean ± SEM (Standard Error Mean). Differences between groups were tested for statistical significance, using unpaired Student's t-test, χ^2 test, one-way-ANOVA followed by Tukey's multiple comparisons test, Significance was expressed as follows in all figures: * p-value < 0.05; ** p-value < 0.01; ***p-value < 0.001; **** p-value < 0.0001.

ANNEX I. *In vitro* validation of the efficacy of the 11 miRNAs *pool* in a Medulloblastoma cell line

The 11 miRNAs pool transfection inhibits cell growth

DAOY cell line was transfected to constitutively express NanoLuc luciferase, an enzyme that is secreted in the medium and can be used as indirect measure of cell growth being released in the medium. The experimental protocol is depicted in *Fig. 1 – A*. Cells were seeded in concentration 15×10^3 cells/cm² in a MW 12 plate in complete DMEM. The day after, a concentration of [250nM] of 11 miRNAs *pool* or *scramble* was transfected using Lipofectamine2000 as chemical vehicle. After 6 hours, the medium was substituted with serum-free complete Neurobasal. Starting from the day of transfection (T0), 1ml of the discarded medium was collected every 24 hours for 4 days (T3). The medium was then stored at -20°C and subsequently analyzed by bioluminescence. The resulting cell growth curve was obtained by cumulative measurement of the total bioluminescence signal (photons/sec) in each time points. The growth curve showed significant difference in the *pool* compared to the *scramble* in each time point considered (*Fig. 1 – C*). Since the cumulative bioluminescence is an indirect measure of the number of cells, cells were harvested after 72h of treatment (T3) and manually counted. The results showed a significative difference between the treated cells and control (*Fig. 1 – D*), thus confirming the outcome of the luciferase assay. In *Fig. 1 – B* are reported representative images of the cultures in each time point.

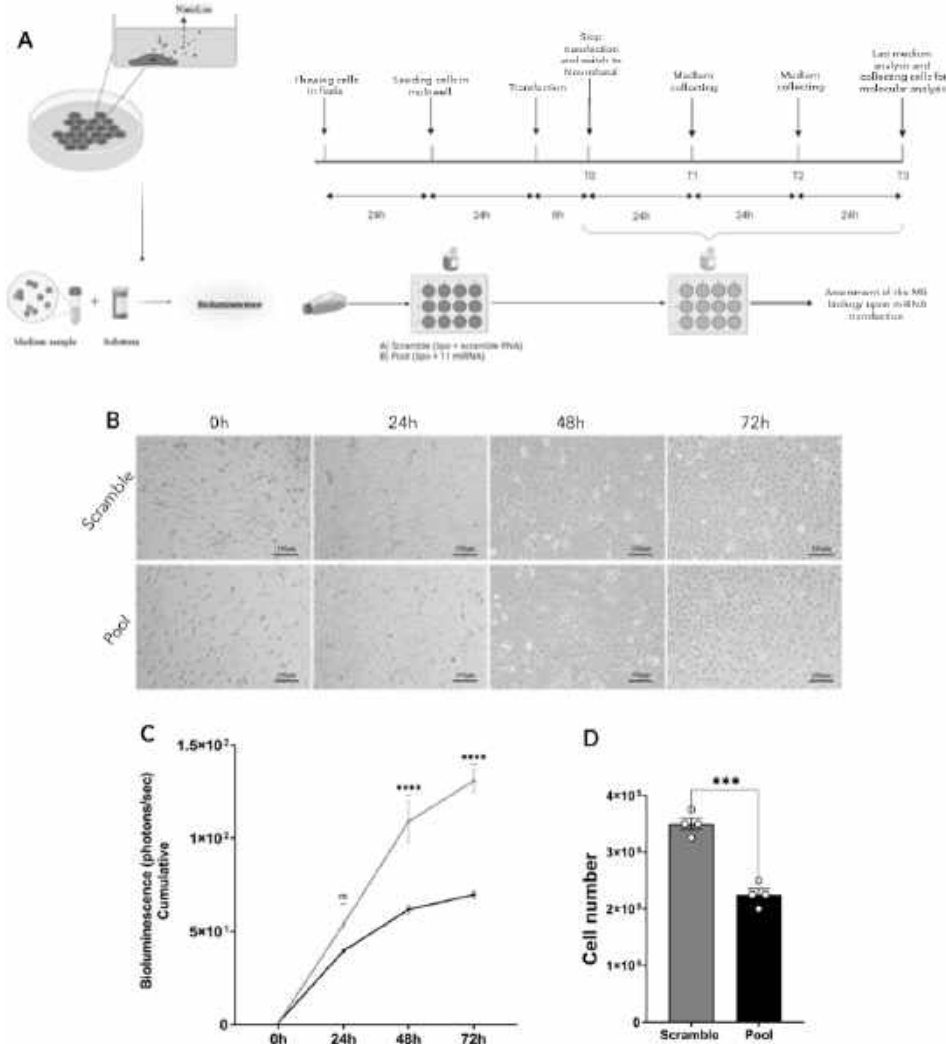


Fig. 1 – The 11 miRNAs pool reduces proliferation of human MB cell line. (A) DAOY cells were seeded in multiwell plates at a concentration of 6×10^4 cells in each well in complete DMEM for 24h. The day after, DMEM was substituted with RPMI-1640 MegaCell medium with Lipofectamine-2000 for transfection of the 11 miRNAs pool or the scramble control. After 6h, medium was changed with complete Neurobasal, and collected each 24h for 4 days. Cells were then collected or fixed in coverslips for immunofluorescence analysis. NanoLuc is constitutively expressed and released by DAOY cells and was used for bioluminescence analysis (photons/sec). (B) After transfection, cell images were acquired every 24h. (C) DAOY cells were treated with scramble or 11 miRNAs pool at a concentration of 250nM for 72h. Medium was collected every 24h and bioluminescence was detected quantifying the NanoLuc secreted by cells. NanoLuc quantity is directly proportional to the number of cells. The experiment was done in biological triplicate and technical quadruplicate. Bars present mean \pm SEM, significance for * $P < 0.05$, ** $P < 0.01$, *** $P < 0.001$. (D) At 72h DAOY cells were detached from the plate of growth and counted. Bars present mean \pm SEM, significance for * $P < 0.05$, ** $P < 0.01$, *** $P < 0.001$. Cell count was in technical quadruplicate.

Lower concentration of the treatment maintains the efficacy on cell growth

To determine the minimum effective dosage of the 11 miRNAs *pool* capable of eliciting the observed effects on cell growth, we conducted a titration experiment following the same protocol described earlier. The concentrations of 250nM, 125nM, 62.5nM, 25nM, 10nM and 5nM were tested (Fig. 1. 2 – A). Cumulative bioluminescence evaluation showed that the effect of the 11 miRNAs *pool* persisted at the lower concentration (5nM) and cell counting performed at 25nM, 10nM and 5nM consolidated this result (Fig. 1. 2 – B and Fig. 1. 2 – C).

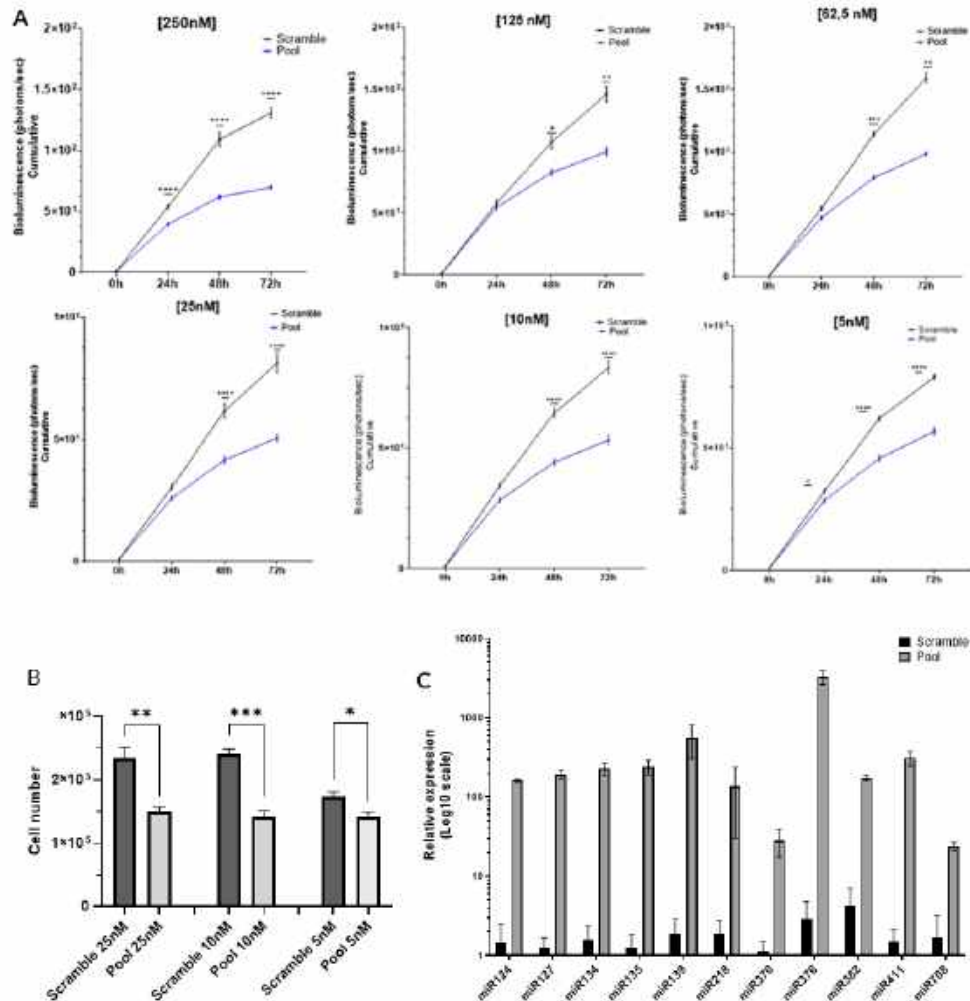


Fig. 1.2 – Titration of the 11 miRNAs pool. (A) DAOY cells were transfected with lower concentrations of scramble or 11 miRNAs pool: 250, 125, 62.5, 25, 10 and 5 nM. Cells did not show a dose-dependent response to the miRNA transfection and the pool resulted effective until 5nM. Experiment was done in technical quadruplicate and bars present mean±SEM, significance for * $P < 0.05$, ** $P < 0.01$, *** $P < 0.001$. (B) At the indicated lower concentrations (25, 10 and 5nM) 72h upon transfection cells were detached and counted with the Neubauer counter chamber at the optical microscope showing a lower number of cells in those treated with the pool. Cell count was in technical quadruplicate, bars present mean±SEM, significance for * $P < 0.05$, ** $P < 0.01$, *** $P < 0.001$. (C) Overexpression of the 11 miRNAs in DAOY cells 72h upon transfection at 10nM to confirm the regularity of the transfection even at this concentration.

The 11 miRNAs pool induces pro-neural differentiation in vitro

DAOY cells were plated in T25 flasks at a concentration of 15×10^3 cells/cm² and treated with *scramble* or *pool* at [250nM], [125nM] and [10 nM]. After 72h cells were collected and processed with PI (propidium iodide) to perform cell cycle analysis by flow cytometry. In Fig. 1.3 – A and Fig. 1.3 – B are reported, respectively, the distribution and percentage of cell populations over the G1/G0, S, G2/M cell cycle phases for each condition. The three concentrations of the 11 miRNAs *pool* showed a higher percentage of cells in G0/G1 phases and a lower percentage of cells in S phase compared to the *scramble* conditions. This suggests that 11 miRNAs *pool* induces an exit from the cell cycle and a stop in G0/G1 phases.

To determine if the increased cell proportion in the G0/G1 phase resulted from differentiation induced by the 11 miRNAs *pool*, we quantified by qPCR the transcript levels for several neuronal or stem markers in cells

treated with *scramble* or *pool* at [10nM] after 72 hours. Relative expression of Nestin, CD44, CD133, NeuN, MAP2, Tuj1 S100 β , GFAP are reported in Fig. I. 4. Results show a significant decrease of CD44 and CD133 stemness markers and a significant increase for NeuN, MAP2, Tuj1 and S100 β markers in cells treated with the *pool* compared to *scramble* samples. GFAP relative expressions show no significant difference. These results suggest that, upon the transfection with the 11 miRNAs *pool*, cells are supported towards a neuronal commitment.

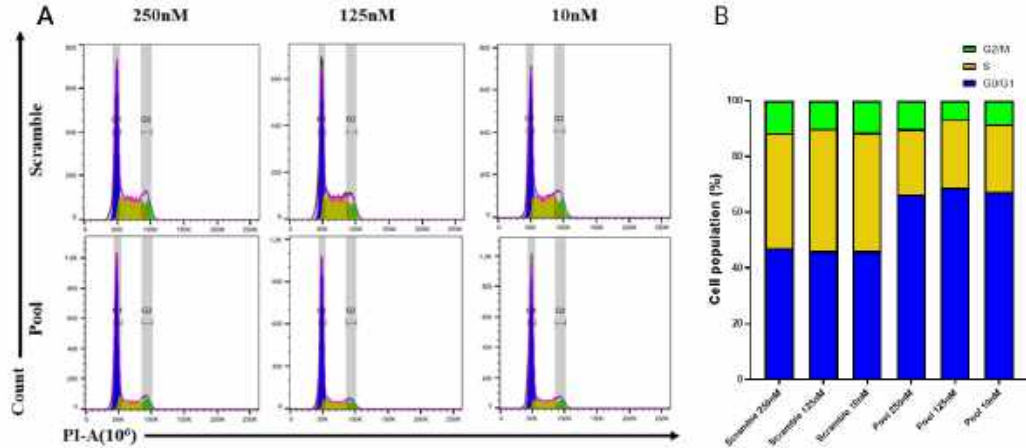


Fig. I. 3 – 11 miRNAs pool stop cells in G0/G1 phase of cell cycle. (A) Flow cytometry evaluation of cell cycle phases of DAOY cells transfected with scramble or 11 miRNAs pool at 250, 125 and 10nM after 72h by using propidium iodide staining (G0/G1 phases in blue, S phase in yellow, M/G2 phases in green). (B) Percentage of cells belonging to the different cell phases.

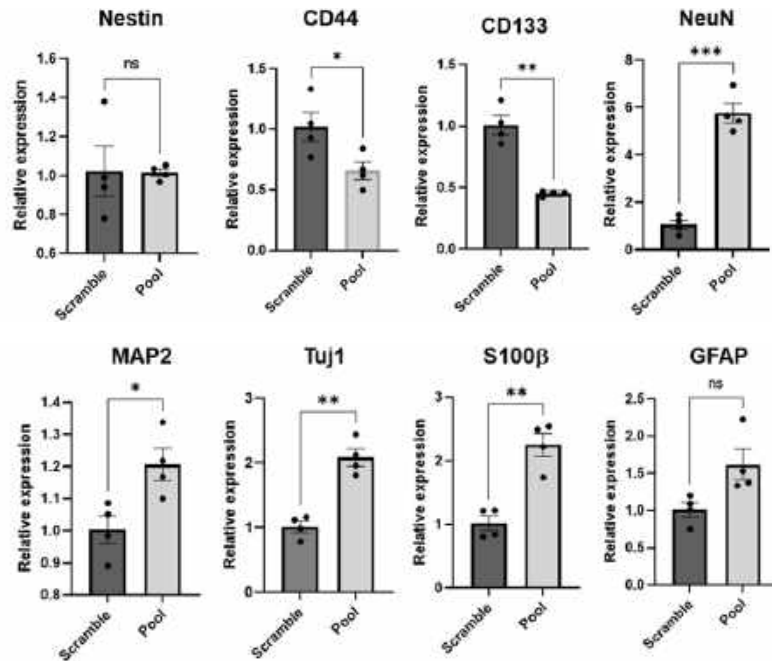


Fig. I. 4 – The 11 miRNAs pool induces cancer stem cells neural differentiation in vitro. 72h upon transfection with 11 miRNAs pool at a concentration of 10nM, it has been evaluated the level of stemness and neural markers through rt-qPCR. Data shown in technical quadruplicates and bars present mean \pm SEM, significance for *P<0.05, **P<0.01, ***P<0.001.

The 11 miRNAs pool does not induce apoptosis in DAOY cells

To evaluate whether the differentiation of DAOY cells induced by the *pool* is parallel to apoptosis of cells, we performed flow cytometry analysis with PI (propidium iodide) and annexin V antibody. Cells were transfected with *scramble* and *pool* at [250nM], [125nM] and [10 nM] in T25 flasks seeded at a concentration of 6×10^3 cells/cm². After 72 hours, cells were collected and processed for flow cytometry analysis. Results showed no difference in apoptotic cell populations at every concentration analyzed (Fig. 1. 5 – A), suggesting that the *pool* does not induce apoptosis after 72h since the transfection *in vitro*. To corroborate these data, we performed quantification by immunofluorescence of the cleaved caspase 3 marker (Cleaved Casp3), protein expressed by apoptotic cells, (Fig. 1. 5 – B). DAOY cells were transfected with the 11 miRNAs *pool* with a concentration of [10nM], then Casp3 marker was quantified and normalized on the total number of cell nuclei. No significant difference in the percentage of apoptotic cells was observed between transfected and control groups 72h after the treatment (Fig. 1. 5 – B).

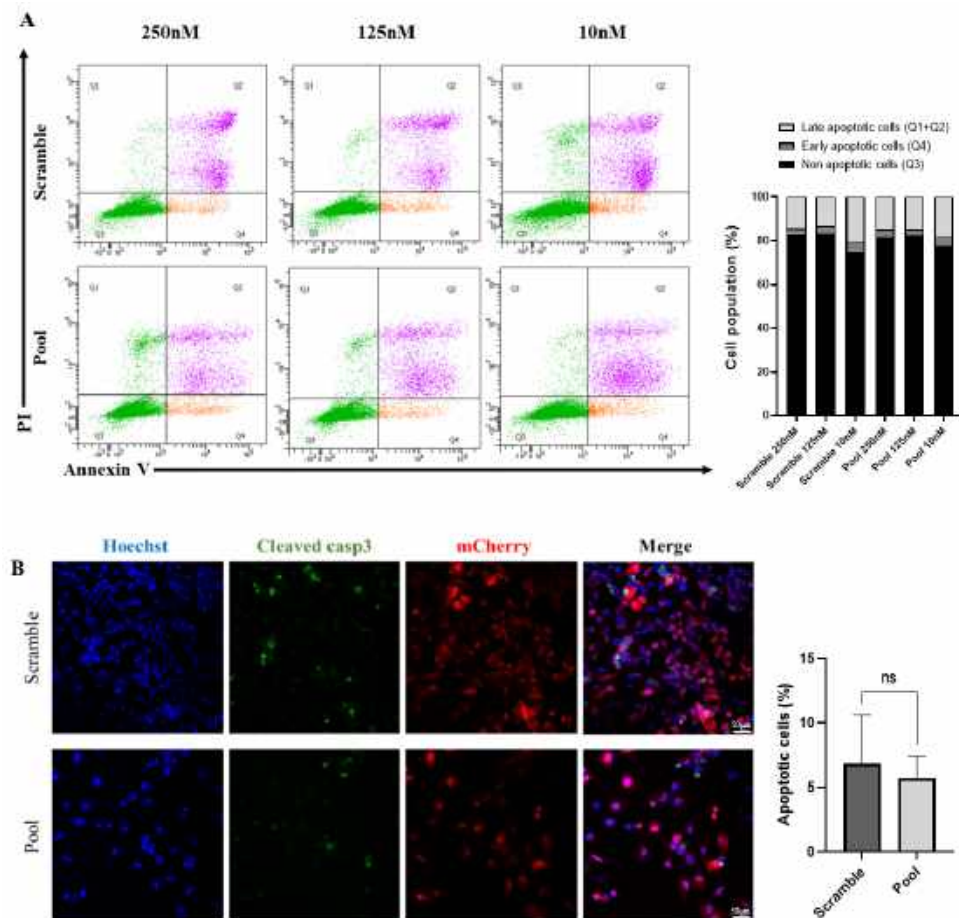


Fig. 1. 5 - The 11 miRNAs pool does not induce apoptosis in MB cells. (A) DAOY cells were transfected with scramble or 11 miRNAs pool at 250, 125 and 10 μ M for 72h. Cells were then collected and stained with Annexin-FITC/PI for the apoptosis measurement with flow cytometry. Annexin V-FITC positive cells were identified as apoptotic cells: early apoptosis (orange) and late apoptosis for cells positive for PI too (pink). (B) Cleaved caspase-3 immunofluorescence in DAOY cells transfected with scramble or 11 miRNAs pool at 10nM for 72h. Hoechst (blue) shows nuclei, cleaved casp3 (green) shows apoptotic cells and mCherry (red) is constitutively expressed by DAOY cells. The quantification of apoptosis was calculated as the number of cells positive for cleaved casp3 normalized on the number of total cells (nuclei - Hoechst).

REVIEWING PROCESS

Reviewer #1 – Dr. Nereo Kalebic

The Thesis focuses on developing a novel mouse model of medulloblastoma and exploring a potential therapeutic role of a *pool* of miRNAs in the same model.

The novelty of the mouse model lies in the strategy to transplant human medulloblastoma cells into embryonic immunocompetent mice, thereby allowing for the generation of the appropriate tumor microenvironment. This approach is based on the previous work of the same group (Hoffmann et al., 2020) in which the authors generated a glioblastoma model. The current model seems even more relevant for the brain cancer field, as medulloblastoma is a pediatric cancer and thus the embryonic transplantation faithfully mimics the events in human patients. The model was very successful as detected by the presence of microglia and macrophages that infiltrated into the tumoral mass. The main weakness of this part of the study is the timing of the analysis. As correctly reported in the Thesis, it would be important to examine if the generated mouse model indeed does not reject the graft after the immune system becomes fully mature. Additionally, to better follow the tumor progression in mouse models, it would be interesting to perform *in vivo* imaging during the first postnatal weeks. In the second part of the Thesis, the generated mouse has been used as a platform to test potential therapeutic efficiency of a *pool* of 11 miRNAs, which were previously shown by the same group to promote neuronal differentiation during adult neurogenesis (Pons-Espinal et al., 2017). This *pool* of miRNAs was transfected into human medulloblastoma cells and transplanted into embryonic mice. The preliminary data suggest that the *pool* of miRNAs has pro-neural and antiproliferative effects. In this context, it would be interesting to better discriminate if the effects of miRNAs are related to increased differentiation or cells only reduce the cell cycle progression and move towards quiescence or senescence. Using specific markers for each of these scenarios and various differentiation lineages along with the morphological analysis of cells could help address this question. BrdU-Ki67 assay suggests an anti-proliferative effects of the 11 miRNAs. It would be interesting to examine how long exactly is the cell cycle of engrafted human medulloblastoma cells and perhaps adjust the timing of BrdU administration and the analysis to make sure that the cells indeed had sufficient time to progress through the cell cycle. The final finding of the Thesis is the potential role of miRNAs in the epithelial-to-mesenchymal transition (EMT). This is a very interesting part as it allows for a future analysis not only of the cancer metastasis upon transfection of the *pool* of miRNAs, but also of the similarities between EMT in cancer and neuronal differentiation during fetal development.

Overall, the work presented in this Thesis can lead to an important advancement in cancer modeling *in vivo*, in understanding the role of 11 miRNAs in medulloblastoma progression and finally in dissecting the molecular and cellular similarities between brain cancers and brain development. In conclusion, I believe the Thesis presents a body of high-quality work that deserves the award of PhD.

Author's answer

I want to thank Dr. Kalebic for the time dedicated to the critical reading of my thesis and his insightful comments, particularly those on the solidness of the immune system representation in the model. The reviewer rightly emphasized the need for monitoring of tumors at post-natal stages, and I concur. As mentioned in the Discussion section, two key possibilities exist: either the immune system is fully functional and actively eliminates the masses, or the MB engraftments have developed mechanisms to evade elimination. A longitudinal assessment of the tumoral engraftments is crucial to differentiate between these scenarios and understand the underlying immune processes at play in our *in utero* orthotopic xenotransplantation model. Current *in vivo* imaging techniques at our institute lack the necessary sensitivity to effectively track our human MB xenografts due to their small size and diffuse nature. These techniques are designed for larger, more compact tumor formations typically found in pre-clinical models. While physical sectioning provided valuable initial insights, it also required a substantial time investment. This prompted us to explore more time-efficient approaches. At the moment, light-sheet fluorescence microscopy or other higher-sensitivity imaging techniques (i.e. micro-CT or PET scans) are under consideration. We are also considering non-invasive approaches using circulating molecules that could indicate tumor activity while simultaneously evaluating immunological response and Tumor Micro-Environment (TME) characteristics.

The reviewer also highlighted the significance of understanding the role of 11 miRNAs on cell cycle. I agree that this aspect is crucial. Building on the Discussion's exploration of the effect of the treatment, in particular its potential role in inducing differentiation or quiescence, we planned to prioritize further research in the differentiation re-programming, as outlined in the "future perspective" section. More in details, we aim to utilize human-specific neuronal differentiation markers, preferably with a nuclear localization signal. These choices aim to increase the accuracy, as human-specific markers ensure greater specificity in refer the outcome to the MB cells, while the nuclear localization provides a clearer visualization and quantification of marker expression within differentiated cells. Through these methods we aim to obtain a more detailed and accurate understanding of the pre-treatment's effect on neuronal differentiation.

I thank the reviewer for raising the pertinent aspect about the senescence as a possible effect of the treatment. This aspect was not directly addressed in this thesis. However, we explored this direction through the β -galactosidase assay *in vitro*, and the analysis is currently being conducted by the colleague responsible for *in vitro* characterization. I agree that understanding which mechanisms underlies the *pool* of 11 miRNAs effect on cell cycle is crucial, and replicating these observations *in vivo* is equally important as cellular behaviour can significantly differ between controlled lab environments and the ecosystem of a living organism. For similar reasons and to also exclude an induction by the 11 miRNAs *pool* of quiescence state, the experiment of BrdU injection was designed to specifically assess whether the pre-treatment could induce an extension of cell cycle length in engrafted cells. As reported in the Discussion, the cell cycle index (determined by BrdU-Ki67⁺/BrdU⁺ cells) could not return any significant finding, possibly due to the improper timing of administration. This highlights the importance of the reviewer's point regarding the need to accurately characterize cell cycle length in engrafted MB cells. Precise characterization with this focus can be performed through either consecutive

sacrifice of mice injected with BrdU at various time points, followed by quantification of BrdU⁺ cells in each group to create a detailed profile of cell cycle progression, or dual labeling with EdU (another thymidine analog), injected alongside BrdU at different time points. This dual labeling approach offers distinct temporal labeling of proliferating cells, providing higher temporal resolution compared to BrdU alone. Examining the behaviour of MB cells is crucial for progressing our comprehension. It is equally vital to acknowledge that both methodologies come with limitations in terms of resources, such as animal utilization and time commitment.

I appreciate the reviewer's comment regarding the potential involvement of Epithelial-Mesenchymal Transition (EMT) in our observations, as we are strongly committed to address this crucial point by targeted experiments specifically designed from insights coming from molecular analysis on the pre-treated cells. We aim to obtain definitive evidence regarding the presence or absence of EMT following the treatment. This will contribute significantly to our understanding of the treatment's mechanism of action and its potential therapeutic implications.

Reviewer 2 – Dr. Giancarlo Belenchi

This PhD Thesis aligns with the extensive research conducted at the host laboratory, focusing on the roles of non-coding RNAs, particularly microRNAs (miRNAs), in cell differentiation and tumor progression. The research builds upon prior findings from Prof. De Pietri Tonelli's laboratory, which identified a cluster of microRNAs capable of collaboratively inducing the differentiation of adult neural stem cells into fully functional neurons. Building upon this observation, the candidate explores the potential of this *pool* of miRNAs to mitigate the proliferation and invasiveness of cancer cells. This investigation involves employing a mouse model of medulloblastoma, a devastating untreatable tumor.

The utilization of miRNAs and short oligonucleotide sequences, mimicking the actions of specific miRNAs, has emerged in recent decades as a potential treatment for various human disorders. This work aligns with this research field and establishes a potentially innovative approach to counteract the progression and invasiveness of medulloblastoma.

The Thesis is well-written and easy to follow. The rationale and the data presented in annex 1, effectively sets the stage for the subsequent experiments. All experiments are well-documented with high-quality images. Dr. La Rosa employs a wide array of techniques, ranging from cellular biology to mouse modeling and in-vivo analysis of xenotransplants.

To enhance the robustness of the results, the candidate might have further strengthened the molecular characterization of the cherry-positive xenotransplanted cells following transfection with the miRNA *pool*, as well as their corresponding control cells. An effective approach could have involved re-purifying these cells, perhaps utilizing laser dissection, to conduct a more in-depth exploration of the pathways associated with reduced invasiveness. This approach could offer a clearer understanding of the underlying mechanisms and could potentially pave the way for future research directions. Identifying new molecular players involved in this process might indeed open avenues for drug-related approaches capable of bypassing the BBB and gaining access to brain tumors more effectively.

However, these experiments are challenging, time-consuming, and bear a risk of failure if the required techniques are unavailable in the host laboratory.

Overall, the data presented by Dr. La Rosa appears robust and holds promising interdisciplinary implications. This demonstration of high-quality work merits the award of a PhD.

Author's answer

I extend my sincere appreciation for the positive feedback on my thesis's quality and well-structured presentation. The comments regarding the solidity of the data presented are a gratifying recognition of my efforts to ensure an informative and significant piece of work.

As concern the Reviewer's suggestion on the implementation of the work by analyzing the molecular features of the tumor cells upon the implantation, I have already conducted a trial of purification of the mCherry⁺ cells by sorting the cells from dissected and digested brain regions exhibiting visible masses. This initial attempt was unsuccessful due to the limited number of cells collected. The scattered location of tumor engraftments

throughout the brain, as also depicted by the tumor distribution reconstruction, is likely the primary cause of this failure. The sequential procedures required for tissue preparation before sorting decrease the overall number of the engrafted cells that can be eventually retrieved. The excision of host brain tissue by roughly removing regions devoid of red fluorescence was also considered to improve the ratio of red-positive cells to host cells, but it failed to meet expectations. Hence, a larger number of animals is necessary to isolate an adequate quantity of cells for subsequent molecular analysis.

The approach suggested by the Reviewer of using laser dissection to resect the interested tissue could be a promising alternative, as it would effectively reduce the presence of host cells and in turn improve signal-to-noise ratio and potentially increase the final yield. Unfortunately, our laboratory does not currently have access to laser dissection equipment. Additionally, as the Reviewer noted, this technique is time-consuming and may pose a substantial risk of failure. A deeper comprehension of miRNA-mediated influence on tumor cells needs the characterization of the engraftments at the molecular level. Your suggestion to pursue this analysis has been incorporated into the Discussion chapter (please see the end of the page for the referenced text), as a critical cornerstone guiding our future research trajectory.

I express my gratitude to Dr. Bellenchi for the willingness to dedicate his time and expertise in evaluating my thesis.

Integrated text (pg. 44):

“[...] The re-purification of engrafted MB cells (i.e. by FACS) could provide a unique perspective into their molecular identity post-implantation. This would dissect not only the intrinsic influence of the host environment but also reveal the distinct molecular signatures induced by the treatment on these cells. It is essential to emphasize the unique value of analyzing engrafted cells rather than studying them under in vitro settings. A comparison of gene- and protein-expression profiles between pre-treated MB cells and the respective controls from in utero engrafts can pinpoint the specific molecular pathways modulated by the 11 miRNAs. This, in turn, allows us to understand the mechanism through which MB cells adapt and evolve within the living organism. Therefore, identifying the targets of 11 miRNAs pool in MB engrafted cells could serve as a pivotal guide, enhancing the precision and focus of our subsequent studies.”

REFERENCES

1. Abdelfattah, A. M., Park, C. & Choi, M. Y. Update on non-canonical microRNAs. *Biomol. Concepts* **5**, 275–287 (2014).
2. Aguilar, C., Mano, M. & Eulalio, A. MicroRNAs at the Host–Bacteria Interface: Host Defense or Bacterial Offense. *Trends Microbiol.* **27**, 206–218 (2019).
3. Akazawa, C., Ishibashi, M., Shimizu, C., Nakanishi, S. & Kageyama, R. A mammalian helix-loop-helix factor structurally related to the product of *Drosophila* proneural gene *atonal* is a positive transcriptional regulator expressed in the developing nervous system. *J. Biol. Chem.* **270**, 8730–8738 (1995).
4. Åkerblom, M. *et al.* MicroRNA-124 is a subventricular zone neuronal fate determinant. *J. Neurosci.* **32**, 8879–8889 (2012).
5. Aloizou, A. M. *et al.* The role of MiRNA-21 in gliomas: Hope for a novel therapeutic intervention? *Toxicol. Reports* **7**, 1514–1530 (2020).
6. Ambros, V. *et al.* LETTERTO THE EDITOR A uniform system for microRNA annotation. 277–279 (2003) doi:10.1261/rna.2183803.One.
7. Ambros, V. The functions of animal microRNAs. *Nature* **431**, 350–355 (2004).
8. Amore, G. *et al.* A Focus on the Cerebellum: From Embryogenesis to an Age-Related Clinical Perspective. *Front. Syst. Neurosci.* **15**, 1–14 (2021).
9. Andescavage, N. N. *et al.* Cerebrospinal Fluid and Parenchymal Brain Development and Growth in the Healthy Fetus. *Dev. Neurosci.* **38**, 420–429 (2017).
10. Arnò, B. *et al.* Neural progenitor cells orchestrate microglia migration and positioning into the developing cortex. *Nat. Commun.* **5**, (2014).
11. Awatramani, R., Soriano, P., Rodriguez, C., Mai, J. J. & Dymecki, S. M. Cryptic boundaries in roof plate and choroid plexus identified by intersectional gene activation. *Nat. Genet.* **35**, 70–75 (2003).
12. Babae, N. *et al.* Systemic miRNA-7 delivery inhibits tumor angiogenesis and growth in murine xenograft glioblastoma. *Oncotarget* **5**, 6687–6700 (2014).
13. Bahena-Ocampo, I. *et al.* miR-10b expression in breast cancer stem cells supports self-renewal through negative PTEN regulation and sustained AKT activation. *EMBO Rep.* **17**, 648–658 (2016).
14. Bahmad, H. F. & Poppiti, R. J. Medulloblastoma cancer stem cells: Molecular signatures and therapeutic targets. *J. Clin. Pathol.* **73**, 243–249 (2020).
15. Bai, A. H. C. *et al.* MicroRNA-182 promotes leptomeningeal spread of non-sonic hedgehog-medulloblastoma. *Acta Neuropathol.* **123**, 529–538 (2012).
16. Barbieri, F. *et al.* Stem-like signatures in human meningioma cells are under the control of CXCL11/CXCL12 chemokine activity. *Neuro. Oncol.* **25**, 1775–1787 (2023).
17. Barca-Mayo, O. & De Pietri Tonelli, D. Convergent microRNA actions coordinate neocortical development. *Cellular and Molecular Life Sciences* vol. 71 2975–2995 at <https://doi.org/10.1007/s00018-014-1576-5> (2014).
18. Bartel, D. P. MicroRNAs: genomics, biogenesis, mechanism, and function. *Cell* **116**, 281–297 (2004).
19. Bergom, C., Gao, C. & Newman, P. J. Mechanisms of PECAM-1-mediated cytoprotection and implications for cancer cell survival. *Leuk. Lymphoma* **46**, 1409–1421 (2005).
20. Bernstein, E. *et al.* Dicer is essential for mouse development. *Nat. Genet.* **35**, 215–217 (2003).
21. Bhat, S. M. *et al.* 3D tumor angiogenesis models: recent advances and challenges. *J. Cancer Res. Clin. Oncol.* **147**, 3477–3494 (2021).
22. Bian, S. *et al.* MicroRNA Cluster miR-17-92 Regulates Neural Stem Cell Expansion and Transition to Intermediate Progenitors in the Developing Mouse Neocortex. *Cell Rep.* **3**, 1398–1406 (2013).
23. Bjerkvig, R., Tysnes, B. B., Aboody, K. S., Najbauer, J. & Terzis, A. J. A. Opinion: the origin of the cancer stem cell: current controversies and new insights. *Nature reviews. Cancer* vol. 5 899–904 at <https://doi.org/10.1038/nrc1740> (2005).
24. Bocci, F., Jolly, M. K., George, J. T., Levine, H. & Onuchic, J. N. A mechanism-based computational model to capture the interconnections among epithelial-mesenchymal transition, cancer stem cells and Notch-Jagged signaling. *Oncotarget* **9**, 29906–29920 (2018).
25. Bonnet, D. & Dick, J. E. Human acute myeloid leukemia is organized as a hierarchy that originates from a primitive hematopoietic cell. *Nat. Med.* **3**, 730–737 (1997).
26. Borgenvik, A. *et al.* Dormant SOX9-Positive Cells Facilitate MYC-Driven Recurrence of

- Medulloblastoma. *Cancer Res.* **82**, 4586–4603 (2022).
27. van Bree, N. F. H. N. & Wilhelm, M. The Tumor Microenvironment of Medulloblastoma: An Intricate Multicellular Network with Therapeutic Potential. *Cancers (Basel)*. **14**, (2022).
 28. Brennecke, J., Hipfner, D. R., Stark, A., Russell, R. B. & Cohen, S. M. bantam encodes a developmentally regulated microRNA that controls cell proliferation and regulates the proapoptotic gene hid in *Drosophila*. *Cell* **113**, 25–36 (2003).
 29. Bribiesca, E. An easy measure of compactness for 2D and 3D shapes. *Pattern Recognit.* **41**, 543–554 (2008).
 30. Brilli, E. *et al.* Neural stem cells engrafted in the adult brain fuse with endogenous neurons. *Stem Cells Dev.* **22**, 538–547 (2013).
 31. Buffo, A. & Rossi, F. Origin, lineage and function of cerebellar glia. *Prog. Neurobiol.* **109**, 42–63 (2013).
 32. Bullock, M. D., Sayan, A. E., Packham, G. K. & Mirnezami, A. H. MicroRNAs: Critical regulators of epithelial to mesenchymal (EMT) and mesenchymal to epithelial transition (MET) in cancer progression. *Biol. Cell* **104**, 3–12 (2012).
 33. Butovsky, O. *et al.* Identification of a unique TGF- β -dependent molecular and functional signature in microglia. *Nat. Neurosci.* **17**, 131–143 (2014).
 34. Butts, T., Green, M. J. & Wingate, R. J. T. Development of the cerebellum: Simple steps to make a ‘little brain’. *Dev.* **141**, 4031–4041 (2014).
 35. Buzas, E. I. Opportunities and challenges in studying the extracellular vesicle corona. *Nat. Cell Biol.* **24**, 1322–1325 (2022).
 36. Cai, X., Hagedorn, C. H. & Cullen, B. R. Human microRNAs are processed from capped, polyadenylated transcripts that can also function as mRNAs. *Rna* **10**, 1957–1966 (2004).
 37. Calabrese, C. *et al.* A Perivascular Niche for Brain Tumor Stem Cells. *Cancer Cell* **11**, 69–82 (2007).
 38. Calin, G. A. *et al.* Frequent deletions and down-regulation of micro-RNA genes miR15 and miR16 at 13q14 in chronic lymphocytic leukemia. *Proc. Natl. Acad. Sci. U. S. A.* **99**, 15524–15529 (2002).
 39. Cao, D. D., Li, L. & Chan, W. Y. MicroRNAs: Key regulators in the central nervous system and their implication in neurological diseases. *Int. J. Mol. Sci.* **17**, 1–28 (2016).
 40. Cardin, S.-E. & Borchert, G. M. Viral MicroRNAs, Host MicroRNAs Regulating Viruses, and Bacterial MicroRNA-Like RNAs BT - Bioinformatics in MicroRNA Research. in (eds. Huang, J. *et al.*) 39–56 (Springer New York, 2017). doi:10.1007/978-1-4939-7046-9_3.
 41. Carlson, B. L., Pokorny, J. L., Schroeder, M. A. & Sarkaria, J. N. Establishment, maintenance and *in vitro* and *in vivo* applications of primary human glioblastoma multiforme (GBM) xenograft models for translational biology studies and drug discovery. *Current protocols in pharmacology / editorial board, S.J. Enna (editor-in-chief) ... [et al.]* vol. Chapter 14 at <https://doi.org/10.1002/0471141755.ph1416s52> (2011).
 42. Carvalho de Oliveira, J., Mathias, C., Oliveira, V. C., Pezuk, J. A. & Brassesco, M. S. The Double Face of miR-708: A Pan-Cancer Player with Dissociative Identity Disorder. *Genes (Basel)*. **13**, (2022).
 43. Chambers, S. M. *et al.* Highly efficient neural conversion of human ES and iPS cells by dual inhibition of SMAD signaling. *Nat. Biotechnol.* **27**, 275–280 (2009).
 44. Chang, T. C. *et al.* Transactivation of miR-34a by p53 Broadly Influences Gene Expression and Promotes Apoptosis. *Mol. Cell* **26**, 745–752 (2007).
 45. Chen, J., Wang, M., Guo, M., Xie, Y. & Cong, Y. S. miR-127 regulates cell proliferation and senescence by targeting BCL6. *PLoS One* **8**, 1–9 (2013).
 46. Chen, Y. *et al.* Silencing of microRNA-708 promotes cell growth and epithelial-to-mesenchymal transition by activating the SPHK2/AKT/ β -catenin pathway in glioma. *Cell Death Dis.* **10**, (2019).
 47. Chen, Z. *et al.* Cellular and molecular identity of tumor-associated macrophages in glioblastoma. *Cancer Res.* **77**, 2266–2278 (2017).
 48. Cheng, L. C., Pastrana, E., Tavazoie, M. & Doetsch, F. MiR-124 regulates adult neurogenesis in the subventricular zone stem cell niche. *Nat. Neurosci.* **12**, 399–408 (2009).
 49. Chivukula, R. R. & Mendell, J. T. Circular reasoning: microRNAs and cell-cycle control. *Trends Biochem. Sci.* **33**, 474–481 (2008).
 50. Cifuentes, D. *et al.* A novel miRNA processing pathway independent of Dicer requires Argonaute2 catalytic activity. *Science* **328**, 1694–1698 (2010).
 51. Clarke, M. F. *et al.* Cancer stem cells - Perspectives on current status and future directions: AACR workshop on cancer stem cells. *Cancer Res.* **66**, 9339–9344 (2006).
 52. Clovis, Y. M., Enard, W., Marinaro, F., Huttner, W. B. & de Pietri Tonelli, D. Convergent repression of

- Foxp2 3' UTR by miR-9 and miR-132 in embryonic mouse neocortex: Implications for radial migration of neurons. *Dev.* **139**, 3332–3342 (2012).
53. Concepcion, C. P., Bonetti, C. & Ventura, A. The MicroRNA-17-92 family of MicroRNA clusters in development and disease. *Cancer J. (United States)* **18**, 262–267 (2012).
 54. Constantin, L. The Role of MicroRNAs in Cerebellar Development and Autism Spectrum Disorder During Embryogenesis. *Mol. Neurobiol.* **54**, 6944–6959 (2017).
 55. Coolen, M., Katz, S. & Bally-Cuif, L. miR-9: A versatile regulator of neurogenesis. *Front. Cell. Neurosci.* **7**, 1–11 (2013).
 56. Corno, D. *et al.* Gene signatures associated with mouse postnatal hindbrain neural stem cells and medulloblastoma cancer stem cells identify novel molecular mediators and predict human medulloblastoma molecular classification. *Cancer Discov.* **2**, 554–568 (2012).
 57. Costa, F. F. *et al.* Identification of microRNAs as potential prognostic markers in ependymoma. *PLoS One* **6**, (2011).
 58. Cottonham, C. L., Kaneko, S. & Xu, L. miR-21 and miR-31 Converge on TIAM1 to Regulate Migration and Invasion of Colon Carcinoma Cells*. *J. Biol. Chem.* **285**, 35293–35302 (2010).
 59. Crasta, K. *et al.* DNA breaks and chromosome pulverization from errors in mitosis. *Nature* **482**, 53–58 (2012).
 60. Daige, C. L. *et al.* Systemic delivery of a miR34a mimic as a potential therapeutic for liver cancer. *Mol. Cancer Ther.* **13**, 2352–2360 (2014).
 61. Daigle, T. L. *et al.* A Suite of Transgenic Driver and Reporter Mouse Lines with Enhanced Brain-Cell-Type Targeting and Functionality. *Cell* **174**, 465–480.e22 (2018).
 62. Davis, T. H. *et al.* Conditional loss of dicer disrupts cellular and tissue morphogenesis in the cortex and hippocampus. *J. Neurosci.* **28**, 4322–4330 (2008).
 63. Debacker, A. J., Voutilainen, J., Catley, M., Blakey, D. & Habib, N. Delivery of Oligonucleotides to the Liver with GalNAc: From Research to Registered Therapeutic Drug. *Mol. Ther.* **28**, 1759–1771 (2020).
 64. Dehay, C. & Kennedy, H. Cell-cycle control and cortical development. *Nat. Rev. Neurosci.* **8**, 438–450 (2007).
 65. Delalay, C. *et al.* MicroRNA-9 Coordinates Proliferation and Migration of Human Embryonic Stem Cell-Derived Neural Progenitors. *Cell Stem Cell* **6**, 323–335 (2010).
 66. Denkert, C. *et al.* Ki67 levels as predictive and prognostic parameters in pretherapeutic breast cancer core biopsies: A translational investigation in the neoadjuvant gepartrio trial. *Ann. Oncol.* **24**, 2786–2793 (2013).
 67. Dennie, J. *et al.* NMR imaging of changes in vascular morphology due to tumor angiogenesis. *Magn. Reson. Med.* **40**, 793–799 (1998).
 68. Denoyelle, C. *et al.* MiR-491-5p-induced apoptosis in ovarian carcinoma depends on the direct inhibition of both BCL-XL and EGFR leading to BIM activation. *Cell Death Dis.* **5**, (2014).
 69. Desmond, M. E. & Jacobson, A. G. Embryonic brain enlargement requires cerebrospinal fluid pressure. *Dev. Biol.* **57**, 188–198 (1977).
 70. Detassis, S., Grasso, M., Del Vescovo, V. & Denti, M. A. microRNAs make the call in cancer personalized medicine. *Front. Cell Dev. Biol.* **5**, 1–20 (2017).
 71. Diehn, M. *et al.* Association of reactive oxygen species levels and radioresistance in cancer stem cells. *Nature* **458**, 780–783 (2009).
 72. Ding, X., Park, S. I., McCauley, L. K. & Wang, C.-Y. Signaling between transforming growth factor β (TGF- β) and transcription factor SNAI2 represses expression of microRNA miR-203 to promote epithelial-mesenchymal transition and tumor metastasis. *J. Biol. Chem.* **288**, 10241–10253 (2013).
 73. Ten Donkelaar, H. J., Lammens, M., Wesseling, P., Thijssen, H. O. M. & Renier, W. O. Development and developmental disorders of the human cerebellum. *J. Neurol.* **250**, 1025–1036 (2003).
 74. Dravid, A., Raos, B., Svirskis, D. & O'Carroll, S. J. Optimised techniques for high-throughput screening of differentiated SH-SY5Y cells and application for neurite outgrowth assays. *Sci. Rep.* **11**, 1–15 (2021).
 75. Du, B. *et al.* MicroRNA-545 suppresses cell proliferation by targeting cyclin D1 and CDK4 in lung cancer cells. *PLoS One* **9**, 1–9 (2014).
 76. Eades, G. *et al.* miR-200a regulates SIRT1 expression and Epithelial to Mesenchymal Transition (EMT)-like transformation in mammary epithelial cells. *J. Biol. Chem.* **286**, 25992–26002 (2011).
 77. Eklund, L., Bry, M. & Alitalo, K. Mouse models for studying angiogenesis and lymphangiogenesis in cancer. *Mol. Oncol.* **7**, 259–282 (2013).
 78. van Essen, M. J., Nayler, S., Becker, E. B. E. & Jacob, J. Deconstructing cerebellar development cell by

- cell. *PLoS Genet.* **16**, 1–14 (2020).
79. Fazi, F. *et al.* A minicircuitry comprised of microRNA-223 and transcription factors NFI-A and C/EBP α regulates human granulopoiesis. *Cell* **123**, 819–831 (2005).
 80. Fazi, F. *et al.* Epigenetic Silencing of the Myelopoiesis Regulator microRNA-223 by the AML1/ETO Oncoprotein. *Cancer Cell* **12**, 457–466 (2007).
 81. Feng, R. & Dong, L. Knockdown of microRNA-127 reverses adriamycin resistance via cell cycle arrest and apoptosis sensitization in adriamycin-resistant human glioma cells. *Int. J. Clin. Exp. Pathol.* **8**, 6107–6116 (2015).
 82. Feng, Z., Zhang, C., Wu, R. & Hu, W. Tumor suppressor p53 meets microRNAs. *J. Mol. Cell Biol.* **3**, 44–50 (2011).
 83. Ferrara, N., Gerber, H.-P. & LeCouter, J. The biology of VEGF and its receptors. *Nat. Med.* **9**, 669–676 (2003).
 84. Le Fèvre, C. *et al.* Ellipsoid calculations versus manual tumor delineations for glioblastoma tumor volume evaluation. *Sci. Rep.* **12**, 1–9 (2022).
 85. Filiano, A. J., Gadani, S. P. & Kipnis, J. Interactions of innate and adaptive immunity in brain development and function. *Brain Res.* **1617**, 18–27 (2015).
 86. Fischer, K. R. *et al.* Epithelial-to-mesenchymal transition is not required for lung metastasis but contributes to chemoresistance. *Nature* **527**, 472–476 (2015).
 87. Forget, A. *et al.* Aberrant ERBB4-SRC Signaling as a Hallmark of Group 4 Medulloblastoma Revealed by Integrative Phosphoproteomic Profiling. *Cancer Cell* **34**, 379–395.e7 (2018).
 88. Friedman, R. C., Farh, K. K. H., Burge, C. B. & Bartel, D. P. Most mammalian mRNAs are conserved targets of microRNAs. *Genome Res.* **19**, 92–105 (2009).
 89. Fukao, T. *et al.* An Evolutionarily Conserved Mechanism for MicroRNA-223 Expression Revealed by MicroRNA Gene Profiling. *Cell* **129**, 617–631 (2007).
 90. Ben Gacem, R., Ben Abdelkrim, O., Ziadi, S., Ben Dhiab, M. & Trimeche, M. Methylation of miR-124a-1, miR-124a-2, and miR-124a-3 genes correlates with aggressive and advanced breast cancer disease. *Tumor Biol.* **35**, 4047–4056 (2014).
 91. Gambari, R., Brognara, E., Spandidos, D. A. & Fabbri, E. Targeting oncomiRNAs and mimicking tumor suppressor miRNAs: Ew trends in the development of miRNA therapeutic strategies in oncology (Review). *Int. J. Oncol.* **49**, 5–32 (2016).
 92. Gangaraju, V. K. & Lin, H. MicroRNAs: key regulators of stem cells. *Nat. Rev. Mol. Cell Biol.* **10**, 116–125 (2009).
 93. Gasch, C., Ffrench, B., O’Leary, J. J. & Gallagher, M. F. Catching moving targets: Cancer stem cell hierarchies, therapy-resistance & considerations for clinical intervention. *Mol. Cancer* **16**, 1–15 (2017).
 94. Gaughwin, P., Ciesla, M., Yang, H., Lim, B. & Brundin, P. Stage-specific modulation of cortical neuronal development by Mmu-miR-134. *Cereb. Cortex* **21**, 1857–1869 (2011).
 95. Gauwerky, C. E., Huebner, K., Isobe, M., Nowell, P. C. & Croce, C. M. Activation of MYC in a masked t(8;17) translocation results in an aggressive B-cell leukemia. *Proc. Natl. Acad. Sci. U. S. A.* **86**, 8867–8871 (1989).
 96. Ge, Y.-F. *et al.* AntagomiR-27a targets FOXO3a in glioblastoma and suppresses U87 cell growth in vitro and *in vivo*. *Asian Pac. J. Cancer Prev.* **14**, 963–968 (2013).
 97. Gebert, L. F. R. & MacRae, I. J. Regulation of microRNA function in animals. *Nat. Rev. Mol. Cell Biol.* **20**, 21–37 (2019).
 98. Gebeshuber, C. A., Zatloukal, K. & Martinez, J. miR-29a suppresses tristetraproline, which is a regulator of epithelial polarity and metastasis. *EMBO Rep.* **10**, 400–405 (2009).
 99. Geribaldi-Doldán, N. *et al.* The Role of Microglia in Glioblastoma. *Front. Oncol.* **10**, 1–8 (2021).
 100. Giangaspero, F. *et al.* Stratification of medulloblastoma on the basis of histopathological grading. *Acta Neuropathol.* **112**, 5–12 (2006).
 101. Gibson, P. *et al.* Subtypes of medulloblastoma have distinct developmental origins. *Nature* **468**, 1095–1099 (2010).
 102. Gillespie, M. S., Ward, C. M. & Davies, C. C. DNA Repair and Therapeutic Strategies in Cancer Stem Cells. *Cancers (Basel)*. **15**, (2023).
 103. Gillies, J. K. & Lorimer, I. A. J. Report regulation of p27Kip1 by miRNA 221/222 in glioblastoma. *Cell Cycle* **6**, 2005–2009 (2007).
 104. Giordana, M. T. *et al.* The distribution of laminin in human brain tumors: An immunohistochemical study. *Acta Neuropathol.* **67**, 51–57 (1985).

105. Giza, D. E., Vasilescu, C. & Calin, G. A. Key principles of miRNA involvement in human diseases. *Discoveries* **2**, e34 (2014).
106. Gonzalez, H., Hagerling, C. & Werb, Z. Roles of the immune system in cancer: From tumor initiation to metastatic progression. *Genes Dev.* **32**, 1267–1284 (2018).
107. Goodrich, L. V., Milenković, L., Higgins, K. M. & Scott, M. P. Altered neural cell fates and medulloblastoma in mouse patched mutants. *Science (80-.)*. **277**, 1109–1113 (1997).
108. Goradel, N. H. *et al.* Regulation of tumor angiogenesis by microRNAs: State of the art. *J. Cell. Physiol.* **234**, 1099–1110 (2019).
109. Gottesman, M. M., Fojo, T. & Bates, S. E. Multidrug resistance in cancer: Role of ATP-dependent transporters. *Nat. Rev. Cancer* **2**, 48–58 (2002).
110. Götz, M. & Huttner, W. B. The cell biology of neurogenesis. *Nat. Rev. Mol. Cell Biol.* **6**, 777–788 (2005).
111. Green, M. J. & Wingate, R. J. T. Developmental origins of diversity in cerebellar output nuclei. *Neural Dev.* **9**, 2–9 (2014).
112. Greene, C., Hanley, N. & Campbell, M. Claudin-5: Gatekeeper of neurological function. *Fluids Barriers CNS* **16**, 1–15 (2019).
113. Gruszka, R., Zakrzewski, K., Liberski, P. P. & Zakrzewska, M. Mrna and mirna expression analyses of the myc/e2f/mir-17-92 network in the most common pediatric brain tumors. *Int. J. Mol. Sci.* **22**, 1–14 (2021).
114. Guo, Y., Bao, Y. & Yang, W. Regulatory miRNAs in colorectal carcinogenesis and metastasis. *Int. J. Mol. Sci.* **18**, (2017).
115. Gururangan, S. *et al.* Efficacy of high-dose chemotherapy or standard salvage therapy in patients with recurrent medulloblastoma. *Neuro. Oncol.* **10**, 745–751 (2008).
116. Ha, J. *et al.* Simplified Brain Organoids for Rapid and Robust Modeling of Brain Disease. *Front. Cell Dev. Biol.* **8**, 1–16 (2020).
117. Ha, M. & Kim, V. N. Regulation of microRNA biogenesis. *Nat. Rev. Mol. Cell Biol.* **15**, 509–524 (2014).
118. Ha, M., Pang, M., Agarwal, V. & Chen, Z. J. Interspecies regulation of microRNAs and their targets. *Biochim. Biophys. Acta - Gene Regul. Mech.* **1779**, 735–742 (2008).
119. Ha, T.-Y. MicroRNAs in Human Diseases: From Cancer to Cardiovascular Disease. *Immune Netw.* **11**, 135 (2011).
120. Hallmann, R. *et al.* The role of basement membrane laminins in vascular function. *Int. J. Biochem. Cell Biol.* **127**, 105823 (2020).
121. Hallonet, M. E. R., Teillet, M. A. & Le Douarin, N. M. A new approach to the development of the cerebellum provided by the quail-chick marker system. *Development* **108**, 19–31 (1990).
122. Hanahan, D. & Weinberg, R. A. Hallmarks of Cancer: The Next Generation. *Cell* **144**, 646–674 (2011).
123. Hatfield, S. D. *et al.* Stem cell division is regulated by the microRNA pathway. *Nature* **435**, 974–978 (2005).
124. He, L. *et al.* A microRNA polycistron as a potential human oncogene. *Nature* **435**, 828–833 (2005).
125. He, Y. *et al.* MiR-124 Promotes the Growth of Retinal Ganglion Cells Derived from Müller Cells. *Cell. Physiol. Biochem.* **45**, 973–983 (2018).
126. Heddleston, J. M., Li, Z., McLendon, R. E., Hjelmeland, A. B. & Rich, J. N. The hypoxic microenvironment maintains glioblastoma stem cells and promotes reprogramming towards a cancer stem cell phenotype. *Cell Cycle* **8**, 3274–3284 (2009).
127. Hemmati, H. D. *et al.* Cancerous stem cells can arise from pediatric brain tumors. *Proc. Natl. Acad. Sci. U. S. A.* **100**, 15178–15183 (2003).
128. Hemmesi, K. *et al.* MiR-135a Inhibits Cancer Stem Cell-Driven Medulloblastoma Development by Directly Repressing Arhgef6 Expression. *Stem Cells* **33**, 1377–1389 (2015).
129. Hendrikse, L. D. *et al.* Failure of human rhombic lip differentiation underlies medulloblastoma formation. *Nature* **609**, 1021–1028 (2022).
130. Henke, E., Nandigama, R. & Ergün, S. Extracellular Matrix in the Tumor Microenvironment and Its Impact on Cancer Therapy. *Front. Mol. Biosci.* **6**, 1–24 (2020).
131. Herkt, M. & Thum, T. Pharmacokinetics and Proceedings in Clinical Application of Nucleic Acid Therapeutics. *Mol. Ther.* **29**, 521–539 (2021).
132. Hoffmann, N. *et al.* A Xenotransplant Model of Human Brain Tumors in Wild-Type Mice. *iScience* **23**, (2020).
133. Hong, D. S. *et al.* Phase 1 study of MRX34, a liposomal miR-34a mimic, in patients with advanced solid tumours. *Br. J. Cancer* **122**, 1630–1637 (2020).
134. Hoshino, M. *et al.* Ptf1a, a bHLH transcriptional gene, defines GABAergic neuronal fates in cerebellum.

- Neuron* **47**, 201–213 (2005).
135. Hu, H. Y. *et al.* Sequence features associated with microRNA strand selection in humans and flies. *BMC Genomics* **10**, 413 (2009).
 136. Huang, M. *et al.* Engineering Genetic Predisposition in Human Neuroepithelial Stem Cells Recapitulates Medulloblastoma Tumorigenesis. *Cell Stem Cell* **25**, 433–446.e7 (2019).
 137. Huntzinger, E. & Izaurralde, E. Gene silencing by microRNAs: contributions of translational repression and mRNA decay. *Nat. Rev. Genet.* **12**, 99–110 (2011).
 138. Hutvagner, G. & Zamore, P. D. A microRNA in a multiple-turnover RNAi enzyme complex. *Science (80-.)*. **297**, 2056–2060 (2002).
 139. Iwadata, Y. Epithelial-mesenchymal transition in glioblastoma progression. *Oncol. Lett.* **11**, 1615–1620 (2016).
 140. Jacobsen, P. F., Jenkyn, D. J. & Papadimitriou, J. M. Establishment of a human medulloblastoma cell line and its heterotransplantation into nude mice. *J. Neuropathol. Exp. Neurol.* **44**, 472–485 (1985).
 141. Januchowski, R., Wojtowicz, K. & Zabel, M. The role of aldehyde dehydrogenase (ALDH) in cancer drug resistance. *Biomed. Pharmacother.* **67**, 669–680 (2013).
 142. Jevtić, P., Edens, L. J., Vuković, L. D. & Levy, D. L. Sizing and shaping the nucleus: Mechanisms and significance. *Curr. Opin. Cell Biol.* **28**, 16–27 (2014).
 143. Johnson, S. M. *et al.* RAS is regulated by the let-7 microRNA family. *Cell* **120**, 635–647 (2005).
 144. Johnson, S. M., Lin, S. Y. & Slack, F. J. The time of appearance of the *C. elegans* let-7 microRNA is transcriptionally controlled utilizing a temporal regulatory element in its promoter. *Dev. Biol.* **259**, 364–379 (2003).
 145. Jones, B. T. *et al.* Target-directed microRNA degradation regulates developmental microRNA expression and embryonic growth in mammals. *Genes Dev.* **37**, 661–674 (2023).
 146. Jones, D. T. W. *et al.* Dissecting the genomic complexity underlying medulloblastoma. *Nature* **488**, 100–105 (2012).
 147. Jurga, A. M., Paleczna, M. & Kuter, K. Z. Overview of General and Discriminating Markers of Differential Microglia Phenotypes. *Front. Cell. Neurosci.* **14**, 1–18 (2020).
 148. Kalebic, N. & Huttner, W. B. Basal Progenitor Morphology and Neocortex Evolution. *Trends Neurosci.* **43**, 843–853 (2020).
 149. Kalluri, R. & Weinberg, R. A. The basics of epithelial-mesenchymal transition. *J. Clin. Invest.* **119**, 1420–1428 (2009).
 150. Kao, S. H., Wu, K. J. & Lee, W. H. Hypoxia, epithelial-mesenchymal transition, and tet-mediated epigenetic changes. *J. Clin. Med.* **5**, 1–14 (2016).
 151. Kawase-Koga, Y., Otaegi, G. & Sun, T. Different timings of dicer deletion affect neurogenesis and gliogenesis in the developing mouse central nervous system. *Dev. Dyn.* **238**, 2800–2812 (2009).
 152. Kim, D. H., Sætrum, P., Snøve, O. & Rossi, J. J. MicroRNA-directed transcriptional gene silencing in mammalian cells. *Proc. Natl. Acad. Sci. U. S. A.* **105**, 16230–16235 (2008).
 153. Kong, W. *et al.* MicroRNA-155 Is Regulated by the Transforming Growth Factor β /Smad Pathway and Contributes to Epithelial Cell Plasticity by Targeting RhoA. *Mol. Cell. Biol.* **28**, 6773–6784 (2008).
 154. Koralov, S. B. *et al.* Dicer Ablation Affects Antibody Diversity and Cell Survival in the B Lymphocyte Lineage. *Cell* **132**, 860–874 (2008).
 155. Kording, F. *et al.* Simultaneous assessment of vessel size index, relative blood volume, and vessel permeability in a mouse brain tumor model using a combined spin echo gradient echo echo-planar imaging sequence and viable tumor analysis. *J. Magn. Reson. Imaging* **40**, 1310–1318 (2014).
 156. Kozomara, A., Birgaoanu, M. & Griffiths-Jones, S. MiRBase: From microRNA sequences to function. *Nucleic Acids Res.* **47**, D155–D162 (2019).
 157. Krichevsky, A. M., Sonntag, K.-C., Isacson, O. & Kosik, K. S. Specific MicroRNAs Modulate Embryonic Stem Cell–Derived Neurogenesis. *Stem Cells* **24**, 857–864 (2006).
 158. Kröger, C. *et al.* Acquisition of a hybrid E/M state is essential for tumorigenicity of basal breast cancer cells. *Proc. Natl. Acad. Sci. U. S. A.* **116**, 7353–7362 (2019).
 159. Lackinger, M. *et al.* A placental mammal-specific micro RNA cluster acts as a natural brake for sociability in mice. *EMBO Rep.* **20**, 1–11 (2019).
 160. Lal, S., Carrera, D., Phillips, J. J., Weiss, W. A. & Raffel, C. An oncolytic measles virus-sensitive Group 3 medulloblastoma model in immune-competent mice. *Neuro. Oncol.* **20**, 1606–1615 (2018).
 161. Łastowska, M., Karkucińska-Więckowska, A., Waschek, J. A. & Niewiadomski, P. Differential expression of mitochondrial biogenesis markers in mouse and human SHH-Subtype Medulloblastoma. *Cells* **8**,

- (2019).
162. Lau, N. C., Lim, L. P., Weinstein, E. G. & Bartel, D. P. An abundant class of tiny RNAs with probable regulatory roles in *Caenorhabditis elegans*. *Science* (80-.). **294**, 858–862 (2001).
 163. Lee, C. *et al.* M1 macrophage recruitment correlates with worse outcome in SHH Medulloblastomas. *BMC Cancer* **18**, 1–8 (2018).
 164. Lee, Y. *et al.* MicroRNA genes are transcribed by RNA polymerase II. *EMBO J.* **23**, 4051–4060 (2004).
 165. Leucht, C. *et al.* MicroRNA-9 directs late organizer activity of the midbrain-hindbrain boundary. *Nat. Neurosci.* **11**, 641–648 (2008).
 166. Leung David W., Cachianes George, Kuang Wun-Jing, Goeddel David V. & Ferrara Napoleone. Vascular endothelial growth factor is a secreted angiogenic mitogen. *Science* (80-.). **246**, 1306–1309 (1989).
 167. Lewis, B. P., Shih, I., Jones-Rhoades, M. W., Bartel, D. P. & Burge, C. B. Prediction of Mammalian MicroRNA Targets. *Cell* **115**, 787–798 (2003).
 168. Lewis, W. H. Experimental studies on the development of the eye in amphibia. I. On the origin of the lens. *Rana palustris*. *Am. J. Anat.* **3**, 505–536 (1904).
 169. Li, X. *et al.* Transcriptional regulation of miR-10a/b by TWIST-1 in myelodysplastic syndromes. *Haematologica* **98**, 414–419 (2013).
 170. Liang, L. & He, X. A narrative review of microRNA therapeutics: understanding the future of microRNA research. *Precis. Cancer Med.* **4**, (2021).
 171. Lin, X. *et al.* HBX-induced miR-5188 impairs FOXO1 to stimulate β -catenin nuclear translocation and promotes tumor stemness in hepatocellular carcinoma. *Theranostics* **9**, 7583–7598 (2019).
 172. Ling, H., Zhang, W. & Calin, G. A. Principles of microRNA involvement in human cancers. *Chin. J. Cancer* **30**, 739–748 (2011).
 173. Linker, C. *et al.* Cell communication with the neural plate is required for induction of neural markers by BMP inhibition: evidence for homeogenetic induction and implications for *Xenopus* animal cap and chick explant assays. *Dev. Biol.* **327**, 478–486 (2009).
 174. Liu, A., Losos, K. & Joyner, A. L. FGF8 can activate Gbx2 and transform regions of the rostral mouse brain into a hindbrain fate. *Development* **126**, 4827–4838 (1999).
 175. Liu, F. *et al.* Upregulation of microRNA-210 regulates renal angiogenesis mediated by activation of VEGF signaling pathway under ischemia/perfusion injury *in vivo* and *in vitro*. *Kidney Blood Press. Res.* **35**, 182–191 (2012).
 176. Liu, Q. *et al.* miR-504 suppresses mesenchymal phenotype of glioblastoma by directly targeting the FZD7-mediated Wnt- β -catenin pathway. *J. Exp. Clin. Cancer Res.* **38**, 358 (2019).
 177. Liu, X. S. *et al.* MicroRNA profiling in subventricular zone after stroke: MiR-124a regulates proliferation of neural progenitor cells through notch signaling pathway. *PLoS One* **6**, 1–11 (2011).
 178. Loh, C. Y. *et al.* The *e-cadherin* and *n-cadherin* switch in epithelial-to-mesenchymal transition: Signaling, therapeutic implications, and challenges. *Cells* vol. 8 (2019).
 179. Lu, J. *et al.* MicroRNA expression profiles classify human cancers. *Nature* **435**, 834–838 (2005).
 180. Lu, M. *et al.* A novel microRNAs expression signature for hepatocellular carcinoma diagnosis and prognosis. *Oncotarget* **8**, 8775–8784 (2017).
 181. Lu, M. *et al.* MicroRNA-370 suppresses the progression and proliferation of human astrocytoma and glioblastoma by negatively regulating β -catenin and causing activation of FOXO3a. *Exp. Ther. Med.* **15**, 1093–1098 (2018).
 182. de Luca, E., Marinaro, F., Niola, F. & Tonelli, D. D. P. Cutting Edge Approaches for the Identification and the Functional Investigation of miRNAs in Brain Science. *Handb. Neurobehav. Genet. Phenotyping* 553–584 (2017) doi:10.1002/9781118540770.ch22.
 183. Lucon, D. R. *et al.* Downregulation of 14q32 micrnas in primary human desmoplastic medulloblastoma. *Front. Oncol.* **3 SEP**, 1–14 (2013).
 184. Luo, X., Liu, J. & Cheng, S. Y. The role of microRNAs during the genesis of medulloblastomas induced by the hedgehog pathway. *J. Biomed. Res.* **25**, 42–48 (2011).
 185. Lv, X., Jiang, H., Liu, Y., Lei, X. & Jiao, J. MicroRNA-15b promotes neurogenesis and inhibits neural progenitor proliferation by directly repressing TET3 during early neocortical development. *EMBO Rep.* **15**, 1305–1314 (2014).
 186. Ma, L., Teruya-Feldstein, J. & Weinberg, R. A. Tumour invasion and metastasis initiated by microRNA-10b in breast cancer. *Nature* **449**, 682–688 (2007).
 187. Ma, S. C. *et al.* CLDN5 affects lncRNAs acting as ceRNA dynamics contributing to regulating blood-brain barrier permeability in tumor brain metastasis. *Oncol. Rep.* **39**, 1441–1453 (2018).

188. Maeda, H. & Khatami, M. Analyses of repeated failures in cancer therapy for solid tumors: poor tumor-selective drug delivery, low therapeutic efficacy and unsustainable costs. *Clin. Transl. Med.* **7**, 1–20 (2018).
189. Majzner, R. G. *et al.* CAR T cells targeting B7-H3, a pan-cancer antigen, demonstrate potent preclinical activity against pediatric solid tumors and brain tumors. *Clin. Cancer Res.* **25**, 2560–2574 (2019).
190. Mak, I. W. Y., Evaniew, N. & Ghert, M. Lost in translation: Animal models and clinical trials in cancer treatment. *Am. J. Transl. Res.* **6**, 114–118 (2014).
191. Makarova, J. A. *et al.* Intracellular and extracellular microRNA: An update on localization and biological role. *Prog. Histochem. Cytochem.* **51**, 33–49 (2016).
192. Makeyev, E. V., Zhang, J., Carrasco, M. A. & Maniatis, T. The MicroRNA miR-124 Promotes Neuronal Differentiation by Triggering Brain-Specific Alternative Pre-mRNA Splicing. *Mol. Cell* **27**, 435–448 (2007).
193. Malatesta, P., Hartfuss, E. & Götz, M. Isolation of radial glial cells by fluorescent-activated cell sorting reveals a neural lineage. *Development* **127**, 5253–5263 (2000).
194. Margol, A. S. *et al.* Tumor-associated macrophages in SHH subgroup of medulloblastomas. *Clin. Cancer Res.* **21**, 1457–1465 (2015).
195. Marin, F. & Puelles, L. Patterning of the embryonic avian midbrain after experimental inversions: A polarizing activity from the isthmus. *Developmental Biology* vol. 163 19–37 at <https://doi.org/10.1006/dbio.1994.1120> (1994).
196. Marzagalli, M., Fontana, F., Raimondi, M. & Limonta, P. Cancer stem cells—key players in tumor relapse. *Cancers (Basel)*. **13**, 1–23 (2021).
197. Maximov, V. *et al.* Tumour-associated macrophages exhibit anti-tumoural properties in Sonic Hedgehog medulloblastoma. *Nat. Commun.* **10**, 1–11 (2019).
198. McAllister, J. P. Pathophysiology of congenital and neonatal hydrocephalus. *Semin. Fetal Neonatal Med.* **17**, 285–294 (2012).
199. Mduma, E., Awuor, A. & Lugina, E. L. Adult medulloblastoma: a case report. *J. Med. Case Rep.* **16**, 330 (2022).
200. Medley, J. C., Panzade, G. & Zinovyeva, A. Y. microRNA strand selection: Unwinding the rules. *Wiley Interdiscip. Rev. RNA* **12**, 1–22 (2021).
201. Meldolesi, J. Neurite outgrowth: This process, first discovered by Santiago Ramon y Cajal, is sustained by the exocytosis of two distinct types of vesicles. *Brain Res. Rev.* **66**, 246–255 (2011).
202. Mens, M. M. J. & Ghanbari, M. Cell Cycle Regulation of Stem Cells by MicroRNAs. *Stem Cell Rev. Reports* **14**, 309–322 (2018).
203. Millard, N. E. & De Braganca, K. C. Medulloblastoma. *J. Child Neurol.* **31**, 1341–1353 (2016).
204. Miska, E. A. *et al.* Microarray analysis of microRNA expression in the developing mammalian brain. *Genome Biol.* **5**, (2004).
205. Mitra, R., Lin, C. C., Eischen, C. M., Bandyopadhyay, S. & Zhao, Z. Concordant dysregulation of miR-5p and miR-3p arms of the same precursor microRNA may be a mechanism in inducing cell proliferation and tumorigenesis: a lung cancer study. *RNA* **21**, 1055–1065 (2015).
206. Mold, J. E. & McCune, J. M. *Immunological Tolerance During Fetal Development. From Mouse to Man. Advances in Immunology* vol. 115 (Elsevier Inc., 2012).
207. Mongroo, P. S. & Rustgi, A. K. The role of the miR-200 family in epithelial-mesenchymal transition. *Cancer Biol. Ther.* **10**, 219–222 (2010).
208. Morel, A. P. *et al.* EMT inducers catalyze malignant transformation of mammary epithelial cells and drive tumorigenesis towards claudin-low tumors in transgenic mice. *PLoS Genet.* **8**, (2012).
209. Morozova, N. *et al.* Kinetic signatures of microRNA modes of action. *Rna* **18**, 1635–1655 (2012).
210. Mourelatos, Z. *et al.* miRNPs: A novel class of ribonucleoproteins containing numerous microRNAs. *Genes Dev.* **16**, 720–728 (2002).
211. Mousavi, S. M. *et al.* Non-coding RNAs and glioblastoma: Insight into their roles in metastasis. *Mol. Ther. - Oncolytics* **24**, 262–287 (2022).
212. Mukherjee, P., Roy, S., Ghosh, D. & Nandi, S. K. Role of animal models in biomedical research: a review. *Lab. Anim. Res.* **38**, 1–17 (2022).
213. Murphy, B. L. *et al.* Silencing of the miR-17~92 cluster family inhibits medulloblastoma progression. *Cancer Res.* **73**, 7068–7078 (2013).
214. Musilova, K. & Mraz, M. MicroRNAs in B-cell lymphomas: how a complex biology gets more complex. *Leukemia* **29**, 1004–1017 (2015).

215. Nadarajah, B., Alifragis, P., Wong, R. O. L. & Parnavelas, J. G. Neuronal migration in the developing cerebral cortex: Observations based on real-time imaging. *Cereb. Cortex* **13**, 607–611 (2003).
216. Najafi, M., Farhood, B. & Mortezaee, K. Cancer stem cells (CSCs) in cancer progression and therapy. *J. Cell. Physiol.* **234**, 8381–8395 (2019).
217. Nassiri, S. M., Ahmadi Afshar, N. & Almasi, P. Insight into microRNAs' involvement in hematopoiesis: current standing point of findings. *Stem Cell Res. Ther.* **14**, 1–26 (2023).
218. Newman, P. J. *et al.* Molecules of the immunoglobulin gene superfamily. *Cell* **1219** (1990).
219. Nielsen, J. A., Lau, P., Maric, D., Barker, J. L. & Hudson, L. D. Integrating microRNA and mRNA expression profiles of neuronal progenitors to identify regulatory networks underlying the onset of cortical neurogenesis. *BMC Neurosci.* **10**, 1–17 (2009).
220. Niu, C. S., Yang, Y. & Cheng, C. D. MiR-134 regulates the proliferation and invasion of glioblastoma cells by reducing Nanog expression. *Int. J. Oncol.* **42**, 1533–1540 (2013).
221. Nurzadeh, M., Naemi, M. & Sheikh Hasani, S. A comprehensive review on oncogenic miRNAs in breast cancer. *J. Genet.* **100**, (2021).
222. O'Brien, J., Hayder, H., Zayed, Y. & Peng, C. Overview of microRNA biogenesis, mechanisms of actions, and circulation. *Front. Endocrinol. (Lausanne)*. **9**, 1–12 (2018).
223. O'Donnell, K. A., Wentzel, E. A., Zeller, K. I., Dang, C. V & Mendell, J. T. c-Myc-regulated microRNAs modulate E2F1 expression. *Nature* **435**, 839–843 (2005).
224. Ohsawa, K., Imai, Y., Sasaki, Y. & Kohsaka, S. Microglia/macrophage-specific protein Iba1 binds to fimbrin and enhances its actin-bundling activity. *J. Neurochem.* **88**, 844–856 (2004).
225. De Oliveira, F., Landeiro, J. & De Castro, I. Adult hemispheric cerebellar medulloblastoma. *Surg. Neurol. Int.* **9**, (2018).
226. Oliveira, S. S. & Morgado-Díaz, J. A. Claudins: Multifunctional players in epithelial tight junctions and their role in cancer. *Cell. Mol. Life Sci.* **64**, 17–28 (2007).
227. Olsen, P. H. & Ambros, V. The lin-4 regulatory RNA controls developmental timing in *Caenorhabditis elegans* by blocking LIN-14 protein synthesis after the initiation of translation. *Dev. Biol.* **216**, 671–680 (1999).
228. Ozben, T. Mechanisms and strategies to overcome multiple drug resistance in cancer. *FEBS Lett.* **580**, 2903–2909 (2006).
229. De Palma, M., Biziato, D. & Petrova, T. V. Microenvironmental regulation of tumour angiogenesis. *Nat. Rev. Cancer* **17**, 457–474 (2017).
230. Pan, G., Liu, Y., Shang, L., Zhou, F. & Yang, S. EMT-associated microRNAs and their roles in cancer stemness and drug resistance. *Cancer Commun.* **41**, 199–217 (2021).
231. Pan, Y., Yu, Y., Wang, X. & Zhang, T. Tumor-Associated Macrophages in Tumor Immunity. *Front. Immunol.* **11**, (2020).
232. Pannuru, P. *et al.* MiR-let-7f-1 regulates SPARC mediated cisplatin resistance in medulloblastoma cells. *Cell. Signal.* **26**, 2193–2201 (2014).
233. Paolicelli, R. C. *et al.* Microglia states and nomenclature: A field at its crossroads. *Neuron* **110**, 3458–3483 (2022).
234. Pei, Y. fei, Lei, Y. & Liu, X. qiang. MiR-29a promotes cell proliferation and EMT in breast cancer by targeting ten eleven translocation 1. *Biochim. Biophys. Acta - Mol. Basis Dis.* **1862**, 2177–2185 (2016).
235. Petersen, C. P., Bordeleau, M. E., Pelletier, J. & Sharp, P. A. Short RNAs repress translation after initiation in mammalian cells. *Mol. Cell* **21**, 533–542 (2006).
236. Phi, L. T. H. *et al.* Cancer stem cells (CSCs) in drug resistance and their therapeutic implications in cancer treatment. *Stem Cells Int.* **2018**, (2018).
237. Phoenix, T. N. *et al.* Medulloblastoma Genotype Dictates Blood Brain Barrier Phenotype. *Cancer Cell* **29**, 508–522 (2016).
238. Pierson, J., Hostager, B., Fan, R. & Vibhakar, R. Regulation of cyclin dependent kinase 6 by microRNA 124 in medulloblastoma. *J. Neurooncol.* **90**, 1–7 (2008).
239. De Pietri Tonelli, D. *et al.* miRNAs are essential for survival and differentiation of newborn neurons but not for expansion of neural progenitors during early neurogenesis in the mouse embryonic neocortex. *Development* **135**, 3911–3921 (2008).
240. Pillai, R. S. *et al.* Inhibition of translational initiation by Let-7 MicroRNA in human cells. *Science* **309**, 1573–1576 (2005).
241. Pilz, D. T. *et al.* LIS1 and XLIS (DCX) mutations cause most classical lissencephaly, but different patterns of malformation. *Hum. Mol. Genet.* **7**, 2029–2037 (1998).

242. Pons-Espinal, M. *et al.* Synergic Functions of miRNAs Determine Neuronal Fate of Adult Neural Stem Cells. *Stem Cell Reports* **8**, 1046–1061 (2017).
243. Prados, M. D. Current Strategies for Management of Medulloblastoma. *Diagnostics* **13**, (2023).
244. Pugh, T. J. *et al.* Medulloblastoma exome sequencing uncovers subtype-specific somatic mutations. *Nature* **488**, 106–110 (2012).
245. Pyonteck, S. M. *et al.* CSF-1R inhibition alters macrophage polarization and blocks glioma progression. *Nat. Med.* **19**, 1264–1272 (2013).
246. Qian, X. *et al.* Star-branched amphiphilic PLA-b-PDMAEMA copolymers for co-delivery of miR-21 inhibitor and doxorubicin to treat glioma. *Biomaterials* **35**, 2322–2335 (2014).
247. Qu, Q. *et al.* Orphan nuclear receptor TLX activates Wnt/B-catenin signalling to stimulate neural stem cell proliferation and self-renewal. *Nat. Cell Biol.* **12**, 31–40 (2010).
248. Quintavalle, C. *et al.* MiR-221/222 overexpression in human glioblastoma increases invasiveness by targeting the protein phosphate PTP. *Oncogene* **31**, 858–868 (2012).
249. Rakic, P. & Sidman, R. L. Histogenesis of cortical layers in human cerebellum, particularly the lamina dissecans. *J. Comp. Neurol.* **139**, 473–500 (1970).
250. Rakic, P. Evolution of the neocortex: a perspective from developmental biology. *Nat. Rev. Neurosci.* **10**, 724–735 (2009).
251. Reid, G. *et al.* Restoring expression of miR-16: A novel approach to therapy for malignant pleural mesothelioma. *Ann. Oncol.* **24**, 3128–3135 (2013).
252. Reillo, I. *et al.* A complex code of extrinsic influences on cortical progenitor cells of higher mammals. *Cereb. Cortex* **27**, 4586–4606 (2017).
253. Reinhart, B. J., Weinstein, E. G., Rhoades, M. W., Bartel, B. & Bartel, D. P. MicroRNAs in plants. *Genes Dev.* **16**, 1616–1626 (2002).
254. Rhoades, M. W. *et al.* Prediction of plant microRNA targets. *Cell* **110**, 513–520 (2002).
255. Riva, D. & Giorgi, C. The cerebellum contributes to higher functions during development. Evidence from a series of children surgically treated for posterior fossa tumours. *Brain* **123**, 1051–1061 (2000).
256. Rogaev, E. I., Borinskaya, S. A., Islamgulov, D. V. & Grigorenko, A. P. Human microRNA in norm and pathology. *Mol. Biol.* **42**, 668–680 (2008).
257. Rønning, C., Sundet, K., Due-Tønnessen, B., Lundar, T. & Helseth, E. Persistent cognitive dysfunction secondary to cerebellar injury in patients treated for posterior fossa tumors in childhood. *Pediatr. Neurosurg.* **41**, 15–21 (2005).
258. Roostaei, T., Nazeri, A., Sahraian, M. A. & Minagar, A. The human cerebellum: A review of physiologic neuroanatomy. *Neurol. Clin.* **32**, 859–869 (2014).
259. Rose, M. F., Ahmad, K. A., Thaller, C. & Zoghbi, H. Y. Excitatory neurons of the proprioceptive, interoceptive, and arousal hindbrain networks share a developmental requirement for Math1. *Proc. Natl. Acad. Sci. U. S. A.* **106**, 22462–22467 (2009).
260. Roussel, M. F. & Stripay, J. L. Modeling pediatric medulloblastoma. *Brain Pathol.* **30**, 703–712 (2020).
261. Ruby, J. G., Jan, C. H. & Bartel, D. P. Intronic microRNA precursors that bypass Drosha processing. *Nature* **448**, 83–86 (2007).
262. Dello Russo, C. *et al.* Exploiting Microglial Functions for the Treatment of Glioblastoma. *Curr. Cancer Drug Targets* **17**, 267–281 (2017).
263. Ryan, B. M. microRNAs in Cancer Susceptibility. *Adv. Cancer Res.* **135**, 151–171 (2017).
264. Sabry, D. *et al.* Role of miRNA-210, miRNA-21 and miRNA-126 as diagnostic biomarkers in colorectal carcinoma: impact of HIF-1 α -VEGF signaling pathway. *Mol. Cell. Biochem.* **454**, 177–189 (2019).
265. Saito, T. & Nakatsuji, N. Efficient gene transfer into the embryonic mouse brain using *in vivo* electroporation. *Dev. Biol.* **240**, 237–246 (2001).
266. Saito, Y. & Jones, P. A. Epigenetic activation of tumor suppressor microRNAs in human cancer cells. *Cell Cycle* **5**, 2220–2222 (2006).
267. Sanuki, R. *et al.* MiR-124a is required for hippocampal axogenesis and retinal cone survival through Lhx2 suppression. *Nat. Neurosci.* **14**, 1125–1136 (2011).
268. Satelli, A. & Li, S. Vimentin in cancer and its potential as a molecular target for cancer therapy. *Cell. Mol. Life Sci.* **68**, 3033–3046 (2011).
269. Sato, T. & Joyner, A. L. The duration of Fgf8 isthmic organizer expression is key to patterning different tectal-isthmo-cerebellum structures. *Development* **136**, 3617–3626 (2009).
270. Schirmer, E. C., Latonen, L. & Tollis, S. Nuclear size rectification: A potential new therapeutic approach to reduce metastasis in cancer. *Front. Cell Dev. Biol.* **10**, 1–17 (2022).

271. Schliermann, A. & Nickel, J. Unraveling the connection between fibroblast growth factor and bone morphogenetic protein signaling. *Int. J. Mol. Sci.* **19**, 1–17 (2018).
272. Schüller, U. *et al.* Forkhead transcription factor FoxM1 regulates mitotic entry and prevents spindle defects in cerebellar granule neuron precursors. *Mol. Cell. Biol.* **27**, 8259–8270 (2007).
273. Schwarz, D. S. *et al.* Asymmetry in the assembly of the RNAi enzyme complex. *Cell* **115**, 199–208 (2003).
274. Schweiger, M. R., Kerick, M., Timmermann, B. & Isau, M. The power of NGS technologies to delineate the genome organization in cancer: from mutations to structural variations and epigenetic alterations. *Cancer Metastasis Rev.* **30**, 199–210 (2011).
275. Semenkow, S. *et al.* An immunocompetent mouse model of human glioblastoma. *Oncotarget* **8**, 61072–61082 (2017).
276. Sempere, L. F. *et al.* Expression profiling of mammalian microRNAs uncovers a subset of brain-expressed microRNAs with possible roles in murine and human neuronal differentiation. *Genome Biol.* **5**, (2004).
277. Seo, J., Ha, J., Kang, E. & Cho, S. The role of epithelial–mesenchymal transition-regulating transcription factors in anti-cancer drug resistance. *Arch. Pharm. Res.* **44**, 281–292 (2021).
278. Seto, A. G. *et al.* Cobomarsen, an oligonucleotide inhibitor of miR-155, co-ordinately regulates multiple survival pathways to reduce cellular proliferation and survival in cutaneous T-cell lymphoma. *Br. J. Haematol.* **183**, 428–444 (2018).
279. Shi, H., Ji, Y., Zhang, D., Liu, Y. & Fang, P. MiR-135a inhibits migration and invasion and regulates EMT-related marker genes by targeting KLF8 in lung cancer cells. *Biochem. Biophys. Res. Commun.* **465**, 125–130 (2015).
280. Shtutman, M. *et al.* The cyclin D1 gene is a target of the β -catenin/LEF-1 pathway. *Proc. Natl. Acad. Sci. U. S. A.* **96**, 5522–5527 (1999).
281. Shu, M. *et al.* Targeting oncogenic miR-335 inhibits growth and invasion of malignant astrocytoma cells. *Mol. Cancer* **10**, 1–17 (2011).
282. Shu, P. *et al.* The spatiotemporal expression pattern of microRNAs in the developing mouse nervous system. *J. Biol. Chem.* **294**, 3444–3453 (2019).
283. Silber, J. *et al.* Expression of miR-124 inhibits growth of medulloblastoma cells. *Neuro. Oncol.* **15**, 83–90 (2013).
284. Singh, S. K. *et al.* Identification of a cancer stem cell in human brain tumors. *Cancer Res.* **63**, 5821–8 (2003).
285. Singh, S. *et al.* Aldehyde dehydrogenases in cellular responses to oxidative/ electrophilic stress. *Free Radic. Biol. Med.* **56**, 89–101 (2013).
286. Smirnova, L. *et al.* Regulation of miRNA expression during neural cell specification. *Eur. J. Neurosci.* **21**, 1469–1477 (2005).
287. Spemann, H. Facsimile reproduction of the cover of an original reprint of the 1924 article by Hans Spemann and Hilde Mangold, with a handwritten dedication by H. Spemann which reads ‘With best regards, H.S.’ (Courtesy of K. Sander, Freiburg). *Archiv* (1924).
288. van Spronsen, M. *et al.* Developmental and Activity-Dependent miRNA Expression Profiling in Primary Hippocampal Neuron Cultures. *PLoS One* **8**, (2013).
289. Squarzoni, P. *et al.* Microglia Modulate Wiring of the Embryonic Forebrain. *Cell Rep.* **8**, 1271–1279 (2014).
290. Stern, C. D. Conrad H. Waddington’s contributions to avian and mammalian development, 1930–1940. *Int. J. Dev. Biol.* **44**, 15–22 (2000).
291. van Stijn, A. *et al.* Differences between the CD34+ and CD34- blast compartments in apoptosis resistance in acute myeloid leukemia. *Haematologica* **88**, 497–508 (2003).
292. Suh, M. R. *et al.* Human embryonic stem cells express a unique set of microRNAs. *Dev. Biol.* **270**, 488–498 (2004).
293. Susanto, E. *et al.* Modeling SHH-driven medulloblastoma with patient iPSC cell-derived neural stem cells. *Proc. Natl. Acad. Sci. U. S. A.* **117**, 20127–20138 (2020).
294. Sutter, R. *et al.* Cerebellar stem cells act as medulloblastoma-initiating cells in a mouse model and a neural stem cell signature characterizes a subset of human medulloblastomas. *Oncogene* **29**, 1845–1856 (2010).
295. Swartling, F. J. *et al.* Pleiotropic role for MYCN in medulloblastoma. *Genes Dev.* **24**, 1059–1072 (2010).
296. Takamizawa, J. *et al.* Reduced expression of the let-7 microRNAs in human lung cancers in association with shortened postoperative survival. *Cancer Res.* **64**, 3753–3756 (2004).

297. Tang, H. *et al.* Interaction of hsa-miR-381 and glioma suppressor LRRC4 is involved in glioma growth. *Brain Res.* **1390**, 21–32 (2011).
298. Tang, T. *et al.* Up-regulation of miR-210 induced by a hypoxic microenvironment promotes breast cancer stem cell metastasis, proliferation, and self-renewal by targeting E-cadherin. *FASEB J.* **32**, 6965–6981 (2018).
299. Tay, Y., Zhang, J., Thomson, A. M., Lim, B. & Rigoutsos, I. MicroRNAs to Nanog, Oct4 and Sox2 coding regions modulate embryonic stem cell differentiation. *Nature* **455**, 1124–1128 (2008).
300. Taylor, S. R. *et al.* MicroRNA-218 instructs proper assembly of hippocampal networks. *bioRxiv* (2022) doi:10.1101/2022.08.24.505085.
301. Testa, G. *et al.* Disentangling the signaling complexity of nerve growth factor receptors by CRISPR/Cas9. *FASEB J.* **36**, 1–16 (2022).
302. Tian, L. *et al.* Mutual regulation of tumour vessel normalization and immunostimulatory reprogramming. *Nature* **544**, 250–254 (2017).
303. Tiberi, L. *et al.* A BCL6/BCOR/SIRT1 Complex Triggers Neurogenesis and Suppresses Medulloblastoma by Repressing Sonic Hedgehog Signaling. *Cancer Cell* **26**, 797–812 (2014).
304. Umeh-Garcia, M. *et al.* A novel bioengineered miR-127 prodrug suppresses the growth and metastatic potential of triple-negative breast cancer cells. *Cancer Res.* **80**, 418–429 (2020).
305. Venkataraman, S. *et al.* MicroRNA 218 acts as a tumor suppressor by targeting multiple cancer phenotype-associated genes in medulloblastoma. *J. Biol. Chem.* **288**, 1918–1928 (2013).
306. Ventura, A. *et al.* Targeted Deletion Reveals Essential and Overlapping Functions of the miR-17~92 Family of miRNA Clusters. *Cell* **132**, 875–886 (2008).
307. Vidal-Itriago, A. *et al.* Microglia morphophysiological diversity and its implications for the CNS. *Front. Immunol.* **13**, 1–16 (2022).
308. Vitanza, N. A. *et al.* Locoregional infusion of HER2-specific CAR T cells in children and young adults with recurrent or refractory CNS tumors: an interim analysis. *Nat. Med.* **27**, 1544–1552 (2021).
309. Volvert, M. L. *et al.* MicroRNA targeting of CoREST controls polarization of migrating cortical neurons. *Cell Rep.* **7**, 1168–1183 (2014).
310. Waller, R. *et al.* Iba-1-/CD68+ microglia are a prominent feature of age-associated deep subcortical white matter lesions. *PLoS One* **14**, 1–18 (2019).
311. Wang, B., Yanez, A. & Novina, C. D. MicroRNA-repressed mRNAs contain 40S but not 60S components. *Proc. Natl. Acad. Sci. U. S. A.* **105**, 5343–5348 (2008).
312. Wang, F., Zhou, F., Kruh, G. D. & Gallo, J. M. Influence of blood-brain barrier efflux pumps on the distribution of vincristine in brain and brain tumors. *Neuro. Oncol.* **12**, 1043–1049 (2010).
313. Wang, L., Wang, X. & Jiang, X. MiR-127 suppresses gastric cancer cell migration and invasion via targeting Wnt7a. *Oncol. Lett.* **17**, 3219–3226 (2019).
314. Wang, V. Y., Rose, M. F. & Zoghbi, H. Y. Math1 expression redefines the rhombic lip derivatives and reveals novel lineages within the brainstem and cerebellum. *Neuron* **48**, 31–43 (2005).
315. Wang, X. *et al.* MiR miR on the wall, who's the most malignant medulloblastoma miR of them all? *Neuro. Oncol.* **20**, 313–323 (2018).
316. Wang, Y. *et al.* A convenient method for distinguishing human and mouse cells in situ. *Acta Biochim. Biophys. Sin. (Shanghai)*. **53**, 124–127 (2021).
317. Wang, Z. Y., Wen, Z. J., Xu, H. M., Zhang, Y. & Zhang, Y. F. Exosomal noncoding RNAs in central nervous system diseases: biological functions and potential clinical applications. *Front. Mol. Neurosci.* **15**, 1–25 (2022).
318. Whitney, J. *et al.* Quantitative Nuclear Histomorphometry Predicts Molecular Subtype and Clinical Outcome in Medulloblastomas: Preliminary Findings. *J. Pathol. Inform.* **13**, 100090 (2022).
319. Wu, F., Yang, Z. & Li, G. Role of specific microRNAs for endothelial function and angiogenesis. *Biochem. Biophys. Res. Commun.* **386**, 549–553 (2009).
320. Wu, L. & Belasco, J. G. Let Me Count the Ways: Mechanisms of Gene Regulation by miRNAs and siRNAs. *Mol. Cell* **29**, 1–7 (2008).
321. Xie, D., Pei, Q., Li, J., Wan, X. & Ye, T. Emerging Role of E2F Family in Cancer Stem Cells. *Front. Oncol.* **11**, 1–12 (2021).
322. Xiong, D. D. *et al.* A nine-miRNA signature as a potential diagnostic marker for breast carcinoma: An integrated study of 1,110 cases. *Oncol. Rep.* **37**, 3297–3304 (2017).
323. Xu, Z. *et al.* MicroRNA-383 inhibits anchorage-independent growth and induces cell cycle arrest of glioma cells by targeting CCND1. *Biochem. Biophys. Res. Commun.* **453**, 833–838 (2014).

324. Yang, L. *et al.* Targeting cancer stem cell pathways for cancer therapy. *Signal Transduct. Target. Ther.* **5**, 8 (2020).
325. Yang, L. *et al.* *Targeting cancer stem cell pathways for cancer therapy. Signal Transduction and Targeted Therapy* vol. 5 (Springer US, 2020).
326. Yang, Z. J. *et al.* Medulloblastoma Can Be Initiated by Deletion of Patched in Lineage-Restricted Progenitors or Stem Cells. *Cancer Cell* **14**, 135–145 (2008).
327. Yang, Z. J. & Wechsler-Reya, R. J. Hit 'Em Where They Live: Targeting the Cancer Stem Cell Niche. *Cancer Cell* **11**, 3–5 (2007).
328. Yao, B. *et al.* Epigenetic mechanisms in neurogenesis. *Nat. Rev. Neurosci.* **17**, 537–549 (2016).
329. Ye, X. & Weinberg, R. A. Epithelial-Mesenchymal Plasticity: A Central Regulator of Cancer Progression. *Trends Cell Biol.* **25**, 675–686 (2015).
330. Yokoyama, A., Takezawa, S., Schüle, R., Kitagawa, H. & Kato, S. Transrepressive Function of TLX Requires the Histone Demethylase LSD1. *Mol. Cell. Biol.* **28**, 3995–4003 (2008).
331. Yoo, A. S. *et al.* MicroRNA-mediated conversion of human fibroblasts to neurons. *Nature* **476**, 228–231 (2011).
332. Zapata-Acevedo, J. F. *et al.* Laminin as a Biomarker of Blood–Brain Barrier Disruption under Neuroinflammation: A Systematic Review. *Int. J. Mol. Sci.* **23**, (2022).
333. Zeng, Z. *et al.* Cancer-derived exosomal miR-25-3p promotes pre-metastatic niche formation by inducing vascular permeability and angiogenesis. *Nat. Commun.* **9**, (2018).
334. Zhang, B., Pan, X., Cobb, G. P. & Anderson, T. A. microRNAs as oncogenes and tumor suppressors. *Dev. Biol.* **302**, 1–12 (2007).
335. Zhang, F., Zhou, Y. & Ding, J. The current landscape of microRNAs (miRNAs) in bacterial pneumonia: opportunities and challenges. *Cell. Mol. Biol. Lett.* **27**, (2022).
336. Zhang, H. *et al.* MicroRNA-9 targets matrix metalloproteinase 14 to inhibit invasion, metastasis, and angiogenesis of neuroblastoma cells. *Mol. Cancer Ther.* **11**, 1454–1466 (2012).
337. Zhang, J. *et al.* Tumor-Associated Macrophages Correlate With Prognosis in Medulloblastoma. *Front. Oncol.* **12**, 1–9 (2022).
338. Zhang, J., Le, T. D., Liu, L. & Li, J. Identifying miRNA sponge modules using biclustering and regulatory scores. *BMC Bioinformatics* **18**, (2017).
339. Zhang, W. *et al.* Microglia-containing human brain organoids for the study of brain development and pathology. *Mol. Psychiatry* **28**, 96–107 (2023).
340. Zhang, Y. *et al.* The MicroRNA-17-92 cluster enhances axonal outgrowth in embryonic cortical neurons. *J. Neurosci.* **33**, 6885–6894 (2013).
341. Zhao, C., Sun, G., Li, S. & Shi, Y. A feedback regulatory loop involving microRNA-9 and nuclear receptor TLX in neural stem cell fate determination. *Nat. Struct. Mol. Biol.* **16**, 365–371 (2009).
342. Zhao, X., Zhang, L., Ting, S.-M. & Aronowski, J. Phagocytosis Assay of Microglia for Dead Neurons in Primary Rat Brain Cell Cultures. *Bio-protocol* **6**, (2016).
343. Zheng, Q. & Hou, W. Regulation of angiogenesis by microRNAs in cancer. *Mol. Med. Rep.* **24**, (2021).
344. Zhou, J. N. *et al.* MicroRNA-125b attenuates epithelial-mesenchymal transitions and targets stem-like liver cancer cells through small mothers against decapentaplegic 2 and 4. *Hepatology* **62**, 801–815 (2015).
345. Zhu, Y. *et al.* miR-145 Antagonizes SNAI1-Mediated Stemness and Radiation Resistance in Colorectal Cancer. *Mol. Ther.* **26**, 744–754 (2018).
346. Ziats, M. N. & Rennert, O. M. Identification of differentially expressed microRNAs across the developing human brain. *Mol. Psychiatry* **19**, 848–852 (2014).
347. Zotova, E. *et al.* Microglial alterations in human Alzheimer's disease following A β 42 immunization. *Neuropathol. Appl. Neurobiol.* **37**, 513–524 (2011).
348. How human are our models? *Nat. Rev. Bioeng.* **1**, 537 (2023).